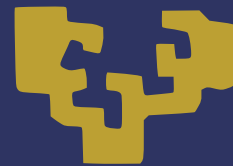




University of the Basque Country

PhD Thesis - 2016



LOWER BOUNDS ON QUANTUM METROLOGICAL PRECISION

Author:
Iagoba Apellaniz

Director:
Géza Tóth



This document was generated with the 2015 distribution of \LaTeX .



2012-2015 lagoba Apellaniz. This work is licensed under the Creative Commons Attribution-ShareAlike 4.0 International License. To view a copy of this license, visit http://creativecommons.org/licenses/by-sa/4.0/deed.en_US.

Prologue

THIS work is part of the doctoral project on Quantum Information which I started on the summer of 2013. This work collects part of the research I have done on these previous years. I will try to be clear throughout all the thesis such that make it readable for a wider audience as it is possible. This way I hope it will be readable by any person with a bachelor in science, particularly in physics or at least with a partial knowledge in Quantum Mechanics. With that in mind the first and the second chapters will be used to introduce the reader into the context on which this thesis was written as well as the basic notions of Quantum Metrology, the enveloping field of the present work. Even though I write this thesis for a broad audience in mind, a basic notion on quantum physics and statistics is needed to follow it properly as I said before. For instance, I will assume among other things that the reader knows what probability is and which are its properties, or what a quantum state is and what it represents. I will give references where to find such complementary material when I think is necessary.

This research I publish in a thesis form is part of the work done within the Research Group in Quantum Information in which Prof. Géza Tóth is the group leader and principal investigator. I have to mention the rest of the members of the group Dr. Philipp Hyllus, Dr. Giuseppe Vitagliano, Dr. Iñigo Urizar-Lanz, Dr. Zoltán Zinborás and Dr. Matthias Kleinmann at the time I was working on the projects of this thesis. Some of them may still be part of the group and some not. Apart from the group of Géza Tóth based in Bilbao, Spain, this thesis also collects some work done in collaboration with the Theoretical Quantum Optics (TQO) group lead by Prof. Otfried Gühne at the University of Siegen, Germany, and the group of Prof. Carsten Klempt at the Leibniz University in Hannover,

based also in Germany. The last one is an experimental group specialized on the creation of exotic quantum states with very many particles with a variety of applications in quantum technology.

First, we investigate the metrological usefulness of a family of states known as the unpolarized Dicke states, which have boosted the sensitivity of magnetometry when lots of particles are used in the sense that quantum enhancements play a very important role to achieve such a precision. Second, we investigate possible lower bounds on the quantum Fisher information, a quantity that characterizes the usefulness of a state for quantum metrology, using the theory of Legendre transforms such that we obtain tight lower bounds based on few measurements of the initial quantum state that will be used for metrology. And last but not least, we investigate the gradient magnetometry, i.e., we develop a theory to study the capabilities of some states to sense the change in space of the magnetic field and we apply that theory to some known states.

Before the thesis work the reader can find the present prologue, the list of publications, the table of contents, and a list of abbreviations, figures and tables. Then, the thesis starts. On the first pages one can find a brief dedicatory and acknowledgements followed by the chapters. The content of the chapters is organized as follows. First, I start with an introduction to describe the current situation of Quantum Information specially Quantum Metrology and I write about the basics of Quantum Metrology and how it emerges from statics and Quantum Mechanics. Second, I present the reader our works in characterizing the family of states known as the unpolarized Dicke states, in optimizing the lower bound for the quantum Fisher information when some expectation values of the states are known and our work in gradient quantum metrology.

Iagoba Apellaniz

Bilbao, November 16, 2016

Publications

Géza Tóth and Iagoba Apellaniz. *Quantum metrology from a quantum information science perspective*. Journal of Physics A: Mathematical and Theoretical, **47** 424006, 2014.

Iagoba Apellaniz, Bernd Lücke, Jan Peise, Carsten Klempt and Géza Tóth. *Detecting metrologically useful entanglement in the vicinity of Dicke states*. New Journal of Physics, **17** 083027, 2015.

Preprints

Iagoba Apellaniz, Matthias Kleinmann, Otfried Gühne and Géza Tóth. *Optimal detection of metrologically useful entanglement*. arXiv:1511.05203.

Out of the scope of this thesis

Giuseppe Vitagliano, Iagoba Apellaniz, Iñigo Luis Egusquiza and Géza Tóth. *Spin squeezing and entanglement for arbitrary spin*. Physical Review A, **89** 032307, 2014.

Giuseppe Vitagliano, Iagoba Apellaniz, Matthias Kleinmann, Bernd Lücke, Carsten Klempt and Géza Tóth. *Entanglement and extreme spin squeezing of unpolarized states* arXiv:1605.07202.

Contents

Acknowledgments	3
1 Introduction	5
2 Backgroud on Quantum Metrology	7
2.1 Background on statistics and the theory of estimation	8
2.1.1 Probability, data samples, average and variance	8
2.1.2 Frecuentist vs. bayesian approach	11
2.1.3 Estimators and Fisher information	11
2.2 Quantum Mechanics from metrology perspective	13
2.2.1 The quantum state, multiparticle state, entanglement	13
2.3 Quantum Metrology	15
2.3.1 Quantum Magnetometry	17
3 Metrology in the vicinity of Dicke states	21
3.1 Unpolarised states for magnetometry	22
3.2 Evolution of the expectation values	23

3.2.1	The optimal precision	26
3.3	Testing the formula against some known states	27
3.4	Using our method with real experimental data	29
4	Witnessing metrologically useful entanglement	33
4.1	Bound from below of a function convex over the states given some arbitrary expectation values	34
4.1.1	Estimation of a general convex function based on the expectation value of an arbitrary observable	34
4.1.2	Measuring several observables	36
4.1.3	Explicit form of the expression to be optimized	36
4.2	Examples	38
4.2.1	Exploiting symmetries	38
4.2.2	Fidelity measurements	39
4.2.3	Spin-squeezed states	43
4.2.4	Dicke states	45
4.3	Calculations for experimental data	46
4.3.1	Few-particle experiments	47
4.3.2	Many-particle experiments	48
4.4	Scaling for $\mathcal{F}_Q[\rho, J_z]$ with N	54
5	Metrology of the gradient magnetic field	57
5.1	Cramér-Rao precision bounds	61
5.1.1	Precision bound for states insensitive to homogeneous fields: Single-parameter dependence	62
5.1.2	Precision bound for states sensitive to homogeneous fields: Two-parameter dependence	64
5.2	Ion chains and two separated ensembles for magnetometry	66
5.3	Magnetometry with an atomic ensemble	70

5.3.1	Precision bound for an atomic ensemble	71
5.3.2	Precision limit for various spin-states	73
6	Conclusions	81
A	Long calculus appearing through the chapters	83
A.1	Simplification of the Eq. (3.13)	83
A.2	Calculation of $ \langle D_{N,m} _z D_{N,N/2}\rangle_x ^2$	84
A.3	Spin-squeezing Hamiltonian	85
B	Miscellaneous mathematical tools	85
B.1	Discussion on angular momentum subspaces for different spins	85
B.2	Husimi Q-representation and the Bloch sphere	88
B.3	Legendre transform	89
B.3.1	Binomial identities	90
	Bibliography	90

Abbreviations, figures and tables

Abbreviations

BEC	-	Bose-Einstein condensate
CLT	-	Central limit theorem
HL	-	Heisenberg limit
HS	-	Heisenberg scaling
PDF	-	Probability distribution function
QFI	-	Quantum Fisher information
SNS	-	Shot-noise scaling
SNL	-	Shot-noise limit
SLD	-	Symmetric logarithmic derivative
SQL	-	Standard quantum limit

Figures

2.1	Quantum Metrology estimation process	16
2.2	Graphical explanation of the error-propagation formula	19
2.3	Diagram for k -producibility sets	19
3.1	Sequence of Dicke state evolution	23

3.2	(a) Evolution of Θ . (b) Evolution of expectation values	26
3.3	Bound against known QFIs for different states.	28
3.4	Evolution of the precision for Θ	31
3.5	(a) Region of precision and experimental data. (b) Constant $\langle J_y^2 \rangle$ section.	32
4.1	Lower bound for fidelities. (a) F_{GHZ} . (b) F_{Dicke}	41
4.2	Solution for 4 particle on the parameter region for spin-squeezed states.	44
4.3	Boundary difference of optimal bound versus Pezzé-Smerzi bound.	45
4.4	6-particles optimal bound on BEC symmetry for the QFI when $\{\langle J_x^2 \rangle, \langle J_y^2 \rangle, \langle J_z^2 \rangle\}$ are measured	46
4.5	Asymptotic behaviour of the bound for increasing particle number for spin-squeezing experimental data	50
4.6	Asymptotic behaviour of the bound for increasing size systems for Dicke like experimental data	54
5.1	1-D chain of atoms gradient evolution sequence	67
5.2	Different set of states and its first and second moments representation.	80
B.1	Graphical representation of the Legendre transform.	89

Tables

4.1	Bounds on QFI for experimental data when fidelities are measured	47
5.1	Bounds on the precisions for different internal states for gradient magnetometry.	80



ZTF-FCT

UNIVERSITY OF THE BASQUE COUNTRY

PHD THESIS

eman ta zabal zazu



Lower bounds on quantum metrological precision

Author:

M. Sc. Iagoba APELLANIZ

Director:

Prof. Géza TÓTH



November 16, 2016

*To my parents, my family
and to all the people
I have had around those years.*

Acknowledgments

I want to thank the people that has supported me in this endeavor. Especially, I want to acknowledge my office and discussion mates, Giuseppe Vitagliano and Iñigo Urizar-Lanz as well as Phillip Hyllus, Matthias Kleinmann and Zoltán Zimborás. A special thank to my director Géza Tóth for all the offered support, without whom my work at hand would not be possible. I also want to thank more people from the department I belong to at the University of the Basque Country, the Department of Theoretical Physics and the History of Science. I appreciate the effort done by people like Iñigo L. Egusquiza in promoting the Ph.D. program of the Department of Theoretical Physics, which has successfully promote plenty of researchers now immersed in wonderful and leading edge research projects world wide. Also I want to acknowledge the Ph.D. students from different departments for the friendship atmosphere one can enjoy working there at this *our* university.

I have been visiting several research groups during those years and I don't forget them, they have accept me as one more between them. So I want to thank a very especial research group for me, the Theoretical Quantum Optics group at the University of Siegen. I would really like to mention the names of all of them but I think it would be quite heavy for the average reader of this thesis. Thank you guys! Also I want to thank people from the group QSTAR at Florence, Italy.

On the other hand I also felt very comfortable at my university, the University of the Basque Country, but I want to thank especially the people that make me grow in all ways as person.

1

Introduction

In the recent years...

The figure of merit for the precision is the inverse of the variance normalized with the number of particles, $(\Delta\theta)^{-2}/N$. It has the following properties:

- (i) The bigger it is the bigger is the precision
- (ii) It is normalized so for the best separable state it is 1. For greater values than 1 it would be a non-classical sign.

SQL

$$(\Delta\theta)^{-2} \leq N \tag{1.1}$$

HL

$$(\Delta\theta)^{-2} \leq N^2 \tag{1.2}$$

This thesis consists of 4 well differentiated parts, apart from the current introduction, on which different topics are developed. In the first part, we will introduce the reader onto the research field

of quantum metrology.

Brief comments on the notation: c_θ and s_θ stand for $\cos(\theta)$ and $\sin(\theta)$ trigonometric functions respectively. We will skip on writing the tensor-product notation \otimes if it is not strictly necessary for the correct comprehension of the text.

2

Background on Quantum Metrology

"In the real world, doing real experiments, statistics began to matter"
Roger J. Barlow

In this chapter we will study the basics of Quantum Metrology, which stands for the science of enhanced metrology by quantum phenomena. On the other hand, metrology, as the science of measuring, has played an essential role for the development of the technology as we know it today. It studies several aspects of the estimation process, such as which strategy to follow in order to improve the precision of an estimation or which is the bound for the precision. Metrology also covers all intermediate process for the estimation, from the design aspects of a precise measuring device, to the most basic concepts of estimation, which lead at the end to a better understanding of it as a whole.

In this sense, with the discovery of the Quantum Physics and the development of Quantum Mechanics, new doors for advances in metrology were open in the early decades of the 20th century. First, Quantum Theory embraced the so-called field of Quantum Information, which merges the notions of the theory of information and computer science, among others sub-fields, with the quantum mechanics. This new field of Quantum Information is in the basis of Quantum Metrology. Moreover, those emerging fields rapidly became into very interesting interdisciplinary playgrounds of science attracting the interest of many scientists as well as resources for their researches. Just to mention that the role of the so-called entanglement, an exclusive feature of Quantum Mechanics which cannot be completely described using classical probabilistic theories, is essential in this context. With the

aim of completely understand this concepts, many scientists world wide have integrated their efforts. Said this, the entanglement also is in the center of theoretical concepts in Quantum Metrology. In the Quantum Metrology framework, we will focus on the achievable precision of the systems. We will show as well different strategies to achieve the desired results.

On the other hand, a very important field of science must be highlighted by its own merits. We are mentioning the statistics, without which many descriptions of the actual and past physical findings would lack of the rigorous interpretation needed for the complexity of data samples. It basically helps to analyse raw data to find special properties out of it.

2.1 Background on statistics and the theory of estimation

In this section, we will enumerate the basic concepts of statistics as well as the estimation process. As we said, the main mathematical tools used by the metrology science belong to statistics. Moreover, we are especially interested in estimation theory. The statistics main characteristic is that it makes the raw data under consideration comprehensible from the human perspective. The data can be anything, from a set of different heights of a basketball team, to the outcomes of a coin toss, or the wavelength of photons coming out of some sample. The aim of this section is to give the reader sufficient material to follow this thesis and make it comprehensible from the beginning*.

2.1.1 Probability, data samples, average and variance

The probability indicates the relative chance of an event to happen. For instance, if there is a box with ten red balls and five blue balls, considering that the balls of the same color are indistinguishable and that we extract one randomly, we have $\frac{5}{10+5} = \frac{1}{3}$ of probability to obtain a blue ball and $\frac{2}{3}$ to obtain a red ball. The reader may notice many properties a probability should have, such as that the probability of any event to happen is always one or that a probability is always given by a number in between zero and one. For more details, there are many interesting textbooks or chapters of some textbook about Probability Theory one could follow if interested. The following References [? ?] are some of those books.

When someone has a data sample at hand, it might come from diverse sources and might be represented using multiple forms such as numbers or words (for instance, a table of names of people), the first thing one tries to accomplish is to analyze the data to extract the relevant properties from it. A data sample always come from a population sample, i.e., the data sample might not be complete

* For a more detailed material, check statistics book as well as mathematics book for scientist and engineers [? ?]

(one could lose some in the process) neither exact (a measuring device always have an error when estimating a magnitude). Hence, the data sample comes attached with a probability for each data element. In the subsequent paragraphs, we will describe this relation and we will enumerate the most useful properties and formulas for the comprehensions of this thesis.

First of all, we will explain our notation which follows the one used on Reference [?]. A probability function gives the probability of an event x to happen when measuring some random variable X , and it is denoted by $\Pr(X = x)$. Second, the N elements of a data sample are considered to come from N random variables with the corresponding N values due to the random nature of the measuring, $\{X_i = x_i\}_{i=1}^N$. The joint probability of those random variables is in general not separable. This is due to the fact that the outcomes could depend on the rest of the outcomes or some other more complex relation that makes the most general case to be non-separable from the probabilistic point of view. Therefore we define this PDF as an N variable function

$$\Pr(\mathbf{X} = \mathbf{x}) \equiv \Pr(X_1 = x_1, X_2 = x_2, \dots, X_N = x_N). \quad (2.1)$$

If separable this is written by

$$\Pr(\mathbf{X} = \mathbf{x}) = \prod_{i=1}^N \Pr(X_i = x_i) \quad (2.2)$$

and it is the case for many relevant cases.

When some property of the system is defined as a function of random variables, the result is also a random variable with another transformed PDF. For example, we measure the position of a body at some moment. If the system was at rest on the origin at initial time and the acceleration is known to be constant, then from the position one can infer on the value of the acceleration by using $A = 2X/t^2$, where X denotes the position at instant t and A the acceleration. If X is a random variable, which is the general case when measuring the position of a body, then the probability is computed in this case by

$$\Pr(A = a) = \frac{dx}{da} \Pr(X = x) = \frac{2}{t^2} \Pr(X = x). \quad (2.3)$$

In general for the multiple random variable case transformations, we must require that

$$|\Pr(\mathbf{X} = \mathbf{x}) dx_1 dx_2 \dots dx_N| = |\Pr(\mathbf{Y} = \mathbf{y}) dy_1 dy_2 \dots dy_N|. \quad (2.4)$$

This leads to some interesting formulas we will discuss later.

We now stick to the simplest case on which the data is a collection of values of the same random variable describing the same physical one-dimensional data population. Some definitions reasonable

to mention in this thesis arise for those kind of data samples: the average, variance, moments and central moments. The arithmetic average (there are other types of average one can find in the textbooks) is computed by

$$\bar{x} = \frac{1}{N} \sum x_i. \quad (2.5)$$

The variance is related with the spread of the data and computed by

$$\sigma^2 = \frac{1}{N} \sum (x_i - \bar{x})^2, \quad (2.6)$$

where σ is the standard deviation. Different moments are computed by $\bar{x}^r = \frac{1}{N} \sum x_i^r$ while central moments are of the form $n_r = \frac{1}{N} \sum (x_i - \bar{x})^r$. Notice that the variance is the second central moment of the data sample. For completeness, when each element of the data consists of more than a number, e.g., (x_i, y_i, z_i) , the co-variance between two data kinds, in the following case X and Y , is obtained by

$$V_{X,Y} = \frac{1}{N} \sum_{i=1}^N (x_i - \bar{x})(y_i - \bar{y}). \quad (2.7)$$

Those functions also apply to the probability distribution functions. While these last ones may be unknown functions for us, as soon as we collect all the possible data or we are in the large number regime the variances of the data sample and of the data population, the means, the co-variances and so on so forth, they must coincide. We will try to keep this distinction as clear as possible. In general the mean values of any function over data sample values $g(x)$ are denoted with a bar over a lowercase variable, e.g., \bar{x}^r for the r -th moment, while the mean values of any function applied to the data population $g(X)$ is written following some textbooks by $E[g(X)]$. One clearly may distinguish two cases here: one for continuous functions where the expectation values or the means are computed integrating over all the possible values, and the other case on which $\Pr(\mathbf{X} = \mathbf{x})$ can take only discrete values. For completeness here are the two definitions

$$E[g(\mathbf{X})] = \begin{cases} \int g(\mathbf{x}) \Pr(\mathbf{X} = \mathbf{x}) d^N \mathbf{x}, \\ \sum_{i,j,\dots} g(\mathbf{x}) \Pr(\mathbf{X} = \mathbf{x}). \end{cases} \quad (2.8)$$

One more definition needs our attention and it is the variance any function $g(X)$ denoted by $V[g(X)] \equiv E[g(X)^2] - E[g(X)]^2$.

2.1.2 Frequentist vs. bayesian approach

2.1.3 Estimators and Fisher information

Let us suppose that the data sample has encoded some wanted parameters $\mathbf{a} \equiv (a_1, a_2, \dots)$. The underlying probability, in general also unknown, may be conditioned by the real values of the wanted parameters \mathbf{a} . The probability of the data sample is therefore written as

$$\Pr(\mathbf{X} = \mathbf{x}|\mathbf{a}), \quad (2.9)$$

where " $|\mathbf{a}$ " indicates its dependency on these parameters. At this point, notice that an estimate of the the wanted parameter based on the data sample has the form of a function the random variables. Therefore as mentioned before, an estimator of a , which is how is called this quantity and is denoted by \hat{a} , is another random variable with a PDF of the form of

$$\Pr(\hat{a}|\mathbf{a}) d\hat{a} = \Pr(\mathbf{X} = \mathbf{x}|\mathbf{a}) dx_1 dx_2 \dots dx_N. \quad (2.10)$$

For short, we omit on writing \mathbf{X} from now on, thus the conditional joint probability of N random variables is written as $\Pr(\mathbf{x}|\mathbf{a})$.

As we said, an estimator is defined to be a function of the data sample. For example, one of such estimators is the estimator of the mean value of the data population, in general unknown. The mean value of the data population, which in general we do not have access to, is denoted usually by μ . Notice that μ is in general different from the mean value of the data sample \bar{x} . A valid estimator for the population mean value would be the arithmetic mean of the data sample, i.e., $\hat{\mu} = \bar{x}$.

An important notion of an estimator is its *efficiency*, i.e., whether it has smaller variance than another. The more efficient estimator the smaller variance it has. Remember than an estimator is a random variable so it must have a variance that comes from the data population, i.e., from $\Pr(\hat{a}|\mathbf{a})$ in this case.

For an estimator of any kind there is a theoretical lower bound for its variance. For the proof of the previous observation, which we compute for continuous random variables without losing of generality, we start with the normalization of the PDF

$$\int \Pr(\mathbf{x}|\mathbf{a}) d^N \mathbf{x} = 1. \quad (2.11)$$

Next, we compute the partial derivative over a such that

$$\int \partial_a \Pr(\mathbf{x}|\mathbf{a}) d^N \mathbf{x} = \int \partial_a (\ln \Pr(\mathbf{x}|\mathbf{a})) \Pr(\mathbf{x}|\mathbf{a}) d^N \mathbf{x} = 0, \quad (2.12)$$

where for simplification, we omit the arguments of the joint probability on the second equality. From Eq. (??), it turns out that the Eq. (??) is the expectation value of $\partial_a(\ln \Pr)$. Finally if we have an unbiased estimator, for which the true value a coincides with the expectation value of the estimator $E[\hat{a}]$, its partial differentiation over a must be equal to one,

$$\partial_a E[\hat{a}] = \partial_a a = 1, \quad (2.13)$$

$$\begin{aligned} 1 &= \partial_a \int \hat{a} \Pr(\mathbf{x}|\mathbf{a}) d^N \mathbf{x} \\ &= \int \hat{a} \partial_a \Pr(\mathbf{x}|\mathbf{a}) d^N \mathbf{x} = \int \hat{a} \partial_a (\ln \Pr(\mathbf{x}|\mathbf{a})) \Pr(\mathbf{x}|\mathbf{a}) d^N \mathbf{x}, \end{aligned} \quad (2.14)$$

where we apply the definition of the expectation value of the estimator \hat{a} for continuous variables and we apply as well similar identities as in Eq. (??).

At this point we invoke the Schwartz inequality for two real multidimensional functions $g(\mathbf{x})$ and $h(\mathbf{x})$ such that $(\int gh d^N \mathbf{x})^2 \leq (\int g^2 d^N \mathbf{x})(\int h^2 d^N \mathbf{x})$. With this we can follow the following recipe to obtain a lower bound for the variance of a general estimator. First the definition of the variance looks like

$$V[\hat{a}] = E[(\hat{a} - a)^2] = \int (\hat{a} - a)^2 \Pr(\mathbf{x}|\mathbf{a}) d^N \mathbf{x}. \quad (2.15)$$

Second, from Eqs. (??) holds that

$$\int (\hat{a} - a) \partial_a (\ln \Pr(\mathbf{x}|\mathbf{a})) \Pr(\mathbf{x}|\mathbf{a}) d^N \mathbf{x} = 1 \quad (2.16)$$

because a is not a function of \mathbf{x} . Hence, using the Schwartz inequality we can write

$$V[\hat{a}] = \int (\hat{a} - a)^2 \Pr(\mathbf{x}|\mathbf{a}) d^N \mathbf{x} \geq \frac{1}{\int [\partial_a (\ln \Pr(\mathbf{x}|\mathbf{a}))]^2 \Pr(\mathbf{x}|\mathbf{a}) d^N \mathbf{x}}, \quad (2.17)$$

which is also known as the Cramér-Rao bound or the Fisher inequality. The denominator on the right hand-side is called generally the Fisher information (FI).

With this review of the most interesting features of "classical" metrology, from the point of view of this thesis, we conclude this section. In the next section, we will record some properties of the Quantum Mechanics and then we will follow with another s with the basis of Quantum Metrology.

2.2 Quantum Mechanics from metrology perspective

The ubiquitous probabilistic nature of Quantum Mechanics forces us to use probabilities on a regular basis. Moreover, if one works on fields connected with experiments or some sort of physical realizations this probabilistic nature of Quantum Mechanics is enhanced. On the other hand, exotic features such as entanglement arise from Quantum Mechanics, which give us unique opportunities to exploit them as resources. The present section is intended to describe these quantum phenomena in more or less detail.

2.2.1 The quantum state, multiparticle state, entanglement

A formal mathematical description of the quantum state is given next. This also allows us to introduce some notation used through the thesis. A *state* in Quantum Mechanics lives on a Hilbert space, \mathcal{H} . The system state, ρ , has the following properties:

- i) It is Hermitian, so it is invariant under the complex transposition, $\rho = \rho^\dagger$ and all its eigenvalues are real.
- ii) Its trace is equal to one, $\text{tr}(\rho) = 1$.
- iii) It is positive semi-definite, i.e, all its eigenvalues are bigger or equal to zero, $\rho = \sum_\lambda p_\lambda \Pi_\lambda$ where $p_\lambda \geq 0$ and $\Pi_\lambda \equiv |\lambda\rangle\langle\lambda|$ is the projector of the eigenstate $|\lambda\rangle$. From (ii), it follows that $\sum_\lambda p_\lambda = 1$.
- iv) If all p_λ are zero except one, the state is called a pure state and is equivalent to the projector of such eigenstate $\rho = \Pi_\lambda \equiv |\lambda\rangle\langle\lambda|$, where $|\lambda\rangle$ denotes a pure *vector* state.
- v) It follows that the quantum states form a convex set where the extreme points are pure states.

The composite system of N different parties live in the Hilbert space $\mathcal{H} = \mathcal{H}^{(1)} \otimes \mathcal{H}^{(2)} \otimes \dots \otimes \mathcal{H}^{(N)}$ or for short $\mathcal{H} = \bigotimes_{i=1}^N \mathcal{H}^{(i)}$, where \otimes stands for tensor product. For instance, this composite Hilbert space could be used to represent a many-particle system, in this case N particles. A *separable* state in this Hilbert space can be described by

$$\rho_{\text{sep}} = \sum_i p_i \rho_i^{(1)} \otimes \rho_i^{(2)} \otimes \dots \otimes \rho_i^{(N)}, \quad (2.18)$$

where p_i are convex weights that sum to one and are equal or bigger than zero. If not the state is said to be *entangled*. We mention it as a formal description of the entanglement []. One may notice at this moment, that relaxing the requirements of Eq. (2.18), one can lead to different classifications of the states. Concepts like genuine multipartite entanglement, k -producible states, or entanglement depth, among others, arose from weakly constrain the Eq. (2.18) [].

It is important to remark one of such classifications in order to characterize the different levels or multipartite entanglement followed in this work. We call a state k -producible, if it *can* be written as a mixture of the tensor product of different multiparticle states with at most k particles,

$$\rho_{k\text{-pro}} = \sum_i p_i \rho_i^{(\alpha, \dots, \beta)} \otimes \rho_i^{(\gamma, \dots, \delta)} \otimes \dots, \quad (2.19)$$

where superscript indexes between parenthesis go from 1 to N and denote to which parties belong the state, and where each index appears once in each sum element. If a state cannot be written as k -producible, then it must be $(k+1)$ -entangled. This defines the entanglement depth. Later on those concepts will arise on the metrology framework [].

Besides those concepts, we present a set of operators that will appear many times in all chapters, namely the angular momentum operators. Again those definitions allow us to introduce notation used on this book. For a single party with discrete d levels and therefore $s = (d-1)/2$, the eigenvalue equation for the angular momentum projection operators are

$$j_l^{(n)} |m\rangle_l^{(n)} = m |m\rangle_l^{(n)} \quad (2.20)$$

for $m = -s, \dots, +s$, where $l = x, y, z$ and where it is usual to omit the subscript and superscript, l and (n) respectively, for simplicity. The square of the total angular momentum, $j^2 = j_x^2 + j_y^2 + j_z^2$, for a single party is simply

$$(j^2)^{(n)} \rho^{(n)} = s(s+1) \rho^{(n)}, \quad (2.21)$$

where $\rho^{(n)}$ is an arbitrary pure or mixed state defined on the $\mathcal{H}^{(n)}$ Hilbert space.

The collective angular momentum projection operators are defined as the sum of their respective single-party spin operators such that they are extended to the rest of the Hilbert spaces by tensor products of the identity operators defined for the rest of subspaces,

$$J_l = \sum_{i=1}^N \mathbb{I}^{(1, \dots, i-1)} \otimes j_l^{(i)} \otimes \mathbb{I}^{(i+1, \dots, N)} \equiv \sum_{i=1}^1 j_l^{(i)}, \quad (2.22)$$

where \mathbb{I} stand for the identity operator and the last formula is the most used since it is easy to notice that the single subspace operator must extended in each case. The square of the angular momentum projections of a many-particle system is not equal to the sum of the square angular momentum

projection of each of the parties and it is obtained by

$$J_l^2 = \sum_{i,j}^N j_l^{(i)} j_l^{(j)} = \sum_{i=1}^N (j_l^2)^{(i)} + \sum_{i \neq j}^N j_l^{(i)} j_l^{(j)}. \quad (2.23)$$

Therefore, the total square angular momentum is neither the sum of all single-party square angular momentum and is computed by

$$J_l^2 = \sum_{i,j}^N j_l^{(i)} j_l^{(j)} = \sum_{i=1}^N (j_l^2)^{(i)} + \sum_{i \neq j}^N j_l^{(i)} j_l^{(j)}, \quad (2.24)$$

where we separated the sum into two pieces, the first corresponds to the sum of all single party angular momentum projections squared and the second corresponds to the product of angular momentum projection operators of two distinct subsystems. Many more combinations of these single-party operators may arise on different contexts. In the Appendix ??, we discuss in more detail the different structures that arise from adding the angular momentum operators, e.g., the symmetric subspace or the fixed total angular momentum subspace.

Evolution:

- Markov
- Limblad

Measurements:

- POVMs

Quantum Information:

2.3 Quantum Metrology

We summarize important recent advances in Quantum Metrology Simple metrological setups allow for encoding some wanted parameter into the state of the system, thus from the readout of the final state one can infer on it. The estimation theory applied to the intrinsic probabilistic nature of quantum states has lead to the the formulation of Quantum Metrology. Merging the probabilistic features of quantum mechanics and the estimation theory is not trivial. Nevertheless, starting from the pioneering works of Wotters, Braunstein and others back in 19XX [], until the works of Giovannetti et al, Paris and others roughly 20 years later [], the field of Quantum Metrology has been stabilized with solid foundations. Later, advanced works in Quantum Metrology appeared [] together with experimental

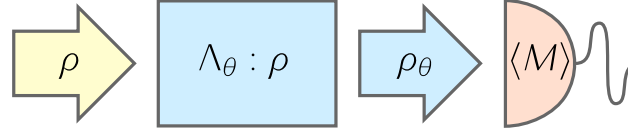


Figure 2.1: Sequence of the different steps for the basics of the estimation process on Quantum Metrology. First, an input state ρ enters the region on which the unknown parameter θ is imprinted on it, for the most general case, represented with Λ_θ . Last, the state that has encoded the parameter θ on it is measured and θ must be inferred from the measured quantity $\langle M \rangle$.

realizations [] which raised the interest in this topic. In this section, we will highlight the most important aspects of this field and with this we will conclude this introductory chapter.

The most basic scheme for a the metrological setup in this context is the following. First, a state is prepared followed by the evolution in which the unknown parameter θ is imprinted into the state. Finally, the outgoing state is characterized by some measurement M which allows to infer in the value of the parameter θ . The details of the evolution, the initial state and the post-characterization using M or a set of different measurements, is crucial for succeed. Figure ?? illustrates the main steps of Quantum Metrology.

In the many-particle case, most of the metrology experiments have been done in systems with simple Hamiltonians that do not contain interaction terms. Such Hamiltonians cannot create entanglement between the particles. A typical situation, is that we rotate our many particle state by some angle and we want to estimate the rotation angle θ . It has been shown that particles exhibiting quantum correlations, or more precisely, quantum entanglement [1, 2], provide a higher precision than an ensemble of not entangled particles. The most important question is how the achievable precision of the angle estimation $(\Delta\theta)^2$ scales with the number of particles. Very general derivations lead to, at best,

$$(\Delta\theta)^2 \sim \frac{1}{N} \quad (2.25)$$

for nonentangled particles. The equation above takes the name *shot-noise scaling* (SNS), the term originating from the shot-noise in electronic circuits, which is due to the discrete nature of the electric charge. On the other hand, quantum entanglement makes it possible to reach

$$(\Delta\theta)^2 \sim \frac{1}{N^2} \quad (2.26)$$

which is called the *Heisenberg scaling* (HS). Notethat if the Hamiltonian of the dynamics has interaction terms, then these bounds can be surpassed [2–8].

It is time to mention that the above calculations have been carried out for an ideal situation. When

an uncorrelated noise is present in the system, it turns out that for large enough particle number the scaling becomes a SNS []. The possible survival of a better scaling under correlated noise, under particular circumstances, or depending on some interpretation of the metrological task, is at the center of attention currently. All these are strongly connected to the question of whether strong multipartite entanglement can survive in a noisy environment.

Finally, note that often, instead of $(\Delta\theta)^2$ one calculates its inverse, which is large for high precision. It scales as $\sim N$ for SNS and as $\sim N^2$ for the HS.

2.3.1 Quantum Magnetometry

Without loss of generality, we present in this section the characterization of the precision of one of the simplest metrological task, namely the estimation of a homogeneous magnetic field based in the interaction between the system and the field. In this section, we will mostly study the interaction of a system with a homogeneous field in the z -direction. In the Chapter 5, we will show a different situation on which the magnetic field changes linearly with the position of the system. With the aim of estimating the strength of the magnetic field, a probe state is used in order to interact with it, coupling the magnetic moment of the state and the external magnetic field. Finally, measuring how the state has changed one could in principle infer on the strength of the magnetic field.

In general, we will say that the magnetic moments of the states come exclusively from the spin angular momentum, neglecting any possible contribution from the orbital angular momentum. This way the physics is simpler. This is justified in the sense that most of the recent experiments on this context have been carried out with ion-traps, BECs or at most cold atomic ensembles, which have indeed a negligible orbital angular momentum.

Beside this considerations, the interaction Hamiltonian can be written as,

$$H = -\boldsymbol{\mu} \cdot \mathbf{B} \quad (2.27)$$

up to some constant factor. Now in the simplest case we will choose the magnetic field to be pointing to some fixed direction, for instance, the z -direction. So the magnetic field vector can be written as $\mathbf{B} = B\mathbf{k}$, where \mathbf{k} is the unitary vector pointing to the z -direction. This way estimation problem is much more simple, since one has not to determine the direction of the magnetic field.

The magnetic moment of the system is proportional to the spin angular momentum, $\boldsymbol{\mu} = -\mu_B g_s \hbar^{-1} \mathbf{J}$, where μ_B and g_s are the Bohr magneton and anomalous gyromagnetic factor respectively. Finally,

one can rewrite the interaction Hamiltonian as,

$$H = \gamma B J_z \quad (2.28)$$

where $\gamma = \mu_B g_s \hbar^{-1}$ and we have used the fact that $\mathbf{J} \cdot \mathbf{k} = J_z$. Finally, the unitary operator leading the evolution of the system can be written as,

$$U = \exp(-i\theta J_z), \quad (2.29)$$

where the magnetic field strength is encoded into the phase-shift $\theta = -\mu_B g_s t B / \hbar$. Here μ_B stand for the Magneton of Bhor and g_s for the giro-magnetic constant for the spin angular momentum, and t is the time spent on the evolution.

We center our attention into multi-partite systems of spin- $\frac{1}{2}$ particles, widely known in the field as qubits. For large particle ensembles, typically only collective quantities can be measured in order to characterize the state and read the outgoing system. Such collective quantities are in this case the angular momentum components defined in Eq. (??) and their combinations. More concretelly, we can measure the expectation values of any

$$J_{\mathbf{n}} := \sum_{l=x,y,z} n_l J_l, \quad (2.30)$$

where $\mathbf{n} = (n_x, n_y, n_z)$ is a unit vector describing the direction of the component.

In order to estimate the phase-shift θ we measure the expectation value of a Hermitian operator, which we will denote here by M in the following. If the evolution time is a constant then estimating θ is equivalent to estimating the magnetic field strength B in Eq. (2.28). The precision of the estimation can be characterized with the error propagation formula as

$$(\Delta\theta)^2 = \frac{(\Delta M)^2}{|\partial_\theta \langle M \rangle|^2}, \quad (2.31)$$

where $\langle M \rangle$ is the expectation value of the operator M , and we used the assumption that the PDF describing the state in order to infer into the expectation value of M from the data sample, is enough to transform $\Pr(M = m|\theta)$ into a PDF as a function of the estimator $\Pr(\hat{\theta}|\theta)$, see the Section ???. Thus, the precision of the estimate depends on how sensitive $\langle M \rangle$ is to the change of θ , and also on how large the variance of M is. Based on the formula Eq. (2.31), one can see that the larger the slope $|\partial_\theta \langle M \rangle|$, the higher the precision. On the other hand, the larger the variance $(\Delta M)^2$, the lower the precision. Figure ?? helps to interpret the quantities appearing in Eq. (2.31).

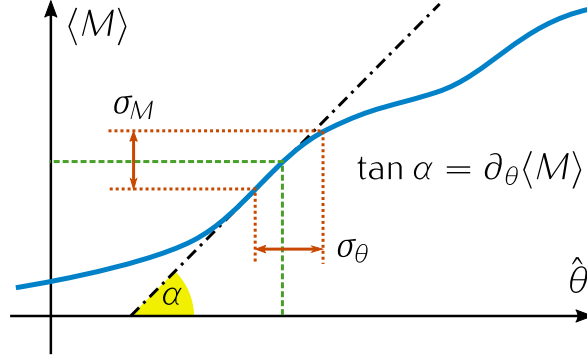


Figure 2.2: (Blue solid) Functional relation between the expectation value $\langle M \rangle$ and the estimator of the wanted parameter $\hat{\theta}$. (Green dashed) One to one correspondence when the estimator $\hat{\theta}$ is based on $\langle M \rangle$. (Red dotted) Obtaining the error of the estimate is based on Eq. (2.31). The slope of the curve at that point, denoted with $\tan \alpha$, directly relates the uncertainty on the measured quantity $\langle M \rangle$ and the error on the estimation σ_θ .

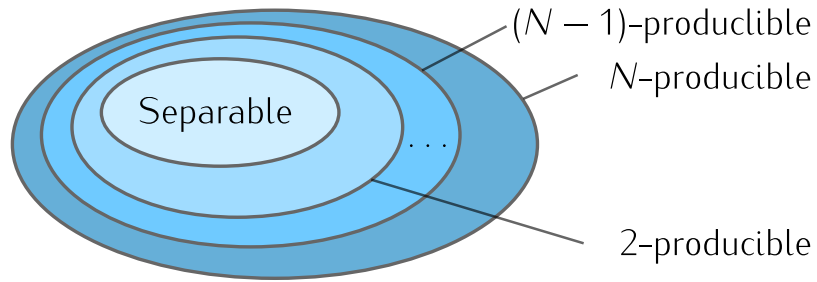


Figure 2.3

$$\mathcal{F}_Q[\rho, J_z] \geq \frac{\langle J_y \rangle^2}{(\Delta J_x)^2} \quad (2.32)$$

3

Metrology in the vicinity of Dicke states

"An experimentalist should not be unduly inhibited by theoretical untidiness"

Robert H. Dicke

In this chapter we will present recent results regarding the metrological usefulness of a family of unpolarised states. Such states can be used as probe states to estimate the homogeneous magnetic field strength, see Section 2.3.1 for references about magnetometry. It turns out that the unpolarised states are the most adequate states to beat the Heisenberg limit, as it was shown on the Section ???. Prime examples of such states are Greenberger–Horne–Zelinger (GHZ) states [9], which have already been realized experimentally many times [10? ? –15]. Hence, these states have attracted the interest of the community.

One of the figures of merit of this such unpolarized, but still useful states is the so-called unpolarized Dicke state [], which consists of, on its z -axis representation, an equal number of qubits pointing up and pointing down while the whole state is at the symmetric subspace. It can be written as follows,

$$|D_{N,N/2}\rangle \equiv |D_N\rangle := \left(\frac{N}{N/2}\right)^{-\frac{1}{2}} \sum_{k \in \sigma_s} \mathcal{P}_k (|1\rangle^{\otimes N/2} |0\rangle^{\otimes N/2}), \quad (3.1)$$

where k are elements of the set of all possible unique permutations of N elements of 2 kinds, σ_s . Such state is known to be highly entangled [] and to reach Heisenberg scaling when used for magnetometry.

For these and other reasons unpolarised Dicke states have been created in photonic systems [], in cold-gases [] and recently in trapped ions [].

One of the most particular features this state has is that since it is a eigenstate of the collective operator J_z with corresponding eigenvalue equal to zero. At the same time, it lives on the subspace where the collective total spin is maximum, i.e, $\langle J^2 \rangle = N(N+2)/4$. With this together with the fact that the state is unpolarised, it turns that it must have a very large uncertainty for the collective spin operators perpendicular to J_z , namely J_x and J_y .

Those properties attracted our attention to those states since the quantum Fisher information, used to characterize the metrological usefulness, is the convex-roof of $4(\Delta J_n)^2$, where \mathbf{n} is the unitary vector pointing in the direction of the magnetic field.

In this chapter, we characterize the metrological usefulness of noisy unpolarized Dicke states with only few collective measurements of the total spin of the ensemble, without the need for the direct measurement of the sensitivity. We also apply our method to recent experimental results with Dicke states.

3.1 Unpolarised states for magnetometry

Having unpolarised states for magnetometry has been shown useful in Section XX. While the quantum Fisher information would give directly the performance one state would have, this is not feasible in general because a complete knowledge of the state is needed to compute such value. On the other hand, we can use the error propagation formula Equation (XX) to obtain a bound on the precision. As one can see on the Figure 3.1 a pure Dicke state is rotated along the z-axis. Say that in this case the initial state is an unpolarised Dicke state of aligned with the x-axis.

The state initially is an eigenstate of the J_x^k operators for $\forall k \in [1, \infty]$. Another feature of the sequence is that $\langle J_l \rangle = 0$ for $\forall l \in x, y, z$. It turns out that measuring the evolution of the second statistical moment of J_x is one of the ways to go. It will start having value equal to zero for the pure unpolarized Dicke state, and rapidly will increase its value as it can be seen on the Figure 3.1. Another heuristic observation is that for $\Theta = \pi/2$ the value of $\langle J_x^2 \rangle$ will be at its maximum been it proportional to $\langle J^2 \rangle$ so to N^2 . Hence, the change on the second moment over the phase shift must be in this case proportional to N^2 . From this and for those states, we lead to the conclusion that one only needs to measure the second moment of the collective spin J_x to observe precisions that scale with the Heisenberg limit. In the following equation we show the error propagation formula that will

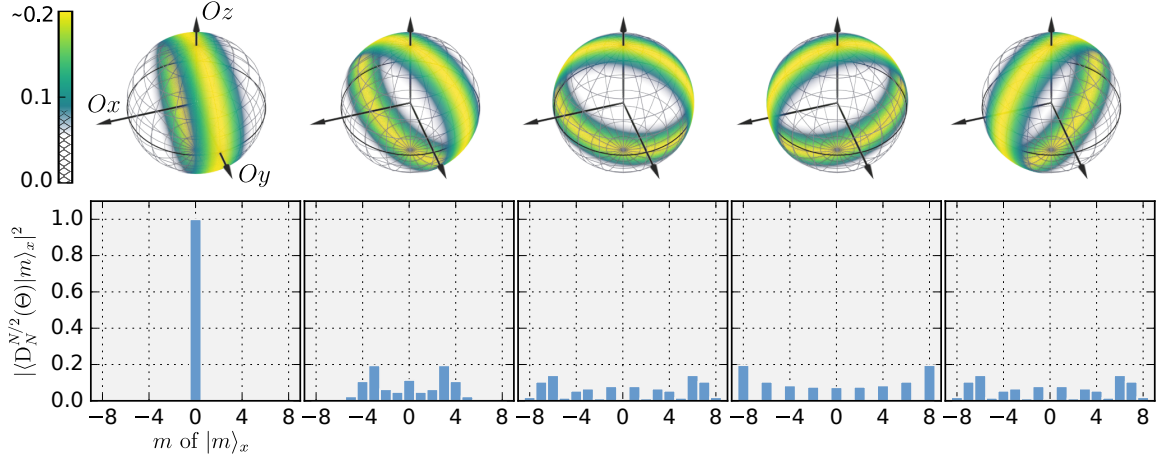


Figure 3.1: Sequence of the evolution of an unpolarized Dicke state of 16 qubits for $\Theta = \{i\pi/6\}_{i=0}^4$. Bloch spheres representing the Husimi quasi-probabilistic distribution of the state, and below PDF of the J_x POVM for each step of the sequence

give us the obtained precision,

$$(\Delta\Theta)^2 = \frac{(\Delta J_x^2)^2}{|\partial_\Theta \langle J_x \rangle|^2}. \quad (3.2)$$

3.2 Evolution of the expectation values

With the aim of computing the precision, Equation (3.2), we will compute the dependence on Θ of the expectation value of the operator J_x and higher order moments. For that first of all we will move onto the Heisenberg picture where the operators evolve in time while the state remains the same. The operator J_x can be written as a function of Θ the following way,

$$J_x(\Theta) = e^{i\Theta J_z} J_x(0) e^{-i\Theta J_z} = J_x(0) c_\Theta - J_y(0) s_\Theta, \quad (3.3)$$

where $J_l(0)$ for $\forall l$ are the collective angular momentum operators at time equal zero, which we will write them simply J_l from now on, and c_Θ and s_Θ are the trigonometric functions introduced on the first chapter.

We need to compute the second and the fourth moments of J_x as it is required by the Equation (3.2). But before any calculation we will make a simplifying assumption which turn to be well supported on the most common situations. The assumption is that both expectation values are even functions on

Θ ,

$$\begin{aligned}\langle J_x^2(\Theta) \rangle &= \langle J_x^2(-\Theta) \rangle, \\ \langle J_x^4(\Theta) \rangle &= \langle J_x^4(-\Theta) \rangle.\end{aligned}\tag{3.4}$$

The square of J_x in the Heisenberg picture is written as follows,

$$J_x^2(\Theta) = J_x^2 c_\Theta^2 + J_y^2 s_\Theta^2 - (J_x J_y + J_y J_x) c_\Theta s_\Theta.\tag{3.5}$$

From the equation above and to fulfill the first constraint on the Equation (3.4) it turns out that the expectation value over our yet to be shown initial state of the operator $(J_x J_y + J_y J_x)$ must vanish. Hence it is equivalent to the first assumption of the Equation (3.4) write that

$$\langle \{J_x, J_y\} \rangle = 0\tag{3.6}$$

where $\{ , \}$ stands for the anticommutator. Apart for been simpler to compute the Equation (3.6) is based also on initial expectation values of the state. We will see that as we said before this is easily guarantied for most important cases.

As we have done recently with the square of J_x now we will do it for J_x^4 . This way one will be able to distinguish which other combination of operators must vanish in order to have Equation (3.4) guarantied. The fourth power of J_x can be written as follows in the Heisenberg picture,

$$\begin{aligned}J_x^4(\Theta) &= J_x^4 c_\Theta^4 + J_y^4 s_\Theta^4 + (J_x^2 J_y^2 + J_x J_y J_x J_y + J_x J_y^2 J_x + J_y J_x J_y J_x + J_y J_x^2 J_y + J_y^2 J_x^2) c_\Theta^2 s_\Theta^2 \\ &\quad - (J_x^3 J_y + J_x^2 J_y J_x + J_x J_y J_x^2 + J_y J_x^3) c_\Theta^3 s_\Theta - (J_x J_y^3 + J_y J_x J_y^2 + J_y^2 J_x J_y + J_y^3 J_x) c_\Theta s_\Theta^3.\end{aligned}\tag{3.7}$$

And again assuming that its expectation value must be an even function on Θ it turns out that the second line must be equal to zero when the expectation value is considered. So $(J_x^3 J_y + J_x^2 J_y J_x + J_x J_y J_x^2 + J_y J_x^3)$ and $(J_x J_y^3 + J_y J_x J_y^2 + J_y^2 J_x J_y + J_y^3 J_x)$ must vanish again over any candidate state to be used as prove state. Hence, the second constraint of the Equation (3.4) can be rewritten as follows,

$$\begin{aligned}\langle \{J_x^2, \{J_x, J_y\}\} \rangle &= 0, \\ \langle \{J_y^2, \{J_x, J_y\}\} \rangle &= 0.\end{aligned}\tag{3.8}$$

Finally, we can write how the evolution of second and fourth moments of the J_x operator must

look like,

$$\langle J_x^2(\Theta) \rangle = \langle J_x^2 \rangle c_\Theta^2 + \langle J_y^2 \rangle s_\Theta^2 \quad (3.9)$$

$$\begin{aligned} \langle J_x^4(\Theta) \rangle &= \langle J_x^4 \rangle c_\Theta^4 + \langle J_y^4 \rangle s_\Theta^4 \\ &\quad + \langle \{J_x^2, J_y^2\} + \{J_x, J_y\}^2 \rangle c_\Theta^2 s_\Theta^2. \end{aligned} \quad (3.10)$$

From here we are able to write the evolution of the variance of the second moment when Equation (3.4) must be obeyed. We obtain

$$\begin{aligned} (\Delta J_x^2(\Theta))^2 &= \langle J_x^4(\Theta) \rangle - \langle J_x^2(\Theta) \rangle^2 \\ &= \langle J_x^4 \rangle c_\Theta^4 + \langle J_y^4 \rangle s_\Theta^4 + \langle \{J_x^2, J_y^2\} + \{J_x, J_y\}^2 \rangle c_\Theta^2 s_\Theta^2 - (\langle J_x^2 \rangle c_\Theta^2 + \langle J_y^2 \rangle s_\Theta^2)^2 \\ &= (\langle J_x^4 \rangle - \langle J_x^2 \rangle^2) c_\Theta^4 + (\langle J_y^4 \rangle - \langle J_y^2 \rangle^2) s_\Theta^4 + (\langle \{J_x^2, J_y^2\} + \{J_x, J_y\}^2 \rangle - 2\langle J_x^2 \rangle \langle J_y^2 \rangle) c_\Theta^2 s_\Theta^2 \\ &= (\Delta J_x^2)^2 c_\Theta^4 + (\Delta J_y^2)^2 s_\Theta^4 + (\langle \{J_x^2, J_y^2\} + \{J_x, J_y\}^2 \rangle - 2\langle J_x^2 \rangle \langle J_y^2 \rangle) c_\Theta^2 s_\Theta^2. \end{aligned} \quad (3.11)$$

The remaining constituent of the Equation (3.2) on which we will base our result for the precision, is the modulus square of the derivative of the second moment of the J_x operator. Using Equation (3.9) for the expression of the evolution of the second moment, the denominator of Equation (3.2) follows

$$\begin{aligned} |\partial_\Theta \langle J_x^2(\Theta) \rangle|^2 &= |-2\langle J_x^2 \rangle c_\Theta s_\Theta + 2\langle J_y^2 \rangle c_\Theta s_\Theta|^2 \\ &= 4\langle J_y^2 - J_x^2 \rangle^2 c_\Theta^2 s_\Theta^2. \end{aligned} \quad (3.12)$$

From the equations above directly follows expression for the precision of Θ ,

$$\begin{aligned} (\Delta\Theta)^2 &= \frac{(\Delta J_x^2)^2 c_\Theta^4 + (\Delta J_y^2)^2 s_\Theta^4 + (\langle \{J_x^2, J_y^2\} + \{J_x, J_y\}^2 \rangle - 2\langle J_x^2 \rangle \langle J_y^2 \rangle) c_\Theta^2 s_\Theta^2}{4\langle J_y^2 - J_x^2 \rangle^2 c_\Theta^2 s_\Theta^2} \\ &= \frac{(\Delta J_x^2)^2 t_\Theta^{-2} + (\Delta J_y^2)^2 t_\Theta^2 + \langle \{J_x^2, J_y^2\} + \{J_x, J_y\}^2 \rangle - 2\langle J_x^2 \rangle \langle J_y^2 \rangle}{4\langle J_y^2 - J_x^2 \rangle^2}. \end{aligned} \quad (3.13)$$

To this calculations further computations follows mainly regarding to the following expectation value $\langle \{J_x^2, J_y^2\} + \{J_x, J_y\}^2 \rangle$. This calculus is left for the Appendix A.1. Finally, the expression Equation (3.13) leads to the following,

$$(\Delta\Theta)^2 = \frac{(\Delta J_x^2)^2 t_\Theta^{-2} + (\Delta J_y^2)^2 t_\Theta^2 + 4\langle J_y^2 \rangle - 3\langle J_z^2 \rangle - 2\langle J_x^2 \rangle (1 + \langle J_y^2 \rangle) + 6\langle J_x J_y^2 J_x \rangle}{4\langle J_y^2 - J_x^2 \rangle^2} \quad (3.14)$$

[WOW IN THE PAPER FINALLY IT IS CORRECT!!]

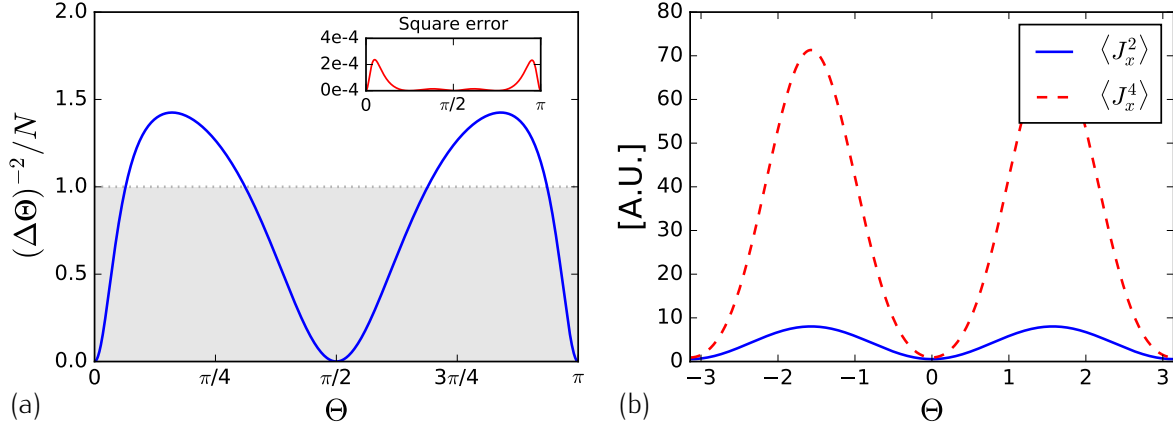


Figure 3.2: (a) Evolution of the precision for 6 qubits based on the simulation of the system and its expectation values. The agreement with the Equation [REF] is shown on the inset plot where the square of the difference between two approaches, the analytical and the simulation, is plotted. The difference is more or less two orders of magnitude below the actual value for the relevant points, which mainly comes because of the error coming from computing the derivative which has to be done approximately between two neighbor points. (b) Verification of the parity with respect to Θ of the expectation values of the second and the fourth moment, so to fulfill the constraint Equation [REF].

We have verified the correctness of our analytical formula with a direct numeric simulation of the Equation [ERROR PROP. FORM.] and the equation above. For that we, have used the ground-state of $H = J_x^2 + J_y$ for 6 qubits, $|\text{GS}\rangle$. This state in principle does not have extra symmetries where further simplifications would take part on the final expression of the formula, so is more adequate for testing. We have computed the evolution of the expectation values of the second and the fourth moments of the operator J_x in the range of half a cycle, i.e, $\Theta \in [0, \pi]$, for thousand of equidistant points. We choose so high density of points on the range in order to compute a more accurate derivative of the expectation value $\partial_\Theta \langle J_x^2 \rangle$ appearing on the Equation [EPF], see Figure [REF] (a). Finally, we have also checked that the constraints assumed at the beginning of this section are fulfilled. For that aim, the range of the evolution time has been $\Theta \in [-\pi, \pi]$ and we have computed the expectation values for five hundreds of equidistant points, see Figure [REF] (b). We can conclude saying that our formula exactly reproduces the evolution of the error propagation formula, Equation [REF].

3.2.1 The optimal precision

One can realize that the whole dependence on the phase shift is in the first two terms of the numerator. This way one can minimize the sum on the first two terms in order to find where the precision is best.

So it follows that,

$$\tan^2(\Theta_{\text{opt}}) = \sqrt{\frac{(\Delta J_x^2)^2}{(\Delta J_y^2)^2}} \quad (3.15)$$

which inserted on the Equation (3.14) gives us the optimal precision when the second moment $\langle J_x^2 \rangle$ is measured based on the initial expectation values of the input state. The optimal precision is written in the following way,

$$(\Delta\Theta)_{\text{opt}}^2 = \frac{\sqrt{(\Delta J_x^2)^2(\Delta J_y^2)^2} + 4\langle J_y^2 \rangle - 3\langle J_z^2 \rangle - 2\langle J_x^2 \rangle(1 + \langle J_y^2 \rangle) + 6\langle J_x J_y^2 J_x \rangle}{4\langle J_y^2 - J_x^2 \rangle^2}. \quad (3.16)$$

We conclude with this section checking our bound for the pure unpolarised Dicke state aligned with the x -axis, $|D_N\rangle_x$, whose precision bound is well known, Equation ([XXX]). With this aim we compute all the expectation values needed for the Equation (3.16) which almost all of them are trivial, $\langle J_x J_y^2 J_x \rangle = \langle J_x^4 \rangle = \langle J_x^2 \rangle = 0$. The rest are obtained in the following way,

$$\langle J_y^2 \rangle = \langle J_z^2 \rangle = \frac{N(N+2)}{8}, \quad (3.17)$$

$$\langle J_y^4 \rangle = \frac{N+2}{8} \left(\frac{3N(N+2)}{16} - \frac{1}{2} \right). \quad (3.18)$$

The Equation (3.17) follows directly from the fact that the state is invariant under rotations on the x -axis, so they are its expectation values, because the sum of all the second moments must give the value of the total angular momentum, in this case the maximum which is $\langle J^2 \rangle = \frac{N(N+2)}{4}$, and because $\langle J_x^2 \rangle = 0$. The proof of the Equation (3.18) needs more algebra and has been left for the Appendix ??.

From the equations above, one lead to the following expression for the precision of the phase shift for a pure unpolarised Dicke state,

$$(\Delta\Theta)^2 = \frac{2}{N(N+2)}, \quad (3.19)$$

which coincides exactly with the inverse quantum Fisher information for such state.

3.3 Testing the formula against some known states

In this section we will compare our criteria based on few expectation values against the corresponding quantum Fisher information obtained for some known input states. Those input states will be first the family of states defined as the ground states of the following Hamiltonian, called the spin-squeezing

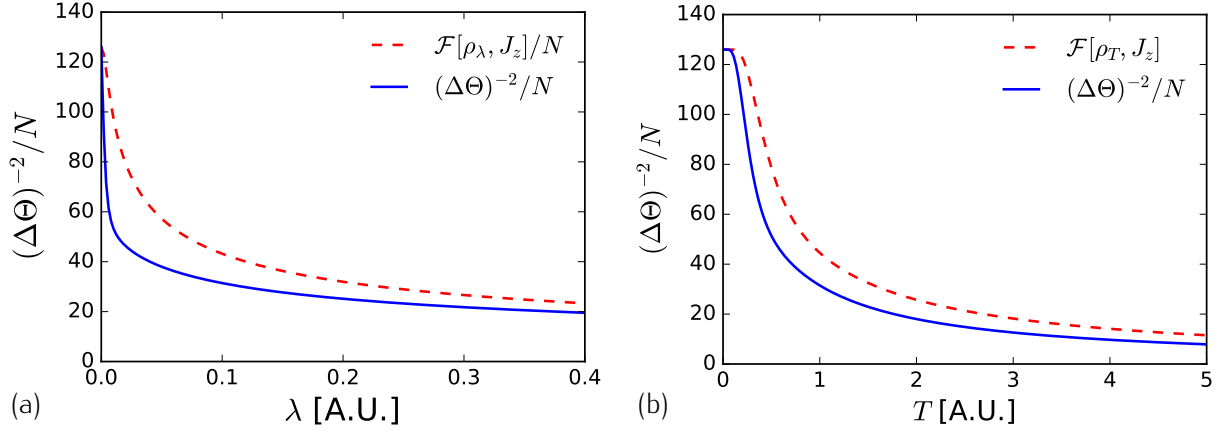


Figure 3.3: Comparison between our formula for the precision and the QFI for different states. (a) Comparison for ground states of H_λ . (b) Comparison with gaussian mixture of Dicke states.

Hamiltonian,

$$H_\lambda = J_x^2 - \lambda J_y. \quad (3.20)$$

For λ equal to zero we have the unpolarized Dicke state, Equation (3.1), and for λ large we recover the coherent totally polarized state pointing onto the y -direction. In the meantime the state is also a spin-squeezed state, therefore the name of the Hamiltonian. The ground state is defined such that

$$\lambda_{\min} = \text{tr}(H_\lambda \rho_\lambda), \quad (3.21)$$

where λ_{\min} is the lowest eigenvalue of H_λ . The state ρ_λ is invariant under permutations of the particles and it is also pure. Moreover the state ρ_λ is symmetric.

The second family of input states we are going to use are the Gaussian mixture of Dicke states around the unpolarized Dicke state, which have the following form as function of β ,

$$\rho_{(T)} \propto \sum_{m=-N/2}^{N/2} e^{-\frac{m^2}{T}} |D_N^m\rangle_x \langle D_N^m|_x. \quad (3.22)$$

After showing how the optimal precision formula behaves compared with the quantum Fisher information for those two families of states, we also have to prove that they indeed fulfill the constraints on Equation (3.4).

For the spin-squeezed state ρ_λ , we have that it is invariant under

On the other hand for the thermal state ρ_T , we have that it is invariant under rotations around

the x -axis

$$\rho_T = e^{-i\alpha J_x} \rho_T e^{i\alpha J_x}, \quad (3.23)$$

for arbitrary $\forall \alpha$.

$$\text{tr}(e^{i\Theta J_z} J_y^m e^{-i\Theta J_z} \rho_T) = \text{tr}(e^{i\Theta J_z} J_y^m e^{-i\Theta J_z} e^{-i\alpha J_x} \rho_T e^{i\alpha J_x}) \quad (3.24)$$

If we choose $\alpha = \pi$ then we rotate all the orthogonal angular momentum operators such that $J_y \rightarrow -J_x$ and $J_z \rightarrow -J_z$. Therefore, $e^{i\pi J_x} e^{i\Theta J_z} J_y^m e^{-i\Theta J_z} e^{-i\pi J_x} = e^{-i\Theta J_z} (-J_y)^m e^{i\Theta J_z}$. Hence, for even m and particularly for $m = 2, 4$ we have that,

$$\text{tr}(e^{i\Theta J_z} J_y^m e^{-i\Theta J_z} \rho_T) = \text{tr}(e^{-i\Theta J_z} J_y^m e^{i\Theta J_z} \rho_T), \quad (3.25)$$

so the Equation (XXX) is granted.

3.4 Using our method with real experimental data

On reference [XXX], it is produced on the laboratory a state with the proper characteristics of an unpolarised Dicke state, small variance on one of the directions and very large one on the perpendicular directions to this. It is also invariant under rotations around x -axis. Effectively, the state has the following form,

$$\rho = \frac{1}{2\pi} \int e^{-i\alpha J_x} \rho_0 e^{i\alpha J_x}, \quad (3.26)$$

where ρ_0 is what we would obtain if we would have access to the phase reference. Hence we have that at $\Theta = 0$ all the statistical moments $\langle J_z^m \rangle = \langle J_y^m \rangle$ are equal.

Simplification of our precision formula on Equation (XXX). First, we simplify the expectation value $\langle J_x J_z^2 J_x \rangle$ in the following way,

$$\begin{aligned} \langle J_x J_z^2 J_x \rangle &= \frac{\langle J_x (J_y^2 + J_z^2) J_x \rangle}{2} = \frac{\langle J_x (J_x^2 + J_y^2 + J_z^2) J_x \rangle - \langle J_x^4 \rangle}{2} \\ &\leq \frac{N(N+2)}{8} \langle J_x^2 \rangle - \frac{\langle J_x^4 \rangle}{2}. \end{aligned} \quad (3.27)$$

Notice that obtaining $\langle J_x J_z^2 J_x \rangle$ is hard experimentally. This simplification can only make our estimation of the precision worse while for symmetric states the equality holds. The bound from below for the

precision can be writtes as,

$$(\Delta\Theta)_{\text{opt}}^2 \leq \frac{\sqrt{(\Delta J_x^2)^2(\Delta J_y^2)^2} + \langle J_y^2 \rangle + \frac{3N(N+2)-8}{4}\langle J_x^2 \rangle - 2\langle J_x^2 \rangle \langle J_y^2 \rangle - 3\langle J_x^4 \rangle}{4\langle J_y^2 - J_x^2 \rangle^2}, \quad (3.28)$$

where some terms were reordered and further simplified.

It is worth to study this case and apply our methods such that we can extract conclusions about the metrological usefulness of the state. The system in consideration is a $N = 7900$ particles system. The measured data for such system is

$$\begin{aligned} \langle J_x^2 \rangle &= 112 \pm 31, & \langle J_y^2 \rangle &= 6 \times 10^6 \pm 0.6 \times 10^6, \\ \langle J_x^4 \rangle &= 40 \times 10^3 \pm 22 \times 10^3, & \langle J_y^4 \rangle &= 6.2 \times 10^{13} \pm 0.8 \times 10^{13}. \end{aligned} \quad (3.29)$$

Hence we obtain the maximum precision,

$$\frac{(\Delta\Theta)_{\text{opt}}^{-2}}{N} \geq 3.7 \pm 1.5 \quad (3.30)$$

with boot straping methods. The direct substitution would yield to a 3.3 gain over the shot-noise limit.

Next we plot the value for the precision substituting directly the measured data into Equation (XXX), see Figure 3.4.

Further simplification of our method can be achieved for states of the kind of the one studied on this section. Based on $\langle AB \rangle \leq \lambda_{\max}(A)\langle B \rangle$ for two commuting positive-semidefinite observables,

$$\langle J_y^4 \rangle \leq \frac{N^2}{4} \langle J_x^2 \rangle. \quad (3.31)$$

We can also approximate $\langle J_x^4 \rangle$ with $\langle J_x^2 \rangle$ in the sense that it is small and that mainly its value comes from technical noise,

$$\langle J_x^4 \rangle \approx \beta \langle J_x^2 \rangle^2. \quad (3.32)$$

This approximation even if it is not a strict bound on the precision can be very useful in order to characterize the metrological usefulness of our input state based only on second statistical moments of only two angular momentum operators, namely $\langle J_z^2 \rangle$ and $\langle J_x^2 \rangle$. Those two expectation values are related with the width of our state and also with how thin we can do it in one of the directions, for metrological purposes, perpendicular to the magnetic field. So in this case we use $\beta = 3$ assuming

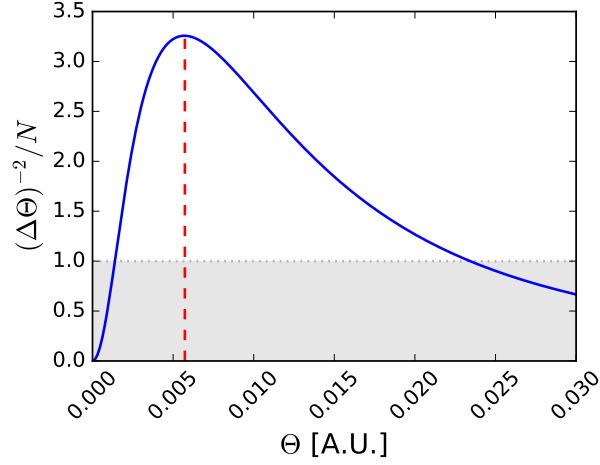


Figure 3.4: The (solid) line shows how the precision of Θ varies through the evolution. Notice that for the initial moment the precision is zero and that it reaches a maximum at $\Theta \approx 0.0057$ highlighted with the vertical (dashed) line. The gray area represent the region where the precision is below the shot-noise limit.

that the distribution function has Gaussian shape.

From these considerations we are able to write a second bound with fewer expectation values for the optimal precision such that,

$$(\Delta\Theta)_{\text{opt}}^2 \leq \frac{\langle J_y^2 \rangle + \frac{3N(N+2)-8}{4}\langle J_x^2 \rangle + \left(\sqrt{\frac{N^2}{2\langle J_y^2 \rangle} - 2} - 2 \right) \langle J_y^2 \rangle \langle J_x^2 \rangle - 9\langle J_x^2 \rangle^2}{4\langle J_y^2 - J_x^2 \rangle^2}. \quad (3.33)$$

We have used this formula to compute the bound on the optimal precision with the measured data shown on Equation (XXX), $(\Delta\Theta)_{\text{opt}}^{-2} \geq 2.9N$, see Figure 3.5.

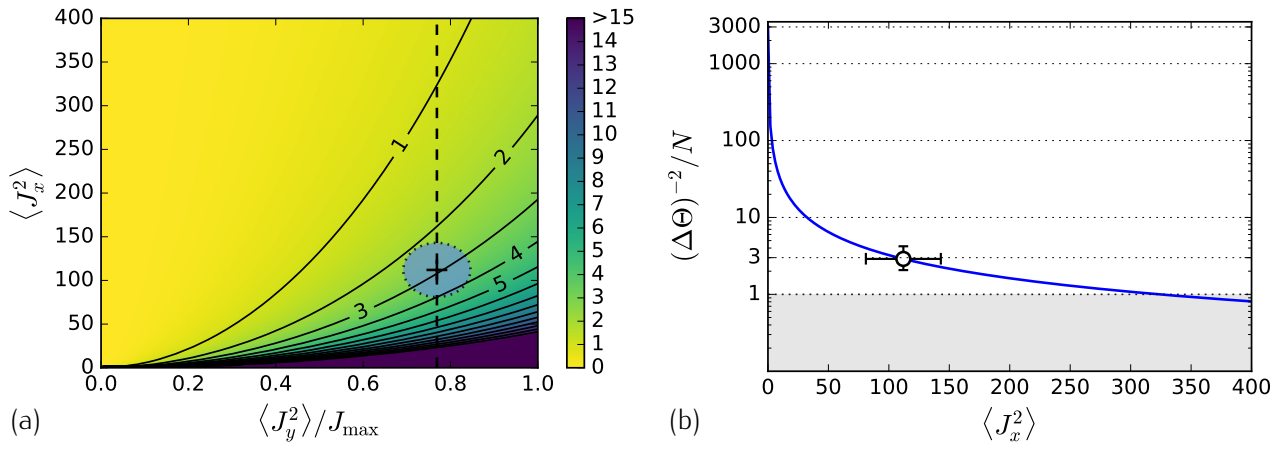


Figure 3.5: Comparison between our formula for the precision and the QFI for different states. a) Comparison for ground states of H_λ . (b) Comparison with gaussian mixture of Dicke states.

4

Witnessing metrologically useful entanglement

*"All the truths of mathematics are linked to each other,
and all means of discovering them are equally admissible."*
Adrien-Marie Legendre

TYPICALLY, one has not access to the density matrix of the system been used for metrology or for other quantum process. Moreover, for systems on which the particle number is very large, this is the case when one wants to do metrology with quantum states, the details of the density matrix are forbidden by practical reasons. Since the quantum Fisher information is based on the complete knowledge of the density matrix, shortcuts to avoid the complete tomography must be developed as we have had shown one practical case on the previous chapter. In this chapter, we obtain a general procedure to get an optimal bound for the quantum Fisher information based on as many expectation values of the initial state as one is ready to measure. Two main features are worth to mention again. First, in general this method gives us an optimal tight bound. Last but not least, the bound is based on the expectation values of the initial state only, so it is not necessary to perform an evolution of the state to estimate how well will it behave. This is in contrast to other approaches one can find in the literature, as it is a time saving concept.

The figure of merit of bounds from below for the quantum Fisher information based on expectation

values of the initial state is the following,

$$\mathcal{F}_Q[\rho, J_z] \geq \frac{\langle J_x \rangle^2}{(\Delta J_y)^2}. \quad (4.1)$$

where the state is polarized along the x -axis and the variance of the J_y operator is smaller than the standard. On the previous chapter we also have shown one of these bound specifically designed for unpolarized Dicke states.

Homogeneous magnetometry, $\mathbf{B} = B\mathbf{k}$ where B is constant in time.

Section [REF], see magnetometry, generator J_z .

Quantum Fisher information $\mathcal{F}_Q[\rho, J_z]$.

4.1 Bound from below of a function convex over the states given some arbitrary expectation values

The problem of getting a lower bound for a convex function on the states having already some expectation values of some arbitrary observables was studied by O. Ghne *et al.* and J. Eisert *et al.* in Refs. [16, 17] respectively, mainly from the perspective of entanglement measures. The illustrated techniques are based on the well known Legendre transform for differentiable functions, see Appedix B.3 for more details. We first review in this section the state-of-the-art solution for this problem. And later on, we extend it to the quantum Fisher information. For simplicity in the next subsection, Sec ??, we assume that a single expectation value is given. An extension to the case on which more expectation values are given will follow in the Subsection ??. Finally, we will summarize it with an explicit formula which will be used to compute the bounds.

4.1.1 Estimation of a general convex function based on the expectation value of an arbitrary observable

When a convex function $g(\rho)$ is given together with an expectation value of some operator $w = \text{tr}(\rho W)$, a tight lower bound, $\mathcal{B}_g(w)$, can be obtained as [16–18]

$$\begin{aligned} g(\rho) &\geq \mathcal{B}_g(w) := \sup_r \{rw - \hat{g}(rW)\} \\ &= \{\inf_{\rho} g(\rho) \mid w = \text{tr}(\rho W)\} \end{aligned} \quad (4.2)$$

where $\hat{g}(rW)$ is the Legendre transform of $g(\rho)$ and the second equality expresses the tightness of the bound. The Legendre transform in this context is defined as

$$\hat{g}(rW) = \sup_{\rho} \{ \langle rW \rangle_{\rho} - g(\rho) \}, \quad (4.3)$$

where the maximisation is over *all* possible states. This method to obtain the lower bound has been used to compute entanglement measures, as we mentioned before [].

Following the theory one can find that in the case on which the convex function $g(\rho)$ is defined as convex roof over all possible convex decompositions of the state, the optimisation of Eq. (4.3) can be reduced to an optimisation over pure states only, thus simplifying the process []

$$\begin{aligned} \hat{g}(rW) &= \sup_{\rho} \{ \langle rW \rangle_{\rho} - g(\rho) \} \\ &= \sup_{\rho} \left\{ r \langle W \rangle_{\rho} - \inf_{\{p_k, |\phi_k\rangle\}} \left\{ \sum_k p_k g(|\phi_k\rangle) \right\} \right\} \\ &= \sup_{\{p_k, |\phi_k\rangle\}} \left\{ \sum_k p_k \langle rW \rangle_{|\phi_k\rangle} - \inf_{\{p_k, |\phi_k\rangle\}} \left\{ \sum_k p_k g(|\phi_k\rangle) \right\} \right\} \\ &= \sup_{\{p_k, |\phi_k\rangle\}} \left\{ \sum_k p_k \{ \langle rW \rangle_{|\phi_k\rangle} - g(|\phi_k\rangle) \} \right\} \\ &= \sup_{|\psi\rangle} \{ \langle rW \rangle_{|\psi\rangle} - g(|\psi\rangle) \}. \end{aligned} \quad (4.4)$$

However, even an optimization over all pure states is feasible numerically only for small systems. We will show later on this section how to circumvent this issue in the case of the QFI. The convex roof construction has the following form

$$g(\rho) = \inf_{\{p_k, |\psi_k\rangle\}} \sum_k p_k g(|\psi_k\rangle), \quad (4.5)$$

where the mixed state is decomposed into $\rho = \sum_k p_k |\psi_k\rangle\langle\psi_k|$. Among other definitions of the QFI on the literature, there is one that defines it as the convex roof of $4(\Delta J_z)^2$, the variance of the generator, as it has been shown on Ref. [19?], we can compute the Legendre transform optimizing for pure states only. Hence, we will be able to use this simplification to apply this method to obtain the lower bound on the QFI. Notice that in this context the QFI is the convex roof of four times the variance of the generator, Eq. (??).

4.1.2 Measuring several observables

For some cases, it is interesting to characterise the quantum state not only with a single measurement but with several. For instance, we could want to use, as it is done with the spin-squeezed states the absolute polarisation and the variance of one of the orthogonal components of the angular momentum to detect entanglement and metrological usefulness []. So far, we studied the case on which a single measurement is used. Its extension to several expectation values is indeed straight-forward. We can generalize Eqs. (4.2) and (4.3) for several observables $\{W_i\}_{i=1}^M$ as follows [16]

$$\mathcal{B}_g(w_1, w_2, \dots) := \sup_r \{r\mathbf{w} - \sup_\rho \{\langle r\mathbf{W} \rangle - g(\rho)\}\}, \quad (4.6)$$

where $\mathbf{a}\mathbf{b} = \sum_{k=1}^M a_k b_k$, the usual notation for scalar products of two vectors.

4.1.3 Explicit form of the expression to be optimized

After we have shown how to find a lower bound for a general convex function of the state based on its expectation values and how to simplify that method for the case on which the function is defined as convex roof, now we are in a position to achieve the main goal of this chapter. First of all, we notice that for the quantum Fisher Information the inner maximization, the Legendre transform, is obtained optimizing a quadratic function on expectation values,

$$\begin{aligned} \hat{\mathcal{F}}_Q(rW) &= \sup_{|\psi\rangle} \{r\langle W \rangle_\psi - 4(\Delta J_z)_\psi^2\} \\ &= \sup_{|\psi\rangle} \{r\langle W \rangle_\psi - 4\langle J_z^2 \rangle_\psi + 4\langle J_z \rangle_\psi^2\} \\ &= \sup_{|\psi\rangle} \{\langle rW - 4J_z^2 \rangle_\psi + \langle 2J_z \rangle_\psi^2\}, \end{aligned} \quad (4.7)$$

where we have used the fact that the QFI can be expressed as convex roof of $(\Delta J_z)^2$ and we again fall into the problem of a single parameter for simplicity on the following derivations. Equation (4.7) can be rewritten as an optimization linear in operator expectation values and over a parameter μ as

$$\hat{\mathcal{F}}_Q(rW) = \sup_{|\psi\rangle, \mu} \{\langle rW - 4J_z^2 \rangle_\psi + 8\mu\langle J_z \rangle_\psi - 4\mu^2\mathbb{I}\}, \quad (4.8)$$

which, making use of $\max\{\langle A \rangle\} = \lambda_{\max}[A]$ for any observable, can be reformulated as

$$\begin{aligned}\hat{\mathcal{F}}_Q(rW) &= \sup_{|\psi\rangle} \left\{ \lambda_{\max}[rW - 4J_z^2 + 8\mu J_z - 4\mu^2] \right\} \\ &= \sup_{|\psi\rangle} \left\{ \lambda_{\max}[rW - 4(J_z - \mu)^2] \right\}\end{aligned}\tag{4.9}$$

where we omitted in writing \mathbb{I} for clarity and $\lambda_{\max}[A]$ stands for the maximum eigenvalue of the operator A . At the extremum, we make the following observation, the derivative with respect to μ must be zero, hence at the optimum $\mu = \langle J_z \rangle_{\text{opt}}$ which represents the expectation value J_z should have considering the optimal state on Eq. (4.7). This also means that we have to test μ values in the interval $-N/2 \leq \mu \leq N/2$ only for spin-half systems.

The full optimization problem to be solved consists of Eqs. (4.2) and (4.9) substituting $g(\rho)$ by $\mathcal{F}_Q[\rho, J_z]$,

$$\mathcal{B}_{\mathcal{F}}(w) = \sup_r \left\{ rw - \sup_{\mu} \left\{ \lambda_{\max}[rW - 4(J_z - \mu)^2] \right\} \right\}.\tag{4.10}$$

It is crucial that the optimization over r is a concave function, since the theory tells us that $\hat{\mathcal{F}}_Q(rW)$ is a convex function [], even when the multi-parametric case is considered. Thus the optimum can be determined easily with simple methods, e.g., the gradient method, looking for the maximum in r . Based on Eq. (4.2), we can see that even if we do not find the global optimum in r , we obtain a valid lower bound. The extension of this bound to the multi-parametric case is done using the recipe given in Eq. (4.6). On the other hand, the function to be optimized for μ does not have a single maximum in general. Moreover, not finding the optimal μ leads to an overestimating of the bound. Thus, a large care must be taken especially when optimizing over μ .

We stress again the generality of this findings beyond linear interferometers covered on the following sections. For nonlinear interferometers [], the phase Θ must be estimate in an unitary dynamics $U = \exp -iG\Theta$, where G is not a sum of single spin operators, hence, is different from the angular momentum components.

Next, we will demonstrate the use of our approach for several experimentally relevant situations. In the many-particle case, often symmetric operators can be used to describe accurately the system, which makes possible to carry out calculations for thousand of particles, as will be presented later on this chapter.

4.2 Examples

In this section, we show how to obtain lower bounds based of the fidelities with respect to the GHZ state and the unpolarized Dicke state as well as with different configurations of powers of collective angular momentum operators, e.g., the set $\{\langle J_y \rangle, \langle J_x \rangle, \langle J_x^2 \rangle\}$.

4.2.1 Exploiting symmetries

When making calculations for quantum systems with an increasing number of qubits, we soon run into difficulties when computing the largest eigenvalue of Eq. (4.9). The reason is that for N qubits, we need to handle $2^N \times 2^N$ size matrices, hence we are limited to systems of 10 to 15 qubits.

We can obtain bounds for much larger particle numbers, if we restrict ourselves to the symmetric subspace \square . This approach can give optimal bounds for many systems, such as Bose-Einstein condensates (BEC) of two-level atoms, which are in a symmetric multiparticle state. The bound computed for the symmetric subspace might be not correct and generally overestimated for general cases.

Finally, it is important to note that if the operators W_k are permutationally invariant and the eigenstate with the maximal eigenvalue in Eq. (4.9) is non-degenerate. And the resulting maximal eigenvalue is the same ...

We follow presenting the proof of the recently mentioned observation for completeness. Let us denote the ground state of a permutationally invariant Hamiltonian by $|\Psi\rangle$. This is at the same time the $T = 0$ thermal ground state, hence it must be a permutationally invariant pure state. For such states $S_{kl}|\Psi\rangle\langle\Psi|S_{kl} = |\Psi\rangle\langle\Psi|$, where S_{kl} is the swap operator exchanging qubits k and l . Based on this, follows that $S_{kl}|\Psi\rangle = c_{kl}|\Psi\rangle$, and $c_{kl} \in -1, +1$. There are three possible cases to consider:

- i) All $c_{kl} = +1$. In this case, for all permutation operator Π_j we have

$$\Pi_j|\Psi\rangle = |\Psi\rangle, \quad (4.11)$$

since any permutation operator Π_j can be constructed as $\Pi_j = \prod_i S_{k_i l_i}$. Equation (4.11) means that the state $|\Psi\rangle$ is symmetric.

- ii) All $c_{kl} = -1$. This means that the state is antisymmetric, however this state exists only for $N = 2$ qubits.

iii) Not all c_{kl} are identical to each other. In this case, there must be k_+, l_+, k_-, l_- such that

$$\begin{aligned} S_{k_+, l_+} |\Psi\rangle &= +|\Psi\rangle, \\ S_{k_-, l_-} |\Psi\rangle &= -|\Psi\rangle. \end{aligned} \quad (4.12)$$

Let us assume that k_+, l_+, k_-, l_- are index different from each other. In this case, $|\Psi'\rangle = S_{k_+, k_-} S_{l_+, l_-} |\Psi\rangle$ another ground state of the Hamiltonian H such that

$$\begin{aligned} S_{k_+, l_+} |\Psi'\rangle &= -|\Psi'\rangle, \\ S_{k_-, l_-} |\Psi'\rangle &= +|\Psi'\rangle. \end{aligned} \quad (4.13)$$

Comparing Eqs. (4.12) and (4.13) we can conclude that $|\Psi'\rangle \neq |\Psi\rangle$, while due to the permutational invariance of H we have that $\langle H \rangle_{\Psi'} = \langle H \rangle_{\Psi}$. Thus, $|\Psi\rangle$ is not a non-degenerate ground state. The proof works in an analogous way for the only nontrivial case $k_+ = k_-$, when $S_{k_+, k_-} = \mathbb{I}$.

Hence, if $N > 2$ then only i) is possible and $|\Psi\rangle$ must be symmetric.

4.2.2 Fidelity measurements

Let us consider the case when W is a projector onto a pure quantum state. First, we consider GHZ states [] hence W is the projector $|\text{GHZ}\rangle\langle\text{GHZ}|$ and $\langle W \rangle = F_{\text{GHZ}}$, the fidelity with respect to the GHZ state. Based on knowing F_{GHZ} , we would like to estimate $\mathcal{F}_Q[\rho, J_z]^\dagger$.

Using Eqs. (??) and (??), we will obtain an analytical tight lower bound on the QFI based on the fidelity F_{GHZ} . The calculation that we have to carry out is computing the bound

$$\mathcal{B}_{\mathcal{F}}(F_{\text{GHZ}}) = \sup_r \{ r F_{\text{GHZ}} - \sup_{\mu} \{ \lambda_{\max}[r |\text{GHZ}\rangle\langle\text{GHZ}| - 4(J_z - \mu)^2] \} \}. \quad (4.14)$$

We will make our calculations in the J_z orthonormal basis, which is defined with the 2^N basis vectors $b_0 = |00 \dots 000\rangle$, $b_1 = |00 \dots 001\rangle$, ..., $b_{(2^N-2)} = |11 \dots 110\rangle$, and $b_{(2^N-1)} = |11 \dots 111\rangle$. It is easy to see that the matrix in the argument of λ_{\max} in the Eq. (4.14) is almost diagonal in the J_z basis. To be more specific, the only non-diagonal matrix block comes from $|\text{GHZ}\rangle\langle\text{GHZ}|$, which has non-trivial

[†] Not a tight lower bounds on the quantum Fisher information based on the fidelity have been presented in [].

matrix elements only in the $\{b_0, b_{(2^N-1)}\}$ basis. Thus, we have to diagonalize the following matrix

$$r|\text{GHZ}\rangle\langle\text{GHZ}| - 4(J_z - \mu)^2 = \begin{pmatrix} \frac{r}{2} - 4(\frac{N}{2} - \mu)^2 & \frac{r}{2} \\ \frac{r}{2} & \frac{r}{2} - 4(\frac{N}{2} + \mu)^2 \end{pmatrix} \oplus D, \quad (4.15)$$

where D is already a $(2^N - 2) \times (2^N - 2)$ diagonal matrix with $D_k = -4(\langle J_z \rangle_{b_k} - \mu)^2$ negative eigenvalues for $k = 1, 2, \dots, (2^N - 2)$. This means that the Eq. (4.15) can be diagonalized as $\text{diag}[\lambda_+, \lambda_-, D_1, D_2, \dots, D_{2^N-2}]$, where the two eigenvalues λ_{\pm} are

$$\lambda_{\pm} = \frac{r}{2} - N^2 - 4\mu^2 \pm \sqrt{16\mu^2 N^2 + \frac{r^2}{4}}. \quad (4.16)$$

Next, we show a way that can simplify our calculations considerably. As indicated in Eq. (4.14), we have to look for the maximal eigenvalue and then optimize it over μ . We exchange the order of the two steps, that is, we look for the maximum of each eigenvalue over μ , and then find the maximal one. Clearly based on the fact that the eigenvalues of D are negative and that we can find a μ such that D_k equal zero but not positive. Due to this, the problem can be simplified to the following equation

$$\begin{aligned} \sup_{\mu} \{\lambda_{\max}[r|\text{GHZ}\rangle\langle\text{GHZ}| - 4(J_z - \mu)^2]\} &:= \max_{\mu} \{0, \sup(\lambda_+)\} \\ &= \begin{cases} 0, & \text{if } r < 0, \\ \frac{r}{2} + \frac{r^2}{16N^2} & \text{if } 0 \leq r \leq 4N^2, \\ -N^2 + r, & \text{if } r > 4N^2, \end{cases} \end{aligned} \quad (4.17)$$

where we did not have to have to look for the maximum of λ_- over μ since clearly $\lambda_+ \geq \lambda_-$. Finally, we have to substitute Eq. (4.17) into Eq. (4.14), and carry out the optimization over r , considering $F_{\text{GHZ}} \in [0, 1]$.

This way we arrive at the solution for the lower bound of the QFI base on the fidelity with respect to the GHZ state as

$$\mathcal{B}_{\mathcal{F}}(F_{\text{GHZ}}) = \begin{cases} N^2(1 - F_{\text{GHZ}})^2, & \text{if } F_{\text{GHZ}} < 1/2, \\ 0, & \text{if } F_{\text{GHZ}} \leq 1/2. \end{cases} \quad (4.18)$$

This equation is plotted in Figure 4.1 (a). Note that in the figure the plot is normalized by N^2 and that the resulting semi-parabola is independent of the number of particles. Moreover, the bound is zero for $F_{\text{GHZ}} \leq 1/2$. This is consistent with the fact that for the product states $\rho = |111 \dots 11\rangle$ or $\rho = |000 \dots 00\rangle$ we have $F_{\text{GHZ}} = 1/2$, while $\mathcal{F}_Q[\rho, J_z] = 0$.

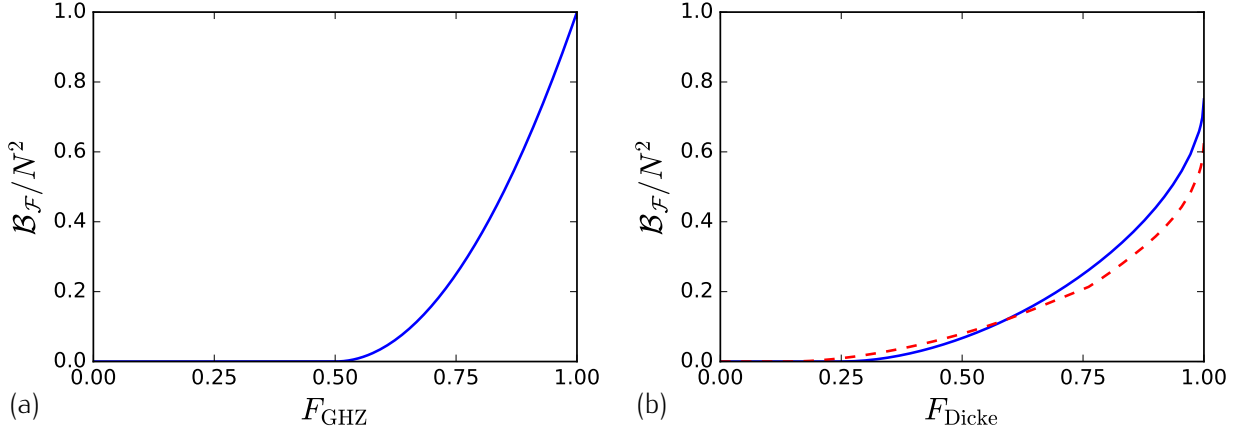


Figure 4.1: (a) Analytical solution of the bound $\mathcal{B}_{\mathcal{F}}$ for different values of the fidelity with respect to the GHZ state. (b) Numerical results for the minimum quantum Fisher information as a function of the fidelity with respect of unpolarise Dicke states perpendicular to the magnetic field, $|D_N^0\rangle$. (blue-line) For systems with 4 particles and (red-dashed) for system with 8 particles. One may notice that when the fidelity is at its maximum the bound approaches to 0.5 as it is the quantum Fisher information for large particle number.

Next, let us consider symmetric unpolarized Dicke state with even N particles along the x -direction, which is given by

$$|D_{N,N/2}\rangle_x = \binom{N}{N/2}^{-\frac{1}{2}} \sum_k \Pi_k (|1\rangle_x^{\otimes N/2} |0\rangle_x^{\otimes N/2}), \quad (4.19)$$

where the summation is over all the different permutations, Π_k , of the product state having $N/2$ particles in $|1\rangle_x$ and the rest $N/2$ in the $|0\rangle_x$ state, the single qubit $j_x^{(n)}$ basis states.

This state is known to be highly entangled [1] and allows for Heisenberg limited interferometry [2]. In the following we will omit the second subscript and we use the notation $|D_N\rangle_x \equiv |D_{N,N/2}\rangle_x$, where we even may skip the subscript x since this Dicke state will be always in the center of our attention, the unpolarized Dicke state perpendicular to the magnetic field in this case along the z -direction. The witness operator that can be used for noisy Dicke states is $W = |D_N\rangle\langle D_N|$, hence the expectation value of the witness is just the fidelity with respect to the Dicke state, i.e., $\langle W \rangle = F_{\text{Dicke}}$. In Figure 4.1 (b), we plotted the results for symmetric Dicke states of various spin numbers. $F_{\text{Dicke}} = 1$ corresponds to $\mathcal{F}_Q[\rho, J_z] = N(N+2)/2$. At this point, note that for the examples presented above, the QFI bound scales as $\mathcal{O}(N^2)$ in the asymptotic limit if the quantum state has been prepared perfectly[‡].

Note that estimating $\mathcal{F}_Q[\rho, J_z]$ based on F_{Dicke} was possible for 40 qubits [TD: Ask geza for the data points for 40 particles] for Fig 4.1 (b), since we carried out the calculations for the symmetric

[‡] $\mathcal{O}(x)$ is the usual Landau notation used to describe the asymptotic behavior for large x [1].

subspace. For our case, the witness operator W is permutationally invariant and it has a non-degenerate eigenstate corresponding to the maximal eigenvalue. Hence, based on the arguments of the Section ?? the bound is valid even for general case, i.e., non-symmetric states.

We now compute several quantities for the large N case. We show that if the fidelity with respect to the Dicke state is larger than a bound then $\mathcal{B}_{\mathcal{F}} > 0$, where we omit the arguments for brevity. Moreover, we have seen in Figure 4.1 (b) that the lower bound on $\mathcal{F}_Q[\rho, J_z]$ as a function of the fidelity F_{Dicke} normalized by N^2 is not the same curve for all N . Next, we will demonstrate by numerical evidence that the lower bound normalized by N^2 collapses to a nontrivial curve for large N .

As a first step, let us consider the completely polarized state along z -direction $|1\rangle_y^{\otimes N}$. This state does not change under rotations around the z -axis, hence $\mathcal{F}_Q[\rho, J_z] = 0$. Its fidelity with respect to the Dicke state, Eq. (4.19), is

$$F_{\text{Dicke}}(|1\rangle_y^{\otimes N}) = \frac{1}{2^N} \binom{N}{N/2} \approx \sqrt{\frac{2}{\pi N}} \quad (4.20)$$

From convexity of the bound on the quantum Fisher information in F_{Dicke} , it immediately follows that for F_{Dicke} smaller than Eq. (4.20) the optimal bound on $\mathcal{F}_Q[\rho, J_z]$ will give zero.

Next, we examine what happens if the fidelity is larger than Eq. (4.20). For that we notice first that $\mathcal{F}_Q[\rho, J_z]$ is the convex roof of $4(\Delta J_z)^2$ []. Hence, if we have a mixed state for which $\mathcal{F}_Q[\rho, J_z]$ is zero, then it can always be decomposed into the mixture of pure states for which $\mathcal{F}_Q[|\Psi\rangle, J_z]$ is zero too. As a consequence, the extremal states of the set of states for which $\mathcal{F}_Q[\rho, J_z] = 0$ are pure states, and we can restrict our search for pure states. The optimization problem we have to solve is given as

$$F_{\text{opt}} = \left\{ \max_{\Psi} |\langle \Psi | D_N \rangle_x|^2 \mid \mathcal{F}_Q[|\Psi\rangle, J_z] = 0 \right\}. \quad (4.21)$$

Pure states $|\Psi\rangle$ that are invariant under $U_{\Theta} = \exp(-iJ_z\Theta)$ for any Θ . Such states are the eigenstates of J_z . In order to maximize the overlap with the Dicke state $|D_N\rangle_x$, we have to look for symmetric eigenstates of J_z . These are the symmetric Dicke states in the z -basis $|D_{N,m}\rangle_z$. Then, using the following identity

$$\sum_{k=0}^q \binom{n}{k} \binom{n}{q-k} (-1)^k = \begin{cases} \binom{n}{q/2} (-1)^{q/2}, & \text{for even } q, \\ 0, & \text{for odd } q. \end{cases} \quad (4.22)$$

one finds that the squared overlap is given by

$$|\langle D_{N,m}|_z|D_N\rangle_x|^2 = \begin{cases} \frac{\binom{N/2}{m/2}^2 \binom{N}{N/2}}{2^N \binom{N}{m}}, & \text{for even } m \text{ and } N, \\ 0, & \text{for odd } m, \end{cases} \quad (4.23)$$

which is maximal, in the case of even N , when $m = N$ or $m = 0$, thus the totally or anti-totally polarized states respectively. We skip the case on which N is odd. For detailed calculations of Eq. (4.23) see Appendix A.2.

Next, we will examine the behavior of our lower bound on $\mathcal{F}_Q[\rho, J_z]$ based on the fidelity F_{Dicke} for large N . In figure ?? [TD: Ask Geza for the data], the calculations up to $N = 500$ present a strong evidence that for fidelity values $F_{\text{Dicke}} = 0.2, 0.5, 0.8$ the lower bound on QFI has a $\mathcal{O}(N^2)$ scaling for increasing N . If this is correct then reaching a fidelity larger than a certain monotonously decreasing bound for large N would imply Heisenberg scaling for the bound on the quantum Fisher information. Note that it is difficult to present a similar numerical evidence for small values of F_{Dicke} since in that case the bound for QFI is nonzero only for large N due to Eq. (4.20).

4.2.3 Spin-squeezed states

In the case of spin squeezing, the quantum state has a large spin in the y -direction, while a decreased variance in the x -direction. By measuring $\langle J_y \rangle$ and $(\Delta J_x)^2$ we can estimate the lower bound for the quantum Fisher Information by Eq. (??). However, this formula does not necessarily give the best lower bound for all values of the collective observables. With our approach we can find the best bound.

To give a concrete example, we choose $W_1 = J_y$, $W_2 = J_x^2$ and $W_3 = J_x$ for the operators to be measured. We vary w_1 and w_2 in some interval. We also require that $w_3 = 0$, since we assume that the mean spin points into the y -direction[§] This is reasonable since in most spin-squeezing experiments we know the direction of the mean spin.

Our result can be seen in Figure 4.2. We chose $N = 4$ particles since for small N the main features of the plot are clearly visible. The hatched area corresponds to non-physical combination of expectation values. States at the boundary can be obtained as ground states of $H_{\text{bnd}}^{(\pm)}(\lambda) = \pm J_x^2 - \lambda J_y$, see Appendix ??. In Figure 4.2, the state fully polarized in the y -direction, and initial state for

[§] Due to symmetries of the problem, when minimizing $\mathcal{F}_Q[\rho, J_z]$ with the constraints on $\langle J_z \rangle$ and $\langle J_x^2 \rangle$, we do not have to add explicitly the constraint $\langle J_x \rangle = 0$. Optimization with only the first two constraints will give the same bound (see Section ??).

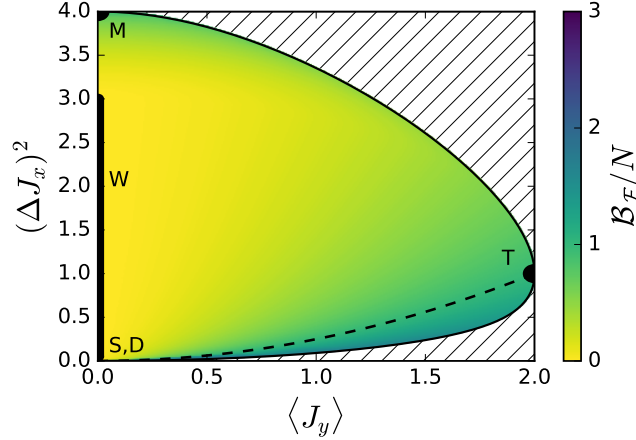


Figure 4.2: We show as a function of the expectation value, $\langle J_y \rangle$, and the variance in the perpendicular direction, $(\Delta J_x)^2$, the minimum sensitivity for a 4-qubit system. (hatched) The physically forbidden region is indicated. (M,T,S,D) Those points indicate where the mixed state (), the totally polarized state (), the single state and the unpolarized Dicke state would be located. (W) on this line sit any of the states which is a mixture between the completely mixed state of the symmetric subspace and the singlet state among others, for instance the completely mixed state of the whole Hilbert space. (dashed) It indicates the shot-noise threshold where below it non-classical sensitivities can be achieved.

spin-squeezing experiments, corresponds to point T. The unpolarized Dicke state along x -direction Eq. (4.19) corresponds to point D. We add that outside the symmetric subspace, there are other states with $\langle J_y \rangle = \langle J_x^2 \rangle = 0$, which also corresponds to point D (in this case denoted by point S). For example, such a state is the multiparticle singlet corresponding to point S. However, usual spin-squeezing procedures remain in the symmetric subspace, thus we discuss only the Dicke state. Spin squeezing makes $(\Delta J_x)^2$ decrease, while $\langle J_y \rangle$ also decreased somewhat. Hence, at least for small squeezing it corresponds moving down from point T to point D following the boundary, while the metrological usefulness is increasing. Below the dashed line $\mathcal{F}_Q[\rho, J_z] > N$, hence the state possesses metrologically useful entanglement []. The equal mixture of $|000 \dots 00\rangle_x$ and $|111 \dots 11\rangle_x$ corresponds to point M, with $\mathcal{F}_Q[\rho, J_z] = N$. Finally, the completely mixed state rests on the line W. It cannot be used for metrology, hence $\mathcal{F}_Q[\rho, J_z] = 0$.

We now compare the difference between our bound and L. Pezze and A. Smerzi bound Eq. (2.32). First, we consider the experimentally relevant region for which $(\Delta J_x)^2 \leq 1$. We find that for points away from the physical boundary at least by 0.001 on the vertical axis, the difference between the two bounds is smaller than 2×10^{-6} . For points at the boundary, the difference is somewhat larger, but still small, the relative difference is smaller than 2% for 4 particles. [TD: Add part of the appendix] Hence, Eq. (2.32) practically coincides with the optimal bound for $(\Delta J_x)^2 < 1$.

We now consider regions on Figure 4.2 for which $(\Delta J_x)^2 > 1$. The difference between the two

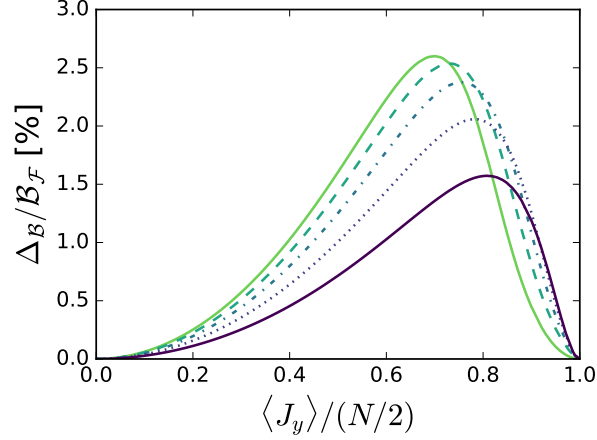


Figure 4.3: Difference between the bound of Pezze-Smerzi and the optimal bound for the quantum Fisher information normalized by the value of the optimal bound itself for the bosonic ground states of $H = J_x^2 - \lambda J_y$ for $\forall \lambda \in [0, \infty)$. From dark to lighter colors (line, point, dash-point, dashed, pointed, line), results for different particle numbers, $N = 4, 6, 10, 20, 1000$ respectively. Heuristically speaking, one can say that for large particle number the difference is biggest when the polarisation is around two thirds of the maximal polarisation and that this difference is about 2.6%.

bound is now larger. It is larger at point M, for which the bound Eq. (2.32) is zero. Hence for measurement values corresponding to points close to M, our method improve the formula Eq. (2.32). It is important from the point of view of applying our method to spin-squeezing experiments that the bound Eq. (2.32) can be substantially improved for $(\Delta J_x)^2 < 1$, if we assume bosonic symmetry for the system, or we measure an additional quantity, such as $\langle J_x^4 \rangle$ as shown in Figure ?? [TD: Ask Geza for data].

4.2.4 Dicke states

In this section, we use our method to find lower bounds on the QFI for states characterized to be close to the Dicke states (4.19), based on collective measurements. We discuss what operators have to be measured to estimate the metrological usefulness of the state. In Section ??, we will test our approach for a realistic system with very many particles.

In order to estimate the metrological usefulness of states created in such experiments, we choose to measure $W_1 = J_x^2$, $W_2 = J_y^2$ and $W_3 = J_z^2$ since the expectation values of these operators uniquely define the ideal Dicke state, and they have been already used for entanglement detection [?]. In cold gas experiments of nowadays, the state created is invariant under transformations of the type $U_x(\phi) = \exp(-iJ_x\phi)$ [20]. For such states $\langle J_y^2 \rangle = \langle J_x^2 \rangle$, which we also use as a constraint in our optimization.

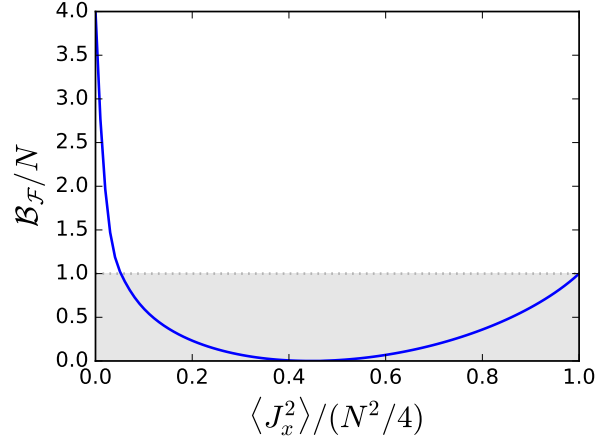


Figure 4.4: Optimal lower bound on the quantum Fisher Information for symmetric states with $\langle J_y^2 \rangle = \langle J_z^2 \rangle$. Even if it is metrologically useful for a wide range of $\langle J_x^2 \rangle$, the numerics shows us a tiny region where the metrological gain is surpassing the shot-noise limit.

Let us demonstrate how our method works in an example for small systems. Figure 4.4 shows the result for 6 qubits for symmetric states for which

$$\langle J_x^2 + J_y^2 + J_z^2 \rangle = \frac{N(N+2)}{4} =: \mathcal{J}_N. \quad (4.24)$$

It can be seen that the lower bound on quantum Fisher Information is the largest for $\langle J_x^2 \rangle = 0$. It reaches the value corresponding to the ideal Dicke state, $\mathcal{F}_Q[\rho, J_z]/N = (N+2)/2 = 4$. It is remarkable that the state is also useful for metrology if $\langle J_x^2 \rangle$ is very large. In this case $\langle J_y^2 \rangle$ and $\langle J_z^2 \rangle$ are smaller than $\langle J_x^2 \rangle$.

4.3 Calculations for experimental data

In this section, we use our method to find tight lower bound on the QFI based on experimental data. In particular, we will determine the bound for several experiments in photons and trapped ions creating GHZ states and Dicke states, in which the fidelity has been measured [11, 13–15, 21–25], which is much easier than obtaining the quantum Fisher Information from the density matrix [26], or estimation it from a metrological procedure [27]. We will obtain a bound on the QFI for a spin-squeezing experiment with thousand of particles [28]. Based on numerical examples, we see that the bound Eq. (2.32) is close to the optimal even for not completely polarized states. Assuming symmetry or knowing additional expectation values can improve the bound Eq. (2.32). Finally, we will also obtain the bound for the QFI for a recent experiment with Dicke states [?]. The estimate of the

Physical system	Target quantum state	Fidelity	$\mathcal{B}_{\mathcal{F}}/N$	Ref.
photons	$ D_4\rangle$	0.844 ± 0.008	1.432 ± 0.044	[?]
		0.78 ± 0.008	1.124 ± 0.236	[25]
		0.8872 ± 0.0055	1.680 ± 0.036	[21]
		0.873 ± 0.005	1.44 ± 0.024	[29]
	$ D_6\rangle$	0.654 ± 0.024	0.564 ± 0.076	[23]
		0.56 ± 0.02	0.304 ± 0.048	[24]
photons	$ GHZ_4\rangle$	0.840 ± 0.007	1.848 ± 0.076	[11]
	$ GHZ_5\rangle$	0.68	0.65	[?]
	$ GHZ_8\rangle$	0.59 ± 0.02	0.256 ± 0.128	[?]
	$ GHZ_8\rangle$	0.776 ± 0.06	2.4376 ± 0.1072	[13]
	$ GHZ_{10}\rangle$	0.561 ± 0.019	0.15 ± 0.11	[13]
trapped-ions	$ GHZ_3\rangle$	0.89 ± 0.03	1.824 ± 0.291	[30]
	$ GHZ_4\rangle$	0.57 ± 0.02	0.08 ± 0.052	[?]
	$ GHZ_6\rangle$	0.509 ± 0.004	0.0018 ± 0.0018	[?]
	$ GHZ_8\rangle$	0.817 ± 0.004	3.21 ± 0.08	[15]
	$ GHZ_{10}\rangle$	0.626 ± 0.006	0.64 ± 0.06	[15]

Table 4.1: Fidelity values and the corresponding bound for the QFI for several experiments with Dicke states and GHZ states. Bounds normalized with N are shown. The ones surpassing the value one, they show quantum entanglement enhanced metrological usefulness. For Dicke states the maximum is achieved at $(N + 2)/2$, i.e., 3 for the $|D_4\rangle$ case and 4 for the $|D_6\rangle$ case. For the case on which GHZ states are used the limit for the normalized bound is N , the particle number.

precision based on considering the particular case when $\langle J_x^2 \rangle$ is measured for parameter estimation [20] is close to the optimal bound computed by our method.

4.3.1 Few-particle experiments

Now, we will estimate the quantum Fisher information based on the fidelity with respect to Dicke states and GHZ states for several experiments with photons and trapped cold ions, following the ideas of Section ??.

Our results are summarized in Table 4.1. The experiments in [13, 25] are with hyperentangled qubits, while in the rest of experiments a single qubit is stored in a particle. Reference [15] describes experiments with 2-14 ions, we presented only results of 2 of them. Finally, for the experiment of Ref. [?] we used the fidelity estimated using reasonable assumptions discussed in that paper, while the worst case fidelity is lower.

We can compare our estimate to the quantum Fisher information of the state for the experiment of

Ref. [21], where the QFI for the density matrix was obtained as $\mathcal{F}_Q[\rho, J_z]/N = (10.326 \pm 0.093)/N = (2.5816 \pm 0.02325)$. As can be seen in Table 4.1, this value is larger than we obtained, however, it was calculated by knowing the entire matrix, while our bound is obtained from the fidelity alone.

4.3.2 Many-particle experiments

In this section, we will estimate the quantum Fisher information based on collective measurements for experiments aiming to create spin-squeezing states and Dicke states.

Spin-squeezing experiment

We turn our attention to a recent many-particle spin-squeezing experiment in cold gases to use our method to find lower bounds on the quantum Fisher information, following the ideas of the Section ???. With that we show that the lower bound given in Eq. (2.32) is close to the optimal. We also demonstrate that we carry out calculations for real systems.

In particular, for our calculations we use the data from spin-squeezing experiments of Ref. [28]. The particle number is $N = 2300$, and the spin squeezing parameter defined as

$$\xi_s^2 = N \frac{(\Delta J_x)^2}{\langle J_y \rangle^2} \quad (4.25)$$

has the value $\xi_s^2 = -8.2\text{dB} = 10^{-8.2/10} = 0.1514$. The spin length $\langle J_y \rangle$ has been close to maximal. In our calculations, we choose

$$\langle J_y \rangle = \alpha \frac{N}{2}, \quad (4.26)$$

where we will test our method with various values for α . For each α we use $(\Delta J_x)^2$ will be given such that we get the experimentally obtained spin-squeezing parameter Eq. (4.25). Moreover, we assume $\langle J_x \rangle = 0$, as the y -direction was the direction of the mean spin in the experiment. Based on Eq. (2.32), the bound for the quantum Fisher information is obtained as

$$\frac{\mathcal{F}_Q[\rho, J_z]}{N} \geq \frac{1}{\xi_s^2} = 6.605. \quad (4.27)$$

For our computations we need a tool to handle large systems. We will carry out the calculations for symmetric states. this way we obtain a lower bound on the QFI that we will denote by \mathcal{B}_{sym} . As already mentioned, we could obtain a bound for the QFI that is valid even for general case, not necessarily symmetric states if the matrix from which compute the maximum eigenvalue Eq. (4.9) has a

non-degenerated largest eigenvalue. This is not the case in general for the spin-squeezing problem. However, we still know that our bound obtained with our calculations on the symmetric subspace cannot be smaller than the optimal bound $\mathcal{B}_{\mathcal{F}}$, which must be bigger or equal to the Eq. (2.32) since it cannot be larger than the optimal bound for general states. These relations can be summarized as

$$\mathcal{B}_{\text{sym}} \geq \mathcal{B}_{\mathcal{F}} \geq \frac{\langle J_y \rangle^2}{(\Delta J_x)^2}, \quad (4.28)$$

where on the right-hand side we just used the bound in Eq. (2.32).

Our calculations lead to

$$\frac{\mathcal{B}_{\text{sym}}(\langle J_y \rangle, (\Delta J_x)^2)}{N} = 6.605 \quad (4.29)$$

for a wide range of values of α . That is, based on numerics, the left-hand side and the right-hand side of Eq. (4.29) seem to be equal. This implies that the lower bound Eq. (2.32) is optimal for estimating the QFI for the system.

We follow giving the details of our calculations for $\alpha = 0.5, 0.85$ and we show examples on which we can improve the bound Eq. (2.32) with our approach, if symmetry is assumed. We present simple scheme that we need to handle large systems, and make calculations for larger particle number. Thus, we need fewer steps for the numerical optimization for large system sizes, which makes our computations faster. Second, while we will be able to carry out the calculation for the particle number of the experiment, we will also see that we could even extrapolate the results from the results obtained for lower particle numbers. This is useful for future application of our method for very large systems.

The basic idea is that we transform the collective quantities from N to a smaller particle number using the scaling relation

$$\langle J_y \rangle = \frac{N'}{2} \alpha, \quad (4.30)$$

$$(\Delta J_x)^2 = \xi_s^2 \frac{N'}{4} \alpha^2. \quad (4.31)$$

We see that for the scaling we consider, for all N' the bound in Eq. (2.32) is valid, i.e., is obtained as

$$\frac{\mathcal{F}_Q[\rho_{N'}, J_z]}{N'} \geq \frac{1}{\xi_s^2} = 6.605. \quad (4.32)$$

Let us first take $\alpha = 0.85$, which is somewhat smaller than the experimental value, however, it helps us to see various characteristics of the method. At the end of the section we will also discuss the results for other values of α . Based on these ideas, we compute the bound \mathcal{B}_{sym} for the quantum

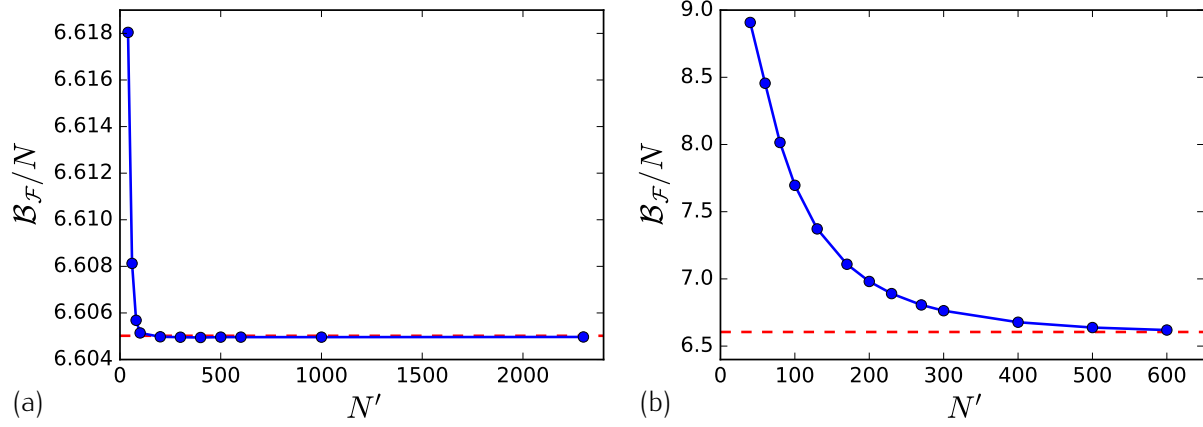


Figure 4.5: [TD: Change vertical label to \mathcal{B}_{sym}] (Color line) Lower bound on the QFI based on $\langle J_y \rangle$ and $(\Delta J_x)^2$ obtained for the symmetric subspace for different particle numbers N' .

Fisher information for an increasing system size N' .

The results can be seen in Figure 4.5 (a). The bound obtained this way is close to the bound in Eq. (4.27) even for small N' . For larger particle number it is constant and coincides with the bound in Eq. (4.27). This also strongly supports the idea that we could use the result for small particle numbers to extrapolate the bound for N . Since for the experimental particle number we obtain that \mathcal{B}_{sym} equals the bound in Eq. (4.27), we find that all three lower bounds in Eq. (4.29) must be equal. Hence, Eq. (2.32) is optimal for the experimental system and α considered before in this section. Besides, these results present also a strong argument for the correctness of our approach.

We now give more details of the calculation. We were able to carry out the optimizations up to $N' = 2300$ with a usual laptop computer using MATLAB programming language[†]. We started the calculation for each given particle number with the r_k parameters obtained for the previous simulation with a smaller particle number. This allows for faster finding of the solution than if we would start the r_k parameters arbitrarily.

Let us consider a spin-squeezing state that is not fully polarized and $\alpha = 0.5$. In Figure 4.5 (b), we can see that for small particle numbers we have a larger bound on $\mathcal{F}_Q[\rho, J_z]$ than the one obtained from Eq. (2.32). Thus for the case on which the particle number would be smaller we could improve the bound Eq. (2.32) by assuming symmetry. On the other hand, for large particle number we recover the bound Eq. (2.32).

Finally, we add a note on the technical detail. We carried out our calculations with the constraints on $(\Delta J_x)^2$ and $\langle J_y \rangle$, with the additional constraint $\langle J_x \rangle = 0$. For the experimental particle numbers, one

[†] For MATLAB R2015a, see <http://www.mathworks.com>.

can show that our results are valid even if we constrained only $(\Delta J_x)^2$ and $\langle J_y \rangle$, and did not use the $\langle J_x \rangle = 0$ constraint. This way, in principle, we could only get a lower bound that is equal to the one we obtained before or lower. However, we obtained before a value identical to the analytical bound Eq. (2.32). The optimal bound cannot be below the analytic bound, since then the analytic bound would overestimate the quantum Fisher information, and it would not be a valid bound. Hence, even an optimization without the $\langle J_x \rangle = 0$ constraint could not obtain a smaller value than our results.

Experiment creating Dicke states

In this section, we present our calculations for an experiment aiming at creating Dicke states in cold gases [31]. The basic ideas are similar to the ones explained in Section 4.2.4 for small systems. The experimental data, as in previous Section ??, are $N = 7900$, $\langle J_y^2 \rangle = 112 \pm 31$, $\langle J_x^2 \rangle = \langle J_z^2 \rangle = 6 \times 10^6 \pm 0.6 \times 10^6$ [20]. Applying some simple transformations, we can make calculations for a very large numbers of particles, and obtain results even for general, non-symmetric systems.

In the general, non-symmetric case, we can handle only small problems. Thus, we have to transform the collective quantities such that the corresponding quantum state, i.e., it has to fulfill

$$\langle J_x^2 \rangle_{\text{sym}} + \langle J_y^2 \rangle_{\text{sym}} + \langle J_z^2 \rangle_{\text{sym}} = \mathcal{J}_N, \quad (4.33)$$

where \mathcal{J}_N is defined on Eq. (4.24). A mapping of this type can be realized equally scaling all second moments of the angular momentum projections as

$$\langle J_l^2 \rangle_{\text{sym},N} = \gamma \langle J_l^2 \rangle_N, \quad (4.34)$$

where we now added the label N to avoid confusions in upcoming equations, $l = x, y, z$ and where we used the coefficient γ to be

$$\gamma = \frac{\mathcal{J}_N}{\langle J_x^2 \rangle_N + \langle J_y^2 \rangle_N + \langle J_z^2 \rangle_N}. \quad (4.35)$$

Note that $\gamma = 1$ if the original state is symmetric.

Next, based on the ideas of this chapter, we calculate the lower bound on the quantum Fisher information for symmetric systems, which we denote it by $\mathcal{B}_{\text{sym},N}$. Then, to obtain the results for the original non-symmetric case, notice the convex nature of the \mathcal{B}_N , which is the bound to be computed for the general case, implies

$$\mathcal{B}_N \leq \frac{1}{N} \mathcal{B}_{\text{sym},N}, \quad (4.36)$$

where $\mathcal{B}_{\text{sym},N}$ corresponds to the bound one would obtain on the symmetric subspace for expectation values given using the Eq. (4.34). This can be seen using an auxiliary state $\tilde{\rho}$ that mixes the symmetric state that in principle has the expectation values appearing on Eq. (4.34) and the singlet state that has zero value for all those expectation values. Hence, if we construct a mixture of this type as follows

$$\tilde{\rho}_N = (1 - \gamma^{-1})\rho_{\text{singlet},N} + \gamma^{-1}\rho_{\text{sym},N}, \quad (4.37)$$

we have that $\tilde{\rho}$ has the same expectation values as the original non-symmetric case. This way, we can relate the bound for general systems to the quantum Fisher information for symmetric cases as

$$\mathcal{B}_N \leq \mathcal{F}_Q[\tilde{\rho}_N, J_z] = \frac{1}{\gamma} \mathcal{F}_Q[\rho_{\text{sym},N}, J_z]. \quad (4.38)$$

Here, the inequality comes due to that our bound cannot be larger than the QFI of any state having the given set of expectation values. On the other hand, the equality holds due to the fact that both $\tilde{\rho}$ and J_z can be written as block-diagonal matrix of blocks corresponding to different eigenvalues of J^2 . In particular, $\rho_{\text{singlet},N}$ has non-zero elements only in the blocks for which $\langle J^2 \rangle = 0$, while $\rho_{\text{sym},N}$ has nonzero elements only in the blocks in which $\langle J^2 \rangle$ is maximal. Notice that J^2 is a shorthand of $J_x^2 + J_y^2 + J_z^2$. Then we can use the general formula [32]

$$\mathcal{F}_Q[\bigoplus_k p_k \rho_k, \bigoplus_k A_k] = \sum_k p_k \mathcal{F}_Q[\rho_k, A_k], \quad (4.39)$$

where ρ_k are density matrices with unit trace, $\sum_k p_k = 1$ and the k index represent the block subspaces of the system and the operators A_k .

Extensive numerics for small systems show that the inequality in Eq. (4.38) is very close to an equality within the numerical precision

$$\mathcal{B}_N \approx \frac{1}{\gamma} \mathcal{B}_{\text{sym},N}. \quad (4.40)$$

To obtain the lower bound \mathcal{B}_N we also use an increasing system size N' as we have done in at the beginning of this section. However, in this case we will not be able to do the calculation for the experimental particle number, and we will use extrapolation from the results obtained for smaller particle numbers.

First, we transform the measured second moments to values corresponding to a symmetric system

using Eqs. (4.34) and (4.35). For our case, $\gamma = 1.301$. This way, we obtain

$$\begin{aligned}\langle J_y^2 \rangle_{\text{sym},N} &= 145.69, \\ \langle J_x^2 \rangle_{\text{sym},N} &= \langle J_z^2 \rangle_{\text{sym},N} = 7.8 \times 10^6.\end{aligned}\tag{4.41}$$

Next, we will carry out calculations for symmetric systems. We will consider a smaller system N' that keeps expectation values such that the corresponding quantum state must be symmetric. Hence, we will use the following relation to find the target expectation values for smaller systems

$$\begin{aligned}\langle J_y^2 \rangle_{\text{sym},N'} &= \langle J_y^2 \rangle_{\text{sym},N}, \\ \langle J_x^2 \rangle_{\text{sym},N'} &= \langle J_z^2 \rangle_{\text{sym},N'} = \frac{1}{2}(\mathcal{J}_{N'}) - \langle J_y^2 \rangle_{\text{sym},N'},\end{aligned}\tag{4.42}$$

where $\mathcal{J}_{N'}$ is defined in Eq. (4.24). Note that with Eq. (4.24) holds for all N' , hence the state must be symmetric. Hence, the main characteristics of the scaling relation can be summarized as follows, $\langle J_y^2 \rangle_{\text{sym},N'}$ remains equal for all N' while $\langle J_x^2 \rangle_{\text{sym},N'}$ and $\langle J_z^2 \rangle_{\text{sym},N'}$ are chosen such that they are equal to each other and the state is symmetric. For large N , this implies a scaling of $\langle J_y^2 \rangle_{\text{sym},N}$ constant and $\langle J_x^2 \rangle_{\text{sym},N} = \langle J_z^2 \rangle_{\text{sym},N} \sim N(N+2)/8$.

Let us now turn to central quantities of our chapter, the lower bounds on the quantum Fisher information. A central point in our scheme is that due to the scaling properties of the system, we can obtain the value for the particle number N from the values of a smaller particle number N' as [33]

$$\mathcal{B}_{\text{sym},N} \approx \frac{\mathcal{J}_N}{\mathcal{J}_{N'}} \mathcal{B}_{\text{sym},N'},\tag{4.43}$$

which we will verify numerically. Note that for large N , we have $\mathcal{J}_N/\mathcal{J}_{N'} \sim N^2/(N')^2$.

As last step, we have to return from the symmetric system to our real system, not fully symmetric one. Based on Eq. (4.43) and assuming Eq. (4.40), a relation for the lower bound for the original problem can be obtained from the bound on the symmetric problem with N' particles as

$$\mathcal{B}_N \approx \frac{1}{\gamma} \frac{\mathcal{J}_N}{\mathcal{J}_{N'}} \mathcal{B}_{\text{sym},N'} = \frac{\langle J_x^2 \rangle_N + \langle J_y^2 \rangle_N + \langle J_z^2 \rangle_N}{\mathcal{J}'_N} \mathcal{B}_{\text{sym},N'}.\tag{4.44}$$

In Figure 4.6, we plotted the right-hand side of Eq. (4.44) as the function of N' divided by N . We can see that $\mathcal{B}_{N'}/N$ is constant or slightly increasing for $N' > 400$. This is a strong evidence that Eq. (4.43) is valid for relatively large particle numbers. With this, we arrive at the result for the

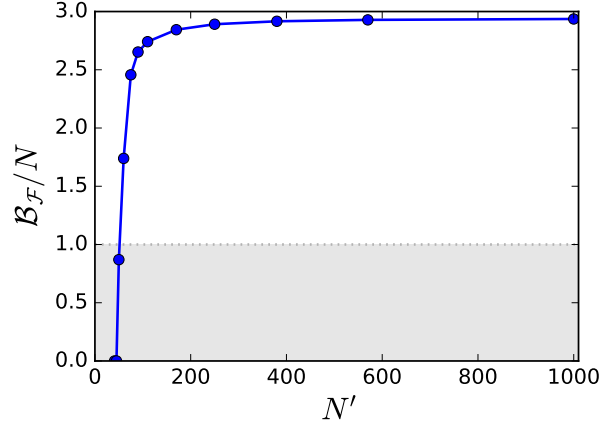


Figure 4.6: Sequence of the evolution of an unpolarized Dicke state of 16 qubits for $\Theta = \{i\pi/6\}_{i=0}^4$. Bloch spheres representing the Hursi distribution of the state, and below PDF of the J_x POVM for each step of the sequence

experimental system

$$\frac{\mathcal{B}_N(\langle J_y^2 \rangle, \langle J_x^2 \rangle = \langle J_z^2 \rangle)}{N} \approx 2.94. \quad (4.45)$$

The \approx sign is used referring to the fact that we assume that the inequality in Eq. (4.38) is close to be saturated and that we did sufficient numerics for an increasing system size N' to have a good asymptotic approach to the real value Eq. (4.43).

It is instructive to compare the value of Eq. (4.45) to the one obtained in Chapter ??, where the same system was characterized base on its metrological usefulness. Such result implies $\mathcal{F}_Q[\rho, J_z]/N \geq 3.3$ which is somewhat bigger than our recent result as we did not use the knowledge of the fourth moments, only the second moments. The closeness of the two results is a strong argument for the correctness of our calculations.

4.4 Scaling for $\mathcal{F}_Q[\rho, J_z]$ with N

Recent important works examine the scaling of the quantum Fisher information with the particle number for metrology under the presence of decoherence [34?]. They consider the QFI defined now for the non-unitary, noisy evolution. They find that for small N it is close to the value obtained by considering coherent dynamics. Hence, even the Heisenberg scaling, $\mathcal{O}(N^2)$, can be reached. However, if N is sufficiently large, then, due to the decoherence during the parameter estimation, the QFI scales as $\mathcal{O}(N)$.

We have to stress that the findings of [34?] are not applicable to our case. Our methods

estimates the quantum Fisher information assuming a perfect unitary dynamics. The quantum Fisher information can be smaller than what we expect ideally only due to the imperfect preparation of the state. We can even find simple conditions on the state preparation that lead to a Heisenberg scaling. Based on Eq. (4.17), if we could realize quantum states ρ_N such that $F_{\text{GHZ}}(\rho_N) \geq 0.5 + \epsilon$ for $N \rightarrow \infty$ for some $\epsilon > 0$, then we would reach $\mathcal{B}_{\mathcal{F}}(F_{\text{GHZ}}) = \mathcal{O}(N^2)$. Strong numerical evidence suggest that a similar relation holds for fidelity F_{Dicke} and $\mathcal{B}_{\mathcal{F}}(F_{\text{GHZ}})$, see Section ??.

[TD: Decide if remove the following sentence. It is very strong] From another point of view, our method can estimate $\mathcal{F}_Q[\rho, J_z]$ for large particle numbers, while a direct measurement of the metrological sensitivity considerably underestimates it.

This is also relevant for [?], where $\mathcal{F}_Q = \mathcal{O}(N^2)$ is reached with weakly entangled states.

5

Accuracy bound for gradient field estimation with atomic ensembles

"To consult the statistician after an experiment is finished is often merely to ask him to conduct a post mortem examination. He can perhaps say what the experiment died of."
Ronald Fisher

In this chapter, one of the most fundamental two-parameter estimation tasks in magnetometry is considered, namely gradient magnetometry. We will add the gradient of the magnetic field as the second parameter beside the constant (homogeneous) part of the field. While most works in magnetometry with a single ensemble focus only on the determination of the strength and direction of magnetic field, certain measurement schemes for the gradient have already been proposed and tested experimentally [XXX]. Some schemes use an imaging of the ensemble with a high spatial resolution, however, they do not count as single-ensemble methods in the sense we use this expression in our paper, since in this case not only collective observables are measured [35–37]. There is a method based on collective measurements of the spin length of a fully polarised ensemble [38]. Finally, there is a scheme where they use as a probe state a many-body singlet states, which is described in Reference [39]. This section provides precision bounds for that scheme, while expanding the quantum states considered to other interesting quantum states, including those that are not invariant under homogeneous fields.

The atoms will be distributed along the x -axis, so $y = z = 0$, and in principle they will be able to

feel differences on the magnetic field at different points of the axis. The magnetic field at the atoms will be given by a linear function on the position x

$$\mathbf{B}(x, 0, 0) = \mathbf{B}_0 + x\mathbf{B}_1 + O(x^2), \quad (5.1)$$

where we will neglect the terms of order two or higher. We will consider the magnetic field pointing along the z -direction only, $\mathbf{B}_0 = B_0\mathbf{k}$ and $\mathbf{B}_1 = B_1\mathbf{k}$, where \mathbf{k} is the unitary vector pointing on the z -direction. For this configuration, due to the Maxwell equations, with no currents or changing electric fields, we have

$$\begin{aligned} \nabla \cdot \mathbf{B} &= 0, \\ \nabla \times \mathbf{B} &= \mathbf{0}. \end{aligned} \quad (5.2)$$

This implies $\sum_{l=x,y,z} \partial_l B_l = 0$ and $\partial_m B_l - \partial_l B_m = 0$ for $\forall l \neq m$, where $\partial_m \equiv \partial/\partial_m$ stands for the partial derivative over the variable l . Thus, the spatial derivatives of the field components are not independent of each other. However, in the case of a linear arranged particle ensemble only the derivative along the x -axis has an influence on the quantum dynamics of the atoms.

We will determine the precision bounds for estimation of the magnetic field gradient B_1 based on the quantum Fisher information (QFI) [40–45]. We will show that for states insensitive to the homogeneous magnetic field, one can reduce the problem to a one-parameter estimation scenario. Such states can arise in a single-ensemble scheme, however, it will be shown that for single-ensembles insensitive to the homogeneous field the Heisenberg limit cannot be reached. Nevertheless, single-ensemble measurements have certain advantages since the spatial resolution can be higher and the experimental requirements are smaller since only a single ensemble must be prepared.

On the other hand, for states sensitive to the homogeneous field, the classical limit can be overcome only if the particle positions are highly correlated with each other. Our calculations are generally valid for any measurement, thus they are relevant to many recent experiments [35–38, 46–49]. We note that in the case of the singlet, our precision bounds are saturated by the metrological scheme presented in Reference [39].

We can also connect our results to entanglement theory [1, 50, 51]. We find that the shot-noise scaling cannot be surpassed with separable states, while the Heisenberg scaling can be reached with entangled states. However, the shot-noise scaling can be surpassed only if the particle positions are correlated, which is the case if the particles attract each other. Moreover, the case of two atomic ensembles, if the spin states of the ensembles are uncorrelated, can also be mapped to our model. This evidently shows how shot-noise scaling can be surpassed with the two-ensemble scenario.

Next, we will present characteristics of our setup. For simplicity, as well as following recent experiments (e.g., Ref. [37]), we will consider an ensemble of spin- j particles placed in a one-dimensional setup, x being the spatial coordinate. Furthermore, we assume that we have particles that behave classically with respect to their spatial state. That is, they cannot be in a superposition of being in two different positions. On the other hand, they have internal degrees of freedom, their spin, that is quantum. This is a very good description to many of the cold gas experiments.

Based on these considerations, we assume that the state is factorizable into a spatial and a spin part as

$$\rho = \rho_x \otimes \rho_s, \quad (5.3)$$

and that the spatial part can be characterized as an incoherent mixture of point-like particles that can be written as

$$\rho_x = \int d^N \mathbf{x} P_N(\mathbf{x}) |\mathbf{x}\rangle \langle \mathbf{x}|. \quad (5.4)$$

Note that the spatial part is diagonal on the position eigenbasis, where the entry x_n of $\mathbf{x} = (x_1, \dots, x_N)$ is the coordinate of the n^{th} particle, and $P_N(\mathbf{x})$ is the spatial probability distribution function of the atoms. This model can be seen as that the density matrix of the spatial part of the state is diagonal on the position eigenbasis and it simplifies much the problem. During the evolution of the state, correlations might arise between the two inner and spatial parts and the product form (5.3) might be not valid to describe the evolution of the system.

We note that our method could be easily extended to the case of Bose-Einstein condensates, not considered in this paper. In that case, the spatial state of the particles would be a pure state, and we would have $\rho_x = (|\Psi\rangle \langle \Psi|)^{\otimes N}$, where $|\Psi\rangle$ is a spatial single-particle state.

Although in our case the parameter to be estimated is B_1 , the time-evolution of the state is usually also affected by the second unknown parameter, the homogeneous field B_0 , which means that we generally have to consider a two-parameter estimation problem. The angular momentum of an individual atom is coupled to the magnetic field, yielding the following interaction term

$$h^{(n)} = \gamma B_z^{(n)} \otimes j_z^{(n)}, \quad (5.5)$$

where the operator $B_z^{(n)} = B_0 + B_1 x^{(n)}$ acts on the spatial part of the Hilbert space. The sum of all one particle interactions provide the total Hamiltonian

$$H = \gamma \sum_{n=1}^N B_z^{(n)} \otimes j_z^{(n)}, \quad (5.6)$$

which will generate the time evolution of the atomic ensemble.

We will estimate the precision of B_1 based on a measurement on the state after it passed through the dynamics expressed by the unitary evolution operator $U = \exp(-i\frac{H}{\hbar}t)$, where t is the time spent by the system under the influence of the magnetic field. Those type of unitary phase shift are the most easy ones to study with the quantum Fisher information, and this is the reason while we choose them to make the jump to the multi-parametric estimation problem. The unitary operator can be rewritten in the following way

$$U = e^{-i(b_0 H_0 + b_1 H_1)}, \quad (5.7)$$

where the $b_i = \gamma B_i t / \hbar$. Here, the generator describing the effect of the homogeneous field is given as

$$H_0 = \sum_{n=1}^N j_z^{(n)} = J_z, \quad (5.8)$$

while the generator describing the effect of the gradient is

$$H_1 = \sum_{n=1}^N x^{(n)} j_z^{(n)}. \quad (5.9)$$

As in Eq. (5.9), we will usually omit \otimes for simplicity, and will use it only if it is necessary to make our explanation clearer.

Note that the operators H_0 and H_1 commute with each other. These two commuting dynamics are the two simplest in an atomic ensemble as they are based on collective operators not requiring an individual access to the particles.

Note also that it is not necessarily true that the operators we have to measure to estimate b_0 and b_1 commute with each other, which problem we will consider case by case. The reason for that is that both operators to be measured act on the same single atomic ensemble. On the other hand, in schemes in which the gradient is calculated based on measurements in two separate atomic ensembles or different atoms in a chain, the measuring operators can always commute with each other [33, 46, 47].

The paper is organized as follows. In Sec. 5.1, the basic concepts used in the paper are presented. In Sec. III, we restrict our calculations to single PI atomic ensembles and we develop some particular cases, such as the singlet spin state or the totally polarised state. In Sec. IV, we discuss our results.

5.1 Cramér–Rao precision bounds

In this section, we show how the Cramér–Rao bound and the QFI help us to obtain the precision bound that is valid for any measurement scenario. We will discuss gradient magnetometry using quantum states that are insensitive to homogeneous fields, which is a single-parameter estimation task. Then, we discuss the case of quantum states sensitive to homogeneous fields. We show that the precision bound obtained does not change under spatial translation. Since this is a two-parameter estimation task, we will introduce the two-parameter Cramér–Rao bound and the corresponding two-parameter QFI matrix, and we adapt those expressions to our problem.

For clarity we present our main tools in subsequent paragraphs before going onto details for states that are not sensitive to the homogeneous field and states that they are. The expression for quantum Fisher information that we use along this paper will be suitable for the transition to the multi-parameter problem, i.e, it is equivalent for the single parameter estimation problem still giving the chance to switch to the multi-parameter case. For two arbitrary operators A and B , it is written as follows

$$\mathcal{F}_Q[\rho, A, B] := 2 \sum_{k,k'} \frac{(\lambda_k - \lambda_{k'})^2}{\lambda_k + \lambda_{k'}} A_{k,k'} B_{k',k}, \quad (5.10)$$

where the subscript for A and B stand for the matrix element on the eigenbasis of the initial state $\rho = \sum_k \lambda_k |k\rangle\langle k|$. If the two operators are the same, the usual form of the QFI on the literature can be recovered with only two arguments [40–45],

$$\mathcal{F}_Q[\rho, A, A] := \mathcal{F}_Q[\rho, A] = 2 \sum_{k,k'} \frac{(\lambda_k - \lambda_{k'})^2}{\lambda_k + \lambda_{k'}} |A_{k,k'}|^2. \quad (5.11)$$

We mention that in our case the operators A and B will commute on all cases making the some computations easier. We also make use of the fact that the QFI as written as in Eq. (5.10) is linear on the second and last arguments,

$$\mathcal{F}_Q[\rho, A, \sum_i b_i] = \sum_i \mathcal{F}_Q[\rho, A, b_i] \quad (5.12)$$

together with $\mathcal{F}_Q[\rho, A, B] = \mathcal{F}_Q[\rho, B, A]$ so the statement holds.

Some more useful properties of the Eq. (5.10). It can be rewritten as follows,

$$\mathcal{F}_Q[\rho, A, B] = 4\langle AB \rangle - 8 \sum_{k,k'} \frac{\lambda_k \lambda_{k'}}{\lambda_k + \lambda_{k'}} A_{k,k'} B_{k',k}. \quad (5.13)$$

This form leads to simple arguments on our derivations on following sections. For pure states it simplifies to,

$$\mathcal{F}_Q[|\psi\rangle, A, B] = 4 \left(\langle AB \rangle_\psi - \langle A \rangle_\psi \langle B \rangle_\psi \right). \quad (5.14)$$

Notice that we recover $\mathcal{F}_Q[\rho, A] = 4(\Delta A)^2$ as can be found in the literature for single parameter estimation with pure states [40, 52]. Another important feature of the qFI in Eq. (5.10) is that it is convex on the space of the states. This property takes the following form,

$$\mathcal{F}_Q[q\rho_1 + (1-p)\rho_2] \leq p\mathcal{F}_Q[\rho_1] + (1-p)\mathcal{F}_Q[\rho_2], \quad (5.15)$$

where we omit in writing the arguments for the operators of the qFI for simplicity.

In the following subsections we show the general form for the precision bounds for states insensitive to the homogeneous fields and for states sensitive to them. We also show that both bounds are invariant under spatial translation of the system which makes the computing for particular cases much easier.

5.1.1 Precision bound for states insensitive to homogeneous fields: Single-parameter dependence

Let us consider quantum states that are insensitive to the homogeneous field. For these states, $[\rho, H_0] = 0$ and hence the evolved state is a function of a single unknown parameter, b_1 .

For the unitary dynamics we consider, the QFI for single-parameter dependence can be expressed in terms of the eigendecomposition of the density matrix, $\rho = \sum_k \lambda_k |k\rangle\langle k|$, in the following way [40–45],

$$\mathcal{F}_Q[\rho, H_1] = 2 \sum_{k,k'} \frac{(\lambda_k - \lambda_{k'})^2}{\lambda_k + \lambda_{k'}} |(H_1)_{k,k'}|^2. \quad (5.16)$$

And due to the Cramér-Rao formula gives us an upper bound for the precision

$$(\Delta b_1)^{-2}|_{\max} = \mathcal{F}_Q[\rho, H_1]. \quad (5.17)$$

Note that it is always possible to find a measurement that saturates the above precision bound. Here, $\mathcal{F}_Q[\rho, H_1]$ denotes the QFI that depends, in the case of unitary transformation of the form Eq. (5.7), on the state ρ and on the generator of the evolution, H_1 .

For the particular case on which the states has the form of Eqs. (??) and (??) the Equation (5.16) can be simplified in the following way, see that we have to compute the matrix elements of H_1 but it

is already diagonal on the spatial subspace. Therefore the following holds for the matrix elements,

$$\begin{aligned}
 (H_1)_{\mathbf{x},k,\mathbf{y},k'} &= \langle \mathbf{x}, k | H_1 | \mathbf{y}, k' \rangle \\
 &= \langle \mathbf{x}, k | \sum_{n=1}^N x^{(n)} j^{(n)} | \mathbf{y}, k' \rangle \\
 &= \delta(\mathbf{x} - \mathbf{y}) \sum_{n=1}^N x_n \langle k | j^{(n)} | k' \rangle.
 \end{aligned} \tag{5.18}$$

We will use the Dirac delta function to further simplify the Equation (5.16), for details of the simplification see the Appendix ??.

For the last part of the proof on which we have to show how translated systems have unchanged the sensitivity over the gradient estimation, we use the Heisenberg picture on which the operators must be reversely transformed instead of the states. Thus, we compute the transformation of H_1 in the following way,

$$\begin{aligned}
 U_d : H_1 &\rightarrow H_1(d) = U_d^\dagger H_1 U_d \\
 &= \sum_{n=1}^N U_d^\dagger x^{(n)} U_d \otimes j_z^{(n)} \\
 &= \sum_{n=1}^N (x^{(n)} - d) j_z^{(n)} \\
 &= H_1 - d H_0.
 \end{aligned} \tag{5.19}$$

Hence, the new unitary evolution operator instead of Equation (5.7) will be

$$U = e^{-i(b_0 H_0 + b_1 H_1(d))} = e^{-i((b_0 - b_1 d) H_0 + b_1 H_1)}, \tag{5.20}$$

which for states insensitive to the homogeneous field, $[\rho, H_0] = 0$, makes the transformation irrelevant.

With this, for states of the form Equations (5.3,??) the following bound for the precision of the estimation of the gradient parameter b_1 holds,

$$(\Delta b_1)^{-2}|_{\max} = \sum_{n,m} \int d^N \mathbf{x} P_N(\mathbf{x}) x_n x_m \mathcal{F}_Q[\rho_s, j_z^{(n)}, j_z^{(m)}], \tag{5.21}$$

where the integral results onto a two-point correlation function of the spatial state.

Moreover, such bound is translationally invariant, i.e, it remains the same after an arbitrary phase-

shift of the form of $U_d = \exp(-i\mathbf{d} \cdot \mathbf{p}_x)$, where \cdot denotes scalar product, \mathbf{d} is a n -length vector of all elements equal to the phase-shift d and \mathbf{p}_x is the vector that collects all the single particle linear momentum operators, $p_x^{(n)}$.

5.1.2 Precision bound for states sensitive to homogeneous fields: Two-parameter dependence

In order to obtain the precision bound for states sensitive to the homogeneous field, one has to consider the effect on the state of a second unknown parameter, in this case b_0 . The homogeneous field will rotate all the spins in the same way, while the field gradient rotates the spins differently depending on the position of the particles. Now, instead to the Cramér-Rao bound (5.17), we have a matrix inequality [40]. We have the QFI matrix \mathcal{F}_Q on one hand, which depends on ρ and the two generators H_0 and H_1 , and the covariance matrix from we are only interested on the variance of the gradient parameter, $(\Delta b_1)^2$ [40]. Just to record, H_0 and H_1 are Hermitian operators and commute with each other and thus the QFI matrix elements are computed as $\mathcal{F}_{ij} \equiv \mathcal{F}_Q[\rho, H_i, H_j]$, following the definition (5.10).

In the two-parameter estimation problem, \mathcal{F} is a 2×2 matrix and the precision bound for the estimation of the gradient is the following,

$$(\Delta b_1)^{-2} \leq \mathcal{F}_{11} - \frac{\mathcal{F}_{01}\mathcal{F}_{10}}{\mathcal{F}_{00}}, \quad (5.22)$$

where \mathcal{F}_{ij} denotes the QFI matrix elements. One must estimate both parameters in most cases since the precision of one depends on the other. The bound is interpreted slightly different from the one-parameter Cramér-Rao bound. In order to be able to saturate the bound the measurements for estimating the two parameters must compatible [40].

To compute the bound (5.21) we need to consider the matrix elements of QFI one by one. First of all, we compute \mathcal{F}_{11} that without assuming anything else has the same form as Equation (5.21)

$$\mathcal{F}_{11} = \sum_{n,m}^N \int d^N \mathbf{x} P_N(\mathbf{x}) x_n x_m \mathcal{F}_Q[\rho_s, j_z^{(n)}, j_z^{(m)}]. \quad (5.23)$$

Second, the most trivial matrix element is \mathcal{F}_{00} which is a function of the internal state ρ_s . To compute

it one must notice that

$$\begin{aligned}
 (H_0)_{\mathbf{x},k,\mathbf{y},k'} &= \langle \mathbf{x}, k | H_0 | \mathbf{y}, k' \rangle \\
 &= \langle \mathbf{x}, k | J_z | \mathbf{y}, k' \rangle \\
 &= \delta(\mathbf{x} - \mathbf{y})(H_0)_{k,k'}.
 \end{aligned} \tag{5.24}$$

And with this it is straightforward to obtain

$$\mathcal{F}_{00} = \mathcal{F}_Q[\rho_s, J_z]. \tag{5.25}$$

Note that this is not a function of the whole state but only of the internal ρ_s state. Finally, we compute both \mathcal{F}_{01} and \mathcal{F}_{10} . To compute this, one may notice first that both matrix elements are equal, $\mathcal{F}_{01} = \mathcal{F}_{10}$. Therefore we have to compute only one of them. The computation follows,

$$\mathcal{F}_{01} = \sum_{n=1}^N \int d^N \mathbf{x} P_N(\mathbf{x}) x_n \mathcal{F}_Q[\rho_s, j_z^{(n)}, J_z]. \tag{5.26}$$

With those results the Equation (5.31) follows. For further details see Appendix ??.

For the last part of the proof, we need to show that his bound is invariant under translations as it is the Equation (5.21). With this aim, using the linearity of the last two arguments of $\mathcal{F}_Q[\rho, A, B]$, Eq. (5.12), the fact that H_0 remains unchanged on the Heisenberg picture and using the shifted H_1 operator, Eq. (5.19), we have that

$$\mathcal{F}_{00}(d) = \mathcal{F}_Q[\rho, H_0(d)] = \mathcal{F}_Q[\rho, H_0], \tag{5.27}$$

$$\begin{aligned}
 \mathcal{F}_{01}(d) &= \mathcal{F}_Q[\rho, H_0(d), H_1(d)] \\
 &= \mathcal{F}_Q[\rho, H_0, H_1 - dH_0] = \mathcal{F}_{01} - d\mathcal{F}_{00},
 \end{aligned} \tag{5.28}$$

$$\begin{aligned}
 \mathcal{F}_{11}(d) &= \mathcal{F}_Q[\rho, H_1(d), H_1(d)] \\
 &= \mathcal{F}_Q[\rho, H_1 - dH_0, H_1 - dH_0] \\
 &= \mathcal{F}_{11} - 2d\mathcal{F}_{01} + d^2\mathcal{F}_{00}.
 \end{aligned} \tag{5.29}$$

Simple algebra shows that the bound for a displaced system is the same bound as is it would not be

displaced,

$$\begin{aligned}
 (\Delta b_1)^{-2} &\leq \mathcal{F}_{11}(d) - \frac{(\mathcal{F}_{01}(d))^2}{\mathcal{F}_{00}} \\
 &= \mathcal{F}_{11} - 2d\mathcal{F}_{01} + d^2\mathcal{F}_{00} \\
 &\quad - \frac{\mathcal{F}_{01}^2 - 2d\mathcal{F}_{01}\mathcal{F}_{00} + d^2\mathcal{F}_{00}^2}{\mathcal{F}_{00}} \\
 &= \mathcal{F}_{11} - \frac{\mathcal{F}_{01}^2}{\mathcal{F}_{00}}.
 \end{aligned} \tag{5.30}$$

Hence, the Observation XXX holds.

For states of the form Equations (5.3, 5.4), the expression to compute the precision bound takes the following form,

$$\begin{aligned}
 (\Delta b_1)^{-2} &\leq \sum_{n,m}^N \int d^N \mathbf{x} P_n(\mathbf{x}) x_n x_m \mathcal{F}_Q[\rho_s, j_z^{(n)}, j_z^{(m)}] \\
 &\quad - \frac{\left(\sum_{n=1}^N \int d^N \mathbf{x} P_n(\mathbf{x}) x_n \mathcal{F}_Q[\rho_s, j_z^{(n)}, J_z] \right)^2}{\mathcal{F}_Q[\rho_s, J_z]}.
 \end{aligned} \tag{5.31}$$

Despite it seems to be complicated, this equation is easily computed for the most common cases such as trapped-ions, cold atomic ensembles the like. This bound as well as Equation (5.21) is invariant under spatial translations of the system.

This observations make the computation of the next sections easier since the now we can place the system arbitrarily wherever we choose. It also allows us to place the origin of our coordinate system where the magnetic field is null. So, the linear magnetic field can be written as $\mathbf{B}(x) = xB_1\mathbf{k}$ where \mathbf{k} is the unitary vector pointing on the z -direction perpendicular to x - and y -axis, making the estimation of the homogenous field irrelevant to compute the precision of the gradient parameter b_1 . Despite the redundant arguments used before, the discourse we have had on the preceding section has a vital importance to understand properly the gradient metrology on this context.

5.2 Ion chains and two separated ensembles for magnetometry

Despite the powerfulness of our tools it is always nice to start with simple but concise examples to see how the results developed on the previous chapter behave. For this goal we choose two state-of-the-art systems for the external states which a priori we know that behave well under the gradient interferometry.

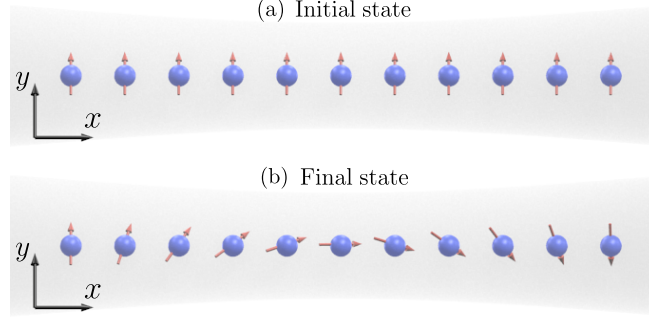


Figure 5.1: A one-dimensional chain of spin- j atoms (blue circles) confined in a potential (grey area). (a) The ensemble is initially totally polarised along a perpendicular direction of the magnetic field B_z and the direction of the chain. The internal state can be written as $|j\rangle_y^{\otimes N}$, the number represents m_y the eigenvalue of the one particle operator $j_y^{(n)}$. (b) One can see how the gradient field affects with a varying field strength the different spins when they are placed in different positions.

The first spatial state will be given by N distinguishable ions all placed to a constant distance from the neighbor constituents on a single dimensional configuration, i.e, an ion-chain [Sanah's paper], see Figure 5.1. We have that for that matter the PDF describing the system is

$$P_N(\mathbf{x}) = \prod_{n=1}^N \delta(x_n - na). \quad (5.32)$$

With this at hand we compute the single point averages and the two point averages corresponding to the ion-chain. For the single point average we have that

$$\int d^N \mathbf{x} P_N(\mathbf{x}) x_n = na, \quad (5.33)$$

and for the two point average we have the following,

$$\int d^N \mathbf{x} P_N(\mathbf{x}) x_n x_m = nma^2. \quad (5.34)$$

We are going to compute the precision bound when the internal state is a product state of all particles pointing onto y -direction, $|j\rangle_y^{\otimes N}$, which is a state sensitive to the homogeneous field, so we

have

$$\begin{aligned}
 (\Delta b_1)^{-2} &\leq \sum_{n,m}^N n m a^2 \mathcal{F}_Q[|j\rangle_y^{\otimes N}, j_z^{(n)}, j_z^{(m)}] \\
 &\quad - \frac{\left(\sum_{n=1}^N a n \mathcal{F}_Q[|j\rangle_y^{\otimes N}, j_z^{(n)}, J_z] \right)^2}{\mathcal{F}_Q[|j\rangle_y^{\otimes N}, J_z, J_z]} \\
 &= a^2 \left\{ \sum_{n=1}^N 2jn^2 - \frac{(\sum_{n=1}^N 2jn)^2}{2jN} \right\} \\
 &= 2a^2 jN \frac{N^2 - 1}{12},
 \end{aligned} \tag{5.35}$$

where we have used the $\mathcal{F}_Q[|\psi\rangle, A, B] = 4(\langle AB \rangle - \langle A \rangle \langle B \rangle)$ identity to compute the calculations.

Despite that Equation (5.35) is a third order function of the particle number N and that it seems to overcome the ultimate limit HL, one should notice that the length of the chain increases as we introduce more particles into the system. To solve this one can normalize the distance between the atoms or simply use some measure of spatial width of the complete system. In our case we decide to use on all results the standard deviation of the averaged particle position as the length measure. It is computed as follows,

$$\mu = \int d^N \mathbf{x} P_N(\mathbf{x}) \frac{\sum_{n=1}^N x_n}{N} \tag{5.36}$$

$$\sigma^2 = \int d^N \mathbf{x} P_N(\mathbf{x}) \frac{\sum_{n=1}^N x_n^2}{N} - \mu^2 \tag{5.37}$$

$$\sigma_{\text{ch}}^2 = a^2 \frac{N^2 - 1}{12}. \tag{5.38}$$

It turns out that this exactly coincides with a factor we have on Equation (5.35). Substituting this onto the result the proof concludes.

For ion-chains where their constituents are separated by a constant distance and where the spin-state ρ_s is the totally polarised state along a perpendicular direction of both the field and the chain direction, in this case y -direction, the precision bound is given by the following formula,

$$(\Delta b_1)^{-2} \leq 2\sigma_{\text{ch}}^2 jN, \tag{5.39}$$

where σ_{ch} denotes the standard deviation of whole position spots on which the particles rest, j is the spin-number of each particle and N is the particle-number.

We continue this illustrative example with the state-of-the-art double-well spatial state. We also will use an internal state that with the maximal QFI so the reader gets familiar with our approach and sees how the best state to measure the gradient parameter looks like on our framework.

The spatial part is described by the following PDF where half of the particles are in one-well and the rest in the other, placed both positions at a distance of a from the origin,

$$P_N(\mathbf{x}) = \prod_{n=1}^N \delta(x_n + (-1)^n a), \quad (5.40)$$

where the "odd" particles go to the "right" and the "even" particles to the "left". With this we are able to compute the single-point and two-point correlation functions as,

$$\int d^N \mathbf{x} P_N(\mathbf{x}) x_n = (-1)^{n+1} a, \quad (5.41)$$

$$\int d^N \mathbf{x} P_N(\mathbf{x}) x_n x_m = (-1)^{n+m} a^2. \quad (5.42)$$

The state $|\psi\rangle$ is insensitive to the homogeneous field so we have that

$$\begin{aligned} (\Delta b_1)^{-2}|_{\max} &= \sum_{n,m}^N (-1)^{n+m} a^2 \mathcal{F}_Q[|\psi\rangle, j_z^{(n)}, j_z^{(m)}] \\ &= a^2 \sum_{n,m}^N (-1)^{n+m} 4(-1)^{n+m} j^2 \\ &= 4a^2 j^2 N^2, \end{aligned} \quad (5.43)$$

where we have used the definition for pure states of QFI, $4(\langle j_z^{(n)} j_z^{(m)} \rangle - \langle j_z^{(n)} \rangle \langle j_z^{(m)} \rangle)$.

On the other hand if we compute now the standard deviation as we did before for the case of the chain, Eqs. (5.36–5.38), we have that in this case $\mu = 0$ and the standard deviation

$$\sigma_{\text{dw}}^2 = \int d^N \mathbf{x} P_N(\mathbf{x}) = a^2, \quad (5.44)$$

with which the proof follows. Before concluding the proof we want to show another more usual approach to the same problem.

It is as follows, given that the QFI is convex on states and having already fixed the external spatial state to be Equation (5.40), the inner state that maximises the QFI is the one that maximises $(\Delta H_1)^2$. In this case, taking into account the particle locations and that we have zero magnetic field at the

origin,

$$H_{1,\text{eff}} = b_1 a (\mathbb{I}_{\text{od}} \otimes J_{z,\text{ev}} - J_{z,\text{od}} \otimes \mathbb{I}_{\text{ev}}), \quad (5.45)$$

where we write the effective Hamiltonian that the particles feel and "od" and "ev" stand for odd and even particle index respectively. From here it is easy to show that the state maximising such variance is the following,

$$|\psi\rangle = \frac{1}{\sqrt{2}}(|0 \cdots 0\rangle_{\text{od}} \otimes |1 \cdots 1\rangle_{\text{ev}} + |1 \cdots 1\rangle_{\text{od}} \otimes |0 \cdots 0\rangle_{\text{ev}}), \quad (5.46)$$

which is equivalent to the state in Equation (5.47). This proves that we have used the right state, and with this we can compute the QFI as in the literature as $\mathcal{F}_Q[|\psi\rangle, H_1] = 4(\Delta H_1)^2 = 4a^2 j^2 N^2$. With this we finally conclude the proof.

The maximally entangled internal state that maximized the QFI too is

$$|\psi\rangle = \frac{1}{\sqrt{2}}(|0101 \cdots 01\rangle + |1010 \cdots 10\rangle). \quad (5.47)$$

Notice that this is a coherent state of all particles on the left "up" and all on the right "down" plus all on the left "down" and all on the right "up". We will choose without loss of generality the particles to be spin- j particles. For this state insensitive to the homogeneous field and in the double-well spatial configuration, Eq. (5.40), the maximal achievable precision is

$$(\Delta b_1)^{-2}|_{\text{max}} = 4\sigma_{\text{dw}}^2 j^2 N^2 \quad (5.48)$$

In this section we have shown to the reader how one should handle the spatial width of the system for classifying it for gradient metrology as well as a state-of-the-art system on which the Heisenberg limit is achieved. Moreover, we have shown how to use the tools developed on previous section to compute simple bounds. In the next section we will focus on single cold-atoms ensembles since they play an important role on today's quantum technology and experiments and many groups are trying to realize them with great success but with few theoretical support from our point of view.

5.3 Magnetometry with an atomic ensemble

In this section, we discuss magnetometry with a single atomic ensemble in a more deep way than in the previous section. For that, we present precision bounds for the estimation of the magnetic field gradient, for states that are insensitive to the homogeneous field. We also present precision bounds for states that are sensitive to the homogeneous field. We consider a one-dimensional cloud of spin- j

atoms placed in a one dimensional trap, which is elongated in the x -direction. The magnetic field points in the z -direction, and has a constant gradient along the x -direction. The setup is depicted in Fig. ???. In the last part of this section, we calculate precision bounds for the gradient estimation for some important multi-particle quantum states, for instance, Dicke states or Greenberger-Horne-Zeilinger (GHZ) states [9]. Note that all these states are permutationally invariant (PI), since we assume a PI procedure to prepare the states.

5.3.1 Precision bound for an atomic ensemble

An atomic ensemble is defined as a finite number of atoms where they cannot be labeled individually. Thus, the initial quantum state is assumed to be PI. Hence apart from ρ_s , the probability distribution function $P_N(\mathbf{x})$, appearing in Equation (??), must also be PI. The permutational invariance of $P_N(\mathbf{x})$ implies that

$$P_N(\mathbf{x}) = \frac{1}{N!} \sum_k \Pi_k[P_N(\mathbf{x})], \quad (5.49)$$

where the summation is over all the possible permutations of the variables x_n denoted by Π_k .

As we have shown on Observations XXX and XXX, the precision bound is invariant under translations on the spatial Hilbert space. This allows us to place the "center of mass" of the system at the origin of the coordinates. With this simplifying assumptions the single-point average of the whole ensemble is

$$\mu = \int d^N \mathbf{x} P_N(\mathbf{x}) x_n = 0, \quad (5.50)$$

where we used the PI nature of $P_n(\mathbf{x})$ to eliminate the sum and the N from the Equation (5.36). We will do the same with the second moments appearing on the variance, Eq. (5.37). Because of this, the size of the system can be related with the single variable, x_n , variance

$$\sigma^2 = \int P_N(\mathbf{x}) x_n^2 d^N \mathbf{x}, \quad (5.51)$$

for any n , which is simplified due to the fact that the system is placed at the origin. In the same way, and due again to the PI nature of $P_N(\mathbf{x})$ we write the covariance of two particle positions as

$$\eta = \int P_N(\mathbf{x}) x_n x_m d^N \mathbf{x} \quad (5.52)$$

for any $n \neq m$. With this we have characterised all two-points correlations that potentially will appear on our calculations. An interesting property of the covariance of this type is that it is a value bounded from below and from above by the variance itself and the particle number N in the following

way,

$$\frac{-\sigma^2}{N-1} \leq \eta \leq \sigma^2. \quad (5.53)$$

So it cannot contribute for a better scaling on the precision than since it scales as much as σ^2 with the particle number. Notice that the lower bound scales worse.

First of all we show an important property of states insensitive to the homogeneous field and we do so using the fact that the QFI for the homogeneous field generator, i.e. J_z , on those states is zero, $\mathcal{F}_Q[\rho, J_z] = 0$. The identity follows,

$$\begin{aligned} \mathcal{F}_Q[\rho, J_z] &= 0 \\ \sum_{n,m}^N \mathcal{F}_Q[\rho, j_z^{(n)}, j_z^{(m)}] &= 0 \\ \sum_{n=1}^N \mathcal{F}_Q[\rho, j_z^{(n)}] &= - \sum_{n \neq m}^N \mathcal{F}_Q[\rho, j_z^{(n)}, j_z^{(m)}] \end{aligned} \quad (5.54)$$

where we use the linearity on the second and third arguments of $\mathcal{F}_Q[\rho, \cdot, \cdot]$ to jump to the second line and subsequently the last line follows.

From the definition of the QFI for states insensitive to the homogeneous field, Eq. (5.21), we compute the bound for single ensembles in the following way,

$$\begin{aligned} (\Delta b_1)^{-2}|_{\max} &= \sum_{n,m}^N \int d^N \mathbf{x} P_N(\mathbf{x}) x_n x_m \mathcal{F}_Q[\rho_s, j_z^{(n)}, j_z^{(m)}] \\ &= \sum_{n=1}^N \sigma^2 \mathcal{F}_Q[\rho, j_z^{(n)}] + \sum_{n \neq m}^N \eta \mathcal{F}_Q[\rho, j_z^{(n)}, j_z^{(m)}]. \end{aligned} \quad (5.55)$$

Together with Equation (5.54) the Observation ?? follows.

The precision is bounded from below for a single atomic ensemble insensitive to homogeneous field with the following quantity

$$(\Delta b_1)^{-2}|_{\max} = (\sigma^2 - \eta) \sum_{n=1}^N \mathcal{F}_Q[\rho_s, j_z^{(n)}]. \quad (5.56)$$

The bound in Eq. (5.56) can be saturated by an optimal measurement. Nevertheless, it is worth to notice that it cannot surpass the shot-noise scaling, $\sim N$, because $\mathcal{F}_Q[\rho_s, j_z^{(n)}]$, the QFI for the single-particle operator $j_z^{(n)}$, cannot be larger than j^2 .

First of all, notice that the second term appearing on Equation (5.31) is proportional to the single-point average $\int d^N \mathbf{x} P_N(\mathbf{x}) x_n$ which by definition is the same for any x_n and by decision is chosen to be zero, since we placed the system at the origin. So, we only have to compute the first term of the Equation (5.31),

$$\begin{aligned}
 (\Delta b_1)^{-2} &\leq \sum_{n,m}^N \int d^N \mathbf{x} P_n(\mathbf{x}) x_n x_m \mathcal{F}_Q[\rho_s, j_z^{(n)}, j_z^{(m)}] \\
 &= \sum_{n=1}^N \sigma^2 \mathcal{F}_Q[\rho, j_z^{(n)}] + \sum_{n \neq m}^N \eta \mathcal{F}_Q[\rho, j_z^{(n)}, j_z^{(m)}] \\
 &= (\sigma^2 - \eta) \sum_{n=1}^N \mathcal{F}_Q[\rho, j_z^{(n)}] + \eta \sum_{n,m}^N \mathcal{F}_Q[\rho, j_z^{(n)}, j_z^{(m)}],
 \end{aligned} \tag{5.57}$$

where we add to the last term $\eta \sum_{n=1}^N \mathcal{F}_Q[\rho, j_z^{(n)}]$ and subtract it from the first term. From this, using the fact that the QFI is linear on the second and third arguments again, the proof holds.

For states sensitive to homogeneous fields, the precision of estimating the gradient is bounded from above as

$$(\Delta b_1)^{-2} \leq (\sigma^2 - \eta) \sum_{n=1}^N \mathcal{F}_Q[\rho_s, j_z^{(n)}] + \eta \mathcal{F}_Q[\rho_s, J_z]. \tag{5.58}$$

The second term on the right-hand side of Eq. (5.58) is new in the sense that it did not appear on the bound for states insensitive to homogeneous fields. Note that the bound in Eq. (5.58) is not necessarily saturable if the optimal measurements to estimate the gradient parameter and the homogeneous parameter do not commute with each other. This question will be discussed in Appendix ???. Note that even if the first term cannot overcome the SL, in the second term the covariance is multiplied by QFI for estimating the homogeneous field and therefore this concrete term can make the bound, for extremely correlated particle positions, to scale as HL.

5.3.2 Precision limit for various spin-states

In this section, we present the precision limits for different classes of important quantum states such as the totally polarised state, the state having the largest precision among separable state, or the singlet state. We see how the precision bounds presented before, Eqs. (5.56, 5.58), are implemented. We show first the results for singlet that are insensitive to homogeneous fields. In this case, the bounds can be achieved by choosing the appropriate magnitude to measure. The rest of the results are for states sensitive to homogeneous fields which in general are not necessarily achievable bounds.

Singlet states

We consider now the singlet state, which is invariant under the influence of a homogeneous field along any direction. So we have to compute the formula for the bound of the precision Eq. (5.56), and we already know that it can be saturated for a certain optimal measurement.

A singlet state is an eigenstate of the collective J_z and J^2 operators, with an eigenvalue zero in both cases. Since this subspace is degenerate we have to take care in order to compute the precision bound. There are many different singlet states for an ensemble of N spin- j particles, and still a great amount of them are PI. Surprisingly the precision bound we compute is the same for any PI singlet. Atomic ensembles in a singlet state have been experimentally created with cold gases [29, 53].

In an N -particle system, there are several singlets pairwise orthogonal to each other. The number of such singlets, D_0 , depends on the particle spin j and the number of particles N .

The most general singlet state can be written in the total angular momentum basis, using D to label the degenerate states, $|J, M_z, D\rangle$, in the following diagonal way

$$\rho_s = \sum_{D=1}^{D_0} \lambda_D |0, 0, D\rangle \langle 0, 0, D|, \quad (5.59)$$

where $\sum_D \lambda_D = 1$. In its complete form the eigenvalues of the spin density matrix are $\lambda_{J, M_z, D} = \delta_{0, J} \lambda_D$.

Looking at Eq. (5.56), we must compute the generalized QFI for the one-particle operator $j_z^{(n)}$ in order to compute the precision bound for PI singlet states. For that purpose we use the fact that when $j_z^{(n)}$ acts on a singlet state, it produces a state outside of the singlet subspace. This can be proved by noting that

$$e^{i\pi J_x} j_z^{(n)} e^{-i\pi J_x} = -j_z^{(n)} \quad (5.60)$$

and that $e^{-i\pi J_x} |0, 0, D\rangle = |0, 0, D\rangle$ holds for any pure singlet state. Employing these equalities, we can arbitrarily flip the sign of $j_z^{(n)}$ so

$$\langle 0, 0, D | j_z^{(n)} | 0, 0, D' \rangle = -\langle 0, 0, D | j_z^{(n)} | 0, 0, D' \rangle, \quad (5.61)$$

which implies

$$\langle 0, 0, D | j_z^{(n)} | 0, 0, D' \rangle = 0, \quad (5.62)$$

for any pair of pure singlet singlet states.

In order to compute the QFI for the singlet state we use Eq. (5.13). Hence we can write the

following for the second term on Eq. (5.13),

$$8 \sum_{D,D'} \frac{\lambda_D \lambda_{D'}}{\lambda_D + \lambda_{D'}} |\langle 0, 0, D | j_z^{(n)} | 0, 0, D' \rangle|^2 = 0. \quad (5.63)$$

It follows that the QFI for any singlet is indeed simply

$$\mathcal{F}_Q[\rho_s, j_z^{(n)}] = 4 \text{tr}(\rho_s (j_z^{(n)})^2). \quad (5.64)$$

For the last part of the proof, we must compute the expectation value of the operator $(j_z^{(n)})^2$. For that we have that

$$\text{tr}(\rho_s (j_k^{(n)})^2) = \text{tr}(\rho_s (j_l^{(n)})^2), \quad (5.65)$$

for any pair $k, l \in x, y, z$ due to the rotational invariance of the singlet, i.e, all the singlets remain invariant under a $SU(2)$ transformation of the kind $U = e^{i\phi \vec{J} \cdot \vec{n}}$, where \vec{n} is an unitary vector belonging to the positional space. We also have that

$$\langle (j_x^{(n)})^2 + (j_y^{(n)})^2 + (j_z^{(n)})^2 \rangle = j(j+1), \quad (5.66)$$

for any state, since it represent the spin number of the particle, which is fixed. Hence, the expectation value of $(j_z^{(n)})^2$ on the singlet is

$$\text{tr}(\rho_s (j_z^{(n)})^2) = \frac{j(j+1)}{3}, \quad (5.67)$$

for all the singlets. Inserting this into Eq. (5.64), we obtain $\mathcal{F}_Q[\rho_s, j_z^{(n)}] = \frac{4j(j+1)}{3}$; and by Eq. (5.56) the statement is proved.

For PI spin states living in the singlet subspace, i.e., states composed of vectors that have zero eigenvalues for J_z and J^2 and all their possible statistical mixtures, the precision of the magnetic gradient parameter is bounded from above as

$$(\Delta b_1)_{\max}^{-2} = \frac{4Nj(j+1)}{3} (\sigma^2 - \eta). \quad (5.68)$$

As mentioned earlier, singlet states are insensitive to homogeneous magnetic fields, hence determining the gradient leads to a single-parameter estimation problem. This implies that there is an optimal operator that saturates the precision bound given by Eq. (5.68). However, it is usually very hard to find this optimal measurement, although a formal procedure for this exists [40]. In Ref. [39], a particular set-up for determining the magnetic gradient with PI singlet states was suggested by the

measurement of the J_x^2 collective operator. For this scenario the precision is given by

$$(\Delta b_1)^{-2} = \frac{|\partial_{b_1} \langle J_x^2 \rangle|^2}{\langle J_x^4 \rangle - \langle J_x^2 \rangle^2}. \quad (5.69)$$

In Appedix ??, we show that this measurement actually provides, in the short-time limit, an optimal precision for gradient metrology.

Totally polarised state

The totally polarised state can easily be prepared experimentally. It has already been used for gradient magnetometry with a single atomic ensemble [35, 37]. For the gradient measurement as for the measurement of the homogeneous field, the polarisation must be perpendicular to the field we want to measure in order to take advantage of the interaction between the particles and the field. Here we chose as before the totally polarized state along the y -axis which is written as $|j\rangle_y^{\otimes N}$. Notice that this state is a state sensitive to the homogeneous field, hence, we must use the Equation (5.58) to compute the bound.

For the pure product states we have that $\mathcal{F}_Q[|\psi\rangle, A] = 4(\Delta A)^2$. Together with, $(\Delta J_z^{(n)})^2 = j/2$ and $(\Delta J_z)^2 = Nj/2$, when the polarisation is perpendicular to the z -direction, the precision will be computed straightforward from Equation (5.58).

Before to do so, let us comment on the heuristics description of the evolution of the system. The homogeneous field rotates all spins by the same angle, while the gradient rotates the spin at different position by a different angle. Due to that, the homogeneous field rotates the collective spin, but does not change its absolute value. On the other hand, the field gradient decreases the absolute value of the spin, which has been used in Ref. [38] for gradient magnetometry, see Fig. 5.1.

Therefore, the Cramér-Rao bound fixes the highest value for the precision of the totally polarised state as follows,

$$(\Delta b_1)^{-2} \leq 2Nj\sigma^2. \quad (5.70)$$

Note that the precision bound for the totally polarised state is smaller than that of the optimal separable state we present later on. We can see clearly that the precision scales as $\mathcal{O}(N)$.

The best separable state

We will now turn our attention to the precision bound for all separable spin states. It is useful to obtain this value so we have a direct comparison of what is the best classically achievable precision.

It will turn out that for $j > \frac{1}{2}$, it is possible to achieve a precision higher than with the fully polarised state. We use the Equation (5.50) and substituting it onto the the low-level definitions of the precision bounds for the gradient magnetometry, Eqs. (5.21, 5.31). We see that if the state is sensitive to the homogeneous field only affects on the implications of the bound, one can be saturated for sure and on the other case it depends on the measurements compatibility as we discussed before. What we have is that the bound is the same $\mathcal{F}_Q[\rho, H_1]$ for both cases. Thus, it is easy to argue that the precision bound is a convex function on the states, even when the external state ρ_x is fixed. Therefore, the separable inner state that maximizes the precision must be a pure product state that maximises all possible $\mathcal{F}_Q[\rho_s, j_z^{(n)}, j_z^{(m)}]$. For pure product states we have first that $\mathcal{F}_Q[\rho_s, j_z^{(n)}, j_z^{(m)}]$ is four times the correlation between the single particle spin operators, which using the well known properties of the pure product states is zero when $n \neq m$. Finally, we have to maximise each $4(\Delta j_z^{(n)})^2$.

As we mentioned before, the best possible precision bound will be reached for a pure product state that maximises all $(\Delta j_z^{(n)})^2$. From the definition of the variance,

$$(\Delta j_z^{(n)})^2 = \langle (j_z^{(n)})^2 \rangle - \langle j_z^{(n)} \rangle^2. \quad (5.71)$$

Hence, We try a state that approaches to zero its polarisation on the z-direction and maximises $\langle (j_z^{(n)})^2 \rangle$. We have that $|\psi\rangle = (|+j\rangle + |-j\rangle)/\sqrt{2}$ is ideal for this. The inner state for all particles is just the product state $\rho_s = |\psi\rangle\langle\psi|^{\otimes N}$. Notice that this state is permutationally invariant, hence it is a tight bound for what can be achieved with PI separable states. The variance of a single particle operator is $(\Delta j_z^{(n)})^2 = j^2$ so the proof holds.

After this discussion we make the following observation. The best achievable precision for separable states is written as

$$(\Delta b_1)^{-2} \leq 4Nj^2\sigma^2, \quad (5.72)$$

where the state itself is sensitive to homogeneous fields. This bound coincides with the totally polarized state studied before when the spin number j is equal to half.

In the following we try to find a better precision bound making use of presumably better entangled states. Note that the bound for the singlet state, even if it is entangled, is above the bound for the totally polarised state but below of the bound defined for the best separable state. Nevertheless, when the singlet state is used effect of the homogeneous magnetic field has not to be compensated since it is insensitive to it and thus the bound can be saturated with an optimal estimator for the gradient field.

The unpolarised Dicke states $|Nj, 0\rangle$ and $|Nj, 0\rangle_x$

Unpolarised Dicke states play an important role in quantum optics and quantum information science. The Dicke state $|Nj, 0\rangle_l$ with a maximal $\langle J_x^2 + J_y^2 + J_z^2 \rangle$ and $\langle J_l \rangle = 0$ for any $l \in x, y, z$ is particularly interesting due to its entanglement properties and its metrological usefulness. This state has been created in photonic experiments [22, 23, 25] and in cold atoms [27, 54], while a Dicke state with $\langle J_z \rangle > 0$ has been created with cold trapped ions [55].

The Dicke state $|Nj, 0\rangle$ is an eigenstate of J_z so insensitive to homogeneous magnetic field pointing into the z -direction, thus the precision can be saturate by some measurement. Whereas, The Dicke state $|Nj, 0\rangle_x$ is sensitive to the homogeneous field. Moreover it is very useful for homogeneous magnetometry as it has been shown in Reference [XXX]. Here we consider large particle numbers, to make the results simpler.

Since both Dicke states are pure, we have that the QFI appearing on Equations (5.56, 5.58) are simply four times the following variances of $j_z^{(n)}$ and J_z . Since both Dicke states are unpolarized, all the first moments $\langle J_l \rangle$ are equal to zero and due to they are PI all $\langle j_l^{(n)} \rangle$ are also zero for all $l \in x, y, z$. Therefore, we only need to compute the second moments to compute the variances.

We will compute all the second moments on all directions of single particle operators $j_l^{(n)}$ as well as the global operators J_l for $|Nj, 0\rangle$. Later on, we will map those result to the Dicke state for the x -direction. We have the following characteristic identities for $|Nj, 0\rangle$, $\langle J_z^2 \rangle = 0$ and $\langle J_{\perp z}^2 \rangle = \frac{Nj(Nj+1)}{2}$ where " $\perp z$ " can be seen as x or y . From the global second moments we can write for the single particle the following,

$$\langle (j_z^{(n)})^2 \rangle = -(N-1) \langle j_z^{(n)} j_z^{(m)} \rangle \quad (5.73)$$

$$\langle (j_{\perp z}^{(n)})^2 \rangle = \frac{j(Nj+1)}{2} - (N-1) \langle j_{\perp z}^{(n)} j_{\perp z}^{(m)} \rangle \quad (5.74)$$

for all $\forall n \neq m$ due to the PI nature of the state. Together with $\langle (j_z^{(n)})^2 + 2(j_{\perp z}^{(n)})^2 \rangle = j(j+1)$ due to the rotational symmetry along the z -axis, we have three independent equations relating all the four moments. In Reference [39], a mapping between the Dicke states of spin- j ensembles and of spin- $\frac{1}{2}$ ensembles was provided, by which the expectation value

$$\langle (j_z^{(n)})^2 \rangle = \frac{(N-1)j^2}{2jN-1} \quad (5.75)$$

was derived. With this we are able to obtain all the rest unknown values we are searching for. In the large N limit, this gives

$$\lim_{N \rightarrow \infty} \langle (j_z^{(n)})^2 \rangle = \frac{j}{2}. \quad (5.76)$$

From Eq. (5.56) we can conclude that $\mathcal{F}_Q[\rho_s, j_z^{(1)}] = 2j$, hence the proof for homogeneous insensitive

$|Nj, 0\rangle$ holds.

Now we have only to apply a mapping between the x - and z -axis to obtain the respective second moments for $|Nj, 0\rangle_x$. We do that on the large N limit,

$$\lim_{N \rightarrow \infty} \langle (j_z^{(n)})^2 \rangle = \frac{j(2j+1)}{4}. \quad (5.77)$$

Finally, we have all the ingredients to go forward on writing the precision bound.

For large N , the precision bound for the Dicke $|Nj, 0\rangle$ state is

$$(\Delta b_1)_{\max}^{-2} = 2Nj(\sigma^2 - \eta), \quad (5.78)$$

whereas for the homogeneous sensitive Dicke state $|Nj, 0\rangle_x$ the precision is bounded from above by

$$(\Delta b_1)^{-2} \leq Nj(2j+1)(\sigma^2 - \eta) + 2Nj(Nj+1)\eta, \quad (5.79)$$

which shows in principle a Heisenberg behavior in the second term on the right-hand side.

The GHZ state

The Greenberger-Horne-Zeilinger (GHZ) states are also highly entangled states that play an important role in quantum physics [9]. They have been created experimentally in photonic systems [10, 12, 56] and trapped ions [14, 15].

The GHZ state is defined for qubits in the following way

$$|\text{GHZ}\rangle = \frac{1}{\sqrt{2}}(|0 \cdots 0\rangle + |1 \cdots 1\rangle). \quad (5.80)$$

This state is very sensitive to the homogeneous field. On the other hand, as shown in Appendix ??, for this state the optimal estimators for the homogeneous field and the gradient field are compatible. It means that both parameters can be estimated at once. Hence, in this case, the bound given in Eq. (5.58) can be saturated by some measurement set-up. In order to calculate this bound explicitly, let us recall that for pure states the QFI is simplified to Eq. (5.14). In the GHZ state the expectation value of $j_z^{(n)}$ and J_z is equal to zero, as it was for the Dicke state, and $\langle (j_z^{(n)})^2 \rangle = j^2$ and $\langle J_z^2 \rangle = N^2 j^2$, hence we obtain the following result

$$(\Delta b_1)_{\max}^{-2} = 4Nj^2\sigma^2 + 4N(N-1)j^2\eta. \quad (5.81)$$

This means that we can reach the Heisenberg-limit with such states, but only in cases where η is

Singlet states	$(\Delta b_1)^{-2} _{\max} = \frac{4Nj(j+1)}{3} (\sigma^2 - \eta)$
Totally polarised state	$(\Delta b_1)^{-2} \leq 2N\sigma^2 j$
Best separable state	$(\Delta b_1)^{-2} \leq 4N\sigma^2 j^2$
$ Nj, 0\rangle$ Dicke state	$(\Delta b_1)^{-2} _{\max} = \frac{Nj}{2} (\sigma^2 - \eta)$
$ Nj, 0\rangle_x$ Dicke state	$(\Delta b_1)^{-2} \leq N(\sigma^2 - \eta)(2j^2 + j) + 2\eta Nj(Nj + 1)$
GHZ state	$(\Delta b_1)^{-2} _{\max} = 4Nj^2(\sigma^2 + (N - 1)\eta)$

Table 5.1: Precision bounds for differential magnetometry for various quantum states. For the definition of the states, see the text. If the bound are proved to be saturable then the $\max_{\text{subscript}}$ is used instead of an inequality.

positive, i.e, that the particles stay spatially correlated.

Summary of results

Finally, we summarise the precision bounds obtained for various quantum states in Table 5.1. In Fig. 5.2, we show the mean values and variances of the collective angular momentum components for these states.

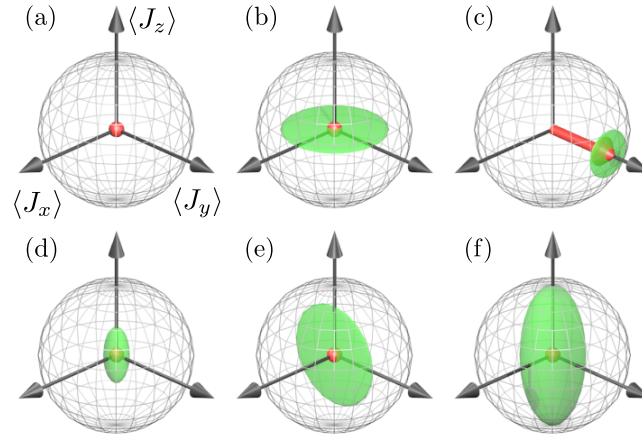


Figure 5.2: Angular momentum components and their variances for various quantum states. The mean value of the collective angular momentum \mathbf{J} is represented by a red dot or arrow. The radius of the sphere is the maximal angular momentum, $r = Nj$. The green uncertainty ellipses describe the uncertainties of the spin components. In this case are represented different states for few particles due to the different scaling of the variances in terms of N , namely, singlet states (a), Dicke state (b), totally polarised state (c), best separable state (d), perpendicular Dicke state (e), and the GHZ (f).

6

Conclusions

H ELLO it's me again

A. Long calculus appearing through the chapters

In this appendix we will develop long calculations appeared throughout different chapters.

A.1 Simplification of $\langle \{J_x^2, J_y^2\} + \{J_x, J_y\}^2 \rangle$

The expectation value appearing on Equation (3.13) which we want to simplify has 6 different terms, all with two J_x and another two J_y ,

$$\langle J_x^2 J_y^2 \rangle + \langle J_x J_y J_x J_y \rangle + \langle J_x J_y^2 J_x \rangle + \langle J_y J_x^2 J_y \rangle + \langle J_y J_x J_y J_x \rangle + \langle J_y^2 J_x^2 \rangle. \quad (\text{A.1})$$

From all those terms the third is somehow referent, since the pure unpolarized Dicke state used as reference is align with the x -axis, so $J_x |D_{N,N/2}\rangle_x = 0$.

We use the commutation relations of the angular momentum operators $[J_k, J_l] = \epsilon_{klm} i J_m$ to rearrange

all operators,

$$\langle J_x^2 J_y^2 \rangle = i\langle J_x J_z J_y \rangle + \langle J_x J_y J_x J_y \rangle, \quad (\text{A.2a})$$

$$\langle J_x J_y J_x J_y \rangle = i\langle J_x J_y J_z \rangle + \langle J_x J_y^2 J_x \rangle, \quad (\text{A.2b})$$

$$\langle J_x J_y^2 J_x \rangle = \langle J_x J_y^2 J_x \rangle, \quad (\text{A.2c})$$

$$\langle J_y J_x^2 J_y \rangle = i\langle J_y J_x J_z \rangle + \langle J_y J_x J_y J_x \rangle, \quad (\text{A.2d})$$

$$\langle J_y J_x J_y J_x \rangle = -i\langle J_z J_y J_x \rangle + \langle J_x J_y^2 J_x \rangle, \quad (\text{A.2e})$$

$$\langle J_y^2 J_x^2 \rangle = -i\langle J_y J_z J_x \rangle + \langle J_y J_x J_y J_x \rangle. \quad (\text{A.2f})$$

One may notice that with those relations is enough to see that we have six $\langle J_x J_y^2 J_x \rangle$, for instance, Equation (A.2a) is $i\langle J_x J_z J_y \rangle$ plus Equation (A.2b) which at the same time is $i\langle J_x J_y J_z \rangle$ plus Equation (A.3c). So each equation has at the end one $\langle J_x J_y^2 J_x \rangle$ plus or minus some expectation value of the product of three operators.

For the three terms operators and again using the commutation relations we can further simplify this expression. Trying to get one $\langle J_x J_y J_z \rangle$ on each term, we obtain the following,

$$i\langle J_x J_z J_y \rangle = \langle J_x^2 \rangle + i\langle J_x J_y J_z \rangle, \quad (\text{A.3a})$$

$$2i\langle J_x J_y J_z \rangle = 2i\langle J_x J_y J_z \rangle, \quad (\text{A.3b})$$

$$i\langle J_y J_x J_z \rangle = \langle J_z^2 \rangle + i\langle J_x J_y J_z \rangle, \quad (\text{A.3c})$$

$$-i\langle J_y J_z J_x \rangle = \langle J_y^2 \rangle - \langle J_z \rangle - i\langle J_x J_y J_z \rangle \quad (\text{A.3d})$$

$$\begin{aligned} -3i\langle J_z J_y J_x \rangle &= -3\langle J_x^2 \rangle - 3i\langle J_y J_z J_x \rangle \\ &= -3\langle J_x^2 \rangle + 3\langle J_y^2 \rangle - 3i\langle J_y J_x J_z \rangle \\ &, = -3\langle J_x^2 \rangle + 3\langle J_y^2 \rangle - 3\langle J_z^2 \rangle - 3i\langle J_x J_y J_z \rangle. \end{aligned} \quad (\text{A.3e})$$

Now if we sum it all, note that the all 3 operators terms simplify, and if we take into account $6\langle J_x J_y^2 J_x \rangle$ the resulting expression is the following,

$$4\langle J_y^2 \rangle - 3\langle J_z^2 \rangle - 2\langle J_x^2 \rangle + 6\langle J_x J_y^2 J_x \rangle \quad (\text{A.4})$$

A.2 Calculation of $|\langle D_{N,m}|_z|D_{N,N/2}\rangle_x|^2$

The Dicke state is defined in Eq: (??), for more details on angular momentum subspaces see Appendix ??
Hello this is the appendix to write about ...

A.3 Spin-squeezing Hamiltonian

B. Miscellaneous mathematical tools

In this appendix we will illustrate basic mathematical tools used all through the thesis. They are shown here because without been figures of merit of the conceptual parts involving this thesis, they are nowadays sufficiently important for any who need some support to understand the notation and basic tools properly.

B.1 Discussion on angular momentum subspaces for different spins

Here we want to show how the whole Hilbert space of the spin angular-momentum of a multi-particle spin- j systems are structured. When same kind of spin- j particles, i.e., qubits or qudits on the Quantum Information language, are the constituents of a system, several important properties and structures arise. We will explain how these Hilbert spaces are added to form a larger Hilbert space while we describe the notation used in this thesis.

First of all, we have the basic single particle d -level system or qudit. When d equals two we have the well known 2-level system or qubit. The basis of such systems have d eigenstates of the spin operator $j_z^{(n)}$, where n stands for the particle label and therefore for its own Hilbert space and the spin-number j is in each case $(d - 1)/2$. Just to remind that j integer stands for bosonic particles whereas j half integers for fermionic ones. So to say the eigenstates are characterized by

$$j_z^{(n)}|m\rangle = m|m\rangle \tag{B.1}$$

for $m = -j, -j+1, \dots, +j-1, +j$. In Quantum Information the two eigenstates $|-1/2\rangle$ and $|+1/2\rangle$ of 2-level systems, or qubits, are identified with $|0\rangle$ and $|1\rangle$ respectively, since the qubit case is the most studied case on which the dichotomized representation of classic *bits*, ones and zeros, is directly related with.

When adding particles into a bigger system convenient representation is key to compute efficiently. A first approach is to add all eigenstates one after the other and permute the states from right to left until complete the whole basis

$$\begin{aligned}
 &|-j, -j, \dots, -j, -j\rangle, \\
 &|-j, -j, \dots, -j, -j+1\rangle, \\
 &\vdots \\
 &|-j, -j, \dots, -j+1, -j\rangle, \\
 &|-j, -j, \dots, -j+1, -j+1\rangle, \\
 &\vdots \\
 &|+j, +j, \dots, +j, +j\rangle,
 \end{aligned} \tag{B.2}$$

where we have used the notation $|m_1, m_2, \dots, m_{N-1}, m_N\rangle \equiv |m_1\rangle \otimes |m_2\rangle \cdots \otimes |m_N\rangle$. This basis is still an eigenbasis of $J_z = \sum_n j_z^{(n)}$, the total angular momentum z-component. On the other hand, it is not a eigenbasis of the total angular momentum $\mathbf{J}^2 = J_x^2 + J_y^2 + J_z^2$ neither they are permutationally invariant, for instance, they are few symmetric states while there is not any anti-symmetric states. So a more convenient representation is explained here in this section.

We will explain shortly how to construct a basis on which all states from the basis are eigenstates of the total angular momentum \mathbf{J}^2 , see Ref. [1]. For that, we have the $J_{\pm} := J_x \pm iJ_y$ operators which increase or decrease eigenvalue of J_z without changing the eigenvalue of \mathbf{J}^2 . Therefore, if we start from $|-j, -j, \dots, -j\rangle$, which is an eigenstate of \mathbf{J}^2 with the maximal eigenvalue $Nj(Nj+1)$, and we apply J_+ subsequently we obtain all the states belonging to this subspace on which \mathbf{J}^2 is maximal [1]. We keep doing this until we have all the subspaces characterized. The eigenbasis can be characterized with three simple numbers $|J, M, D\rangle$, the total angular momentum number, the angular momentum projection quantum number into the z-direction, $M = -J, -J+1, \dots, +J-1, +J$, and the degeneracy number of the J subspaces, $D = 1, 2, \dots, D_J$.

We now show the definition of some of the most used states throughout this thesis. For the spin- $\frac{1}{2}$ particles, i.e., qubits, several states arose. We have all the symmetric states where m particles are in the $|1\rangle$ state and the rest $N-m$ are in $|0\rangle$. Since the symmetric subspace is not degenerated in this

case we omit the degeneracy number

$$\begin{aligned}
 |J = N/2, M = N/2\rangle &\equiv |1, 1, 1, \dots, 1, 1\rangle, \\
 |N/2, N/2 - 1\rangle &\equiv N^{-1/2} \sum_k \mathcal{P}_k(|1\rangle \otimes |0\rangle^{\otimes N-1}), \\
 &\vdots \\
 |N/2, M\rangle &\equiv \binom{N}{N/2 - M}^{-1/2} \sum_k \mathcal{P}_k(|1\rangle^{\otimes N/2 - M} \otimes |0\rangle^{\otimes N + M - N/2}), \\
 &\vdots \\
 |N/2, -N/2\rangle &\equiv |0, 0, 0, \dots, 0, 0\rangle,
 \end{aligned} \tag{B.3}$$

where the sums appearing are over all possible different permutations of the state \mathcal{P}_k . Notice the similarity with respect to the Dicke states Eq. (??). The two mode Dicke state, a symmetric state when the particles can take two different values for the state, is directly mapped to the case on which N qubits are together and the bosonic symmetry is imposed. Therefore, the following equivalence holds

$$|D_{N, \tilde{m}}\rangle \equiv |J = N/2, M = N/2 - \tilde{m}\rangle, \tag{B.4}$$

compare Eq. (??) and the general expression of Eq. (B.3).

For now, we present another well known state, the permutationally invariant singlet for spin- $\frac{1}{2}$ qubits. This state has been recently found to be unique and therefore it has been able to rewrite it in several ways []. The first most trivial definition is that it is permutational invariant ground state of $H = J^2$, from which it can be written as the thermal state at zero temperature for such a Hamiltonian. The second definition is that the PI singlet can be written also as the equally weighted mixture of all the degenerated singlets, i.e., $|J = 0, M = 0, D\rangle$ for $D = 1, 2, \dots, D_0$. An the last definition comes from mixing all the possible permutations of the product of pairwise singlets, $|\Psi^-\rangle := \frac{1}{\sqrt{2}}(|1\rangle \otimes |0\rangle - |0\rangle \otimes |1\rangle)$. Finally, we write those equivalences

$$\lim_{\beta \rightarrow \infty} \frac{\exp(-J^2 \beta)}{\text{tr}(\exp(-J^2 \beta))} \equiv \frac{1}{D_0} \sum_{D=1}^{D_0} |0, 0, D\rangle \langle 0, 0, D| \equiv \left(\frac{N!}{2^{N/2} (N/2)!} \right)^{-1/2} \sum_{k \in \sigma_s} \mathcal{P}_k(|\Psi^-\rangle \langle \Psi^-|^{\otimes N/2}), \tag{B.5}$$

where β is the inverse of the Boltzman constant k_B times the temperature T , and σ_s is the set of all possible unique permutations, in this case $\frac{N!}{2^{N/2} (N/2)!}$.

B.2 Husimi Q-representation and the Bloch sphere

To represent states with angular momentum bigger than $J = \frac{1}{2}$ is convinient to use the so-called Husimi Q -representation [1] on the Bloch-sphere. In fact it is straightforward to represent in a 3D-sphere all the possible states as it is done for qubits.

The Husimi Q -representation must be normalized to 1. Hence,

$$\int Q_\rho(\Omega) d\Omega = 1, \quad (\text{B.6})$$

where Ω represents the solid angle of the sphere, i.e., the function is a function of φ and θ , the azimuth angle and the polar angle respectively, and $d\Omega = \sin(\theta)d\varphi d\theta$. We will use it to describe states belonging to the symmetric subspace or for states belonging to the maximum angular momentum. Therefore, the $Q_\rho(\Omega)$ function will be proportional to the fidelities of totally polarized states that point to different directions represented by Ω .

In the case of many qubits such totally polarized states can be written as

$$|N/2, N/2\rangle_\Omega \equiv |\Omega\rangle := |1\rangle_\Omega \otimes |1\rangle_\Omega \otimes |1\rangle_\Omega \otimes \dots |1\rangle_\Omega, \quad (\text{B.7})$$

where can be reformulated as the eigenstate with the maximum eigenvalue for $J_\Omega = \cos(\varphi)\sin(\theta)J_x + \sin(\varphi)\sin(\theta)J_y + \cos(\theta)J_z$ operator. An alternative way to obtain such totally polarized states $|\Omega\rangle$ is to rotate a totally polarized state along the z -direction by θ angle along the y -axis and then applying a rotation of φ angle along the z -axis. Hence,

$$\begin{aligned} |\Omega\rangle &= e^{-i\varphi J_z} e^{-i\theta J_y} |11\dots 1\rangle \\ J_\Omega |\Omega\rangle &= \frac{N}{2} |\Omega\rangle \end{aligned} \quad (\text{B.8})$$

We write the quasi-probability $Q(\Omega)$ proportional to the fidelity with respect to $|\Omega\rangle$ of the state

$$Q_\rho(\Omega) \propto \text{tr}(\rho |\Omega\rangle\langle\Omega|). \quad (\text{B.9})$$

The normalization constant comes from Eq. (B.6), where a prove state such as the totally mixed state on the symmetric subspace can be used for which $\text{tr}(\frac{\mathbb{I}}{N+1} |\Omega\rangle\langle\Omega|) = \frac{1}{N+1}$. Integrating the Eq. (B.6) we obtain the proportionality factor and it is shown in the following equation

$$Q_\rho(\Omega) = \frac{1}{4\pi(N+1)} \text{tr}(\rho |\Omega\rangle\langle\Omega|), \quad (\text{B.10})$$

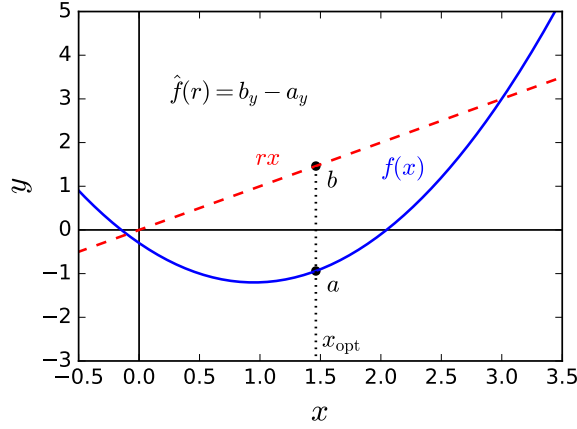


Figure B.1: Graphical representation of the Legendre transform. (blue-line) Convex function, $f(x) = x^2 - 1.9x - 0.3$, to be transformed. (red-dashed) Constant slope line passing by the coordinate system origin, rx . The Legendre transform is the maximal difference between rx and $f(x)$ at the same x . In this case, the vertical distance between a and b .

which must be true for N qubits in the symmetric subspace. Similar definitions could be accomplished for different subspaces or even for different spin number of the constituents.

B.3 Legendre transform

The Legendre transform of a convex function, say $f : x \rightarrow f(x)$, is defined as the maximum distance between the function the line rx and $f(x)$ at same x . It can be written as follows,

$$\hat{f}(r) := \max_x \{rx - f(x)\}, \quad (\text{B.11})$$

where $\hat{f}(r)$ represents the transformed function [18]. A geometric representation of the transform is given on the Figure B.1.

The inverse transformation is simply obtained by applying again the same technique. One fully recovers the

$$f(x) = \max_r \{rx - \hat{f}(r)\}. \quad (\text{B.12})$$

Let us develop the example shown in the Figure B.1, where the function is $f(x) = x^2 - 1.9x - 0.3$. In this case the problem is well defined on the complete real axis. Now, one has to find the maximum of $g(r, x) = rx - f(x)$ for all $\forall r$. This maximum is easily obtained in this particular case with usual techniques. One has to solve for x the following equation $\partial_x g(r, x) = 0$. Thus, the maximum is at

$x_{\text{opt}} = \frac{r+1.9}{2}$ and hence, the Legendre transform is the following,

$$\hat{f}(r) = \frac{r^2}{4} + 0.95r + 1.2025. \quad (\text{B.13})$$

If one applies again the transformation the resulting function is again the original one.

B.3.1 Binomial identities

Bibliography

- [1] Otfried Ghne and Gza Tth. *Entanglement detection*. Physics Reports, **474** 1–75, 2009.
- [2] Alfredo Luis. *Nonlinear transformations and the heisenberg limit*. Physics Letters A, **329** 8–13, 2004.
- [3] Mario Napolitano, Marco Koschorreck, Brice Dubost, Naeimeh Behbood, Robert J Sewell, and Morgan W. W. Mitchell. *Interaction-based quantum metrology showing scaling beyond the heisenberg limit*. Nature, **471** 486–489, March 2011.
- [4] Sergio Boixo, Steven T. Flammia, Carlton M. Caves, and JM Geremia. *Generalized limits for single-parameter quantum estimation*. Physical Review Letters, **98** 090401, Feb 2007.
- [5] Daniel Braun and John Martin. *Heisenberg-limited sensitivity with decoherence-enhanced measurements*. Nature Communications, **2** 223, March 2011.
- [6] S. M. Roy and Samuel L. Braunstein. *Exponentially enhanced quantum metrology*. Physical Review Letters, **100** 220501, Jun 2008.

-
- [7] S. Choi and B. Sundaram. *Bose-einstein condensate as a nonlinear ramsey interferometer operating beyond the heisenberg limit*. Physical Review A, **77** 053613, May 2008.
- [8] A. M. Rey, L. Jiang, and M. D. Lukin. *Quantum-limited measurements of atomic scattering properties*. Physical Review A, **76** 053617, Nov 2007.
- [9] Daniel M Greenberger, Michael A Horne, Abner Shimony, and Anton Zeilinger. *Bell's theorem without inequalities*. **58** 1131–1143, 1990.
- [10] Jian-Wei Pan, Dik Bouwmeester, Matthew Daniell, Harald Weinfurter, and Anton Zeilinger. *Experimental test of quantum nonlocality in three-photon Greenberger-Horne-Zeilinger entanglement*. Nature, **403** 515, Feb 2000.
- [11] Zhi Zhao, Tao Yang, Yu-Ao Chen, An-Ning Zhang, Marek Żukowski, and Jian-Wei Pan. *Experimental violation of local realism by four-photon Greenberger-Horne-Zeilinger entanglement*. Physical Review Letters, **91** 180401, Oct 2003.
- [12] Chao-Yang Lu, Xiao-Qi Zhou, Otfried Gühne, Wei-Bo Gao, Jin Zhang, Zhen-Sheng Yuan, Alexander Goebel, Tao Yang, and Jian-Wei Pan. *Experimental entanglement of six photons in graph states*. Nature Physics, **3** 91–95, 2007.
- [13] Wei-Bo Gao, Chao-Yang Lu, Xing-Can Yao, Ping Xu, Otfried Gühne, Alexander Goebel, Yu-Ao Chen, Cheng-Zhi Peng, Zeng-Bing Chen, and Jian-Wei Pan. *Experimental demonstration of a hyper-entangled ten-qubit schrödinger cat state*. Nature Physics, **6** 331–335, 2010.
- [14] CA Sackett, D Kielpinski, BE King, C Langer, V Meyer, CJ Myatt, M Rowe, QA Turchette, WM Itano, DJ Wineland, and C Monroe. *Experimental entanglement of four particles*. Nature, **404** 256–259, 2000.
- [15] Thomas Monz, Philipp Schindler, Julio T. Barreiro, Michael Chwalla, Daniel Nigg, William A. Coish, Maximilian Harlander, Wolfgang Hänsel, Markus Hennrich, and Rainer Blatt. *14-qubit entanglement: Creation and coherence*. Physical Review Letters, **106** 130506, Mar 2011.
- [16] O. Gühne, M. Reimpell, and R. F. Werner. *Estimating entanglement measures in experiments*. Phys. Rev. Lett., **98**, mar 2007.
- [17] J Eisert, F G S L Brandão, and K M R Audenaert. *Quantitative entanglement witnesses*. New Journal of Physics, **9** 46–46, mar 2007.
- [18] R.T. Rockafellar. *Convex Analysis*. Princeton University Press, 1996.

- [19] Géza Tóth. *Detection of multipartite entanglement in the vicinity of symmetric dicke states*. Journal of the Optical Society of America B: Optical Physics, **24** 275–282, Feb 2007.
- [20] Iagoba Apellaniz, Bernd Lücke, Jan Peise, Carsten Klempt, and Géza Tóth. *Detecting metrologically useful entanglement in the vicinity of dicke states*. New Journal of Physics, **17** 083027, Aug 2015.
- [21] Roland Krischek, Christian Schwemmer, Witlef Wieczorek, Harald Weinfurter, Philipp Hyllus, Luca Pezzé, and Augusto Smerzi. *Useful multiparticle entanglement and sub-shot-noise sensitivity in experimental phase estimation*. Physical Review Letters, **107** 080504, Aug 2011.
- [22] N. Kiesel, C. Schmid, G. Tóth, E. Solano, and H. Weinfurter. *Experimental observation of four-photon entangled dicke state with high fidelity*. Physical Review Letters, **98** 063604, Feb 2007.
- [23] Witlef Wieczorek, Roland Krischek, Nikolai Kiesel, Patrick Michelberger, Géza Tóth, and Harald Weinfurter. *Experimental entanglement of a six-photon symmetric dicke state*. Physical Review Letters, **103** 020504, Jul 2009.
- [24] R. Prevedel, G. Cronenberg, M. S. Tame, M. Paternostro, P. Walther, M. S. Kim, and A. Zeilinger. *Experimental realization of dicke states of up to six qubits for multiparty quantum networking*. Physical Review Letters, **103** 020503, Jul 2009.
- [25] A. Chiuri, C. Greganti, M. Paternostro, G. Vallone, and P. Mataloni. *Experimental quantum networking protocols via four-qubit hyperentangled dicke states*. Physical Review Letters, **109** 173604, Oct 2012.
- [26] Philipp Hyllus, Wiesław Laskowski, Roland Krischek, Christian Schwemmer, Witlef Wieczorek, Harald Weinfurter, Luca Pezzé, and Augusto Smerzi. *Fisher information and multiparticle entanglement*. Physical Review A, **85** 022321, Feb 2012.
- [27] Bernd Lücke, Manuel Scherer, Jens Kruse, Luca Pezzé, Frank Deuretzbacher, Phillip Hyllus, Jan Peise, Wolfgang Ertmer, Jan Arlt, Luis Santos, Agosto Smerzi, and Carsten Klempt. *Twin matter waves for interferometry beyond the classical limit*. Science, **334** 773–776, November 2011.
- [28] Christian Gross, Tilman Zibold, Eike Nicklas, Jerome Esteve, and Markus K Oberthaler. *Non-linear atom interferometer surpasses classical precision limit*. Nature, **464** 1165–1169, 2010.
- [29] Géza Tóth and Morgan W Mitchell. *Generation of macroscopic singlet states in atomic ensembles*. New Journal of Physics, **12** 053007, 2010.

-
- [30] D Leibfried, MD Barrett, T Schaetz, J Britton, J Chiaverini, WM Itano, JD Jost, C Langer, and DJ Wineland. *Toward heisenberg-limited spectroscopy with multiparticle entangled states*. Science, **304** 1476–1478, 2004.
- [31] Bernd Lücke, Jan Peise, Giuseppe Vitagliano, Jan Arlt, Luis Santos, Géza Tóth, and Carsten Klempt. *Detecting multiparticle entanglement of dicke states*. Physical Review Letters, **112** 155304, Apr 2014.
- [32] Géza Tóth and Iago Apellaniz. *Quantum metrology from a quantum information science perspective*. Journal of Physics A: Mathematical and Theoretical, **47** 424006, 2014.
- [33] Yong-Liang Zhang, Huan Wang, Li Jing, Liang-Zhu Mu, and Heng Fan. *Fitting magnetic field gradient with heisenberg-scaling accuracy*. Scientific Reports, **4** 7390, Dec 2014.
- [34] BM Escher, RL de Matos Filho, and L Davidovich. *General framework for estimating the ultimate precision limit in noisy quantum-enhanced metrology*. Nature Physics, **7** 406–411, 2011.
- [35] M. Vengalattore, J. M. Higbie, S. R. Leslie, J. Guzman, L. E. Sadler, and D. M. Stamper-Kurn. *High-resolution magnetometry with a spinor bose-einstein condensate*. Physical Review Letters, **98** 200801, May 2007.
- [36] Min-Kang Zhou, Zhong-Kun Hu, Xiao-Chun Duan, Bu-Liang Sun, Jin-Bo Zhao, and Jun Luo. *Precisely mapping the magnetic field gradient in vacuum with an atom interferometer*. Physical Review A, **82** 061602, Dec 2010.
- [37] M. Koschorreck, M. Napolitano, B. Dubost, and M. W. Mitchell. *High resolution magnetic vector-field imaging with cold atomic ensembles*. Applied Physics Letters, **98** 074101, 2011.
- [38] Naeimeh Behbood, F. Martin Ciurana, Giorgio Colangelo, Mario Napolitano, Morgan W. Mitchell, and Robert J Sewell. *Real-time vector field tracking with a cold-atom magnetometer*. Applied Physics Letters, **102** 173504, 2013.
- [39] Iñigo Urizar-Lanz, Philipp Hyllus, Iñigo Luis Egusquiza, Morgan W. Mitchell, and Géza Tóth. *Macroscopic singlet states for gradient magnetometry*. Physical Review A, **88** 013626, Jul 2013.
- [40] Matteo G. A. Paris. *Quantum estimation for quantum technology*. International Journal of Quantum Information, **7** 125–137, 2009.
- [41] Samuel L. Braunstein and Carlton M. Caves. *Statistical distance and the geometry of quantum states*. Physical Review Letters, **72** 3439–3443, May 1994.

- [42] A.S. Holevo. *Probabilistic and Statistical Aspects of Quantum Theory*. North-Holland, Amsterdam, 1982.
- [43] C.W. Helstrom. *Quantum Detection and Estimation Theory*. Academic Press, New York, 1976.
- [44] Dénes Petz. *Covariance and fisher information in quantum mechanics*. Journal of Physics A: Mathematical and General, **35** 929, 2002.
- [45] Dénes Petz. *Quantum information theory and quantum statistics*. Springer, Berlin, Heilderberg, 2008.
- [46] W. Wasilewski, K. Jensen, H. Krauter, J. J. Renema, M. V. Balabas, and E. S. Polzik. *Quantum noise limited and entanglement-assisted magnetometry*. Physical Review Letters, **104** 133601, Mar 2010.
- [47] K Eckert, P Hyllus, D Bruss, Uffe Vestergaard Poulsen, M Lewenstein, C Jentsch, T Müller, EM Rasel, and W Ertmer. *Differential atom interferometry beyond the standard quantum limit*. Physical Review A, **73** 013814, 2006.
- [48] S Wildermuth, S Hofferberth, I Lesanovsky, S Groth, P Krüger, J Schmiedmayer, and I Bar-Joseph. *Sensing electric and magnetic fields with bose-einstein condensates*. Applied Physics Letters, **88** 264103, 2006.
- [49] Florian Wolfgramm, Alessandro Cere, Federica A Beduini, Ana Predojević, Marco Koschorreck, and Morgan W Mitchell. *Squeezed-light optical magnetometry*. Physical Review Letters, **105** 053601, 2010.
- [50] Reinhard F. Werner. *Quantum states with einstein-podolsky-rosen correlations admitting a hidden-variable model*. Physical Review A, **40** 4277–4281, Oct 1989.
- [51] Ryszard Horodecki, Paweł Horodecki, Michał Horodecki, and Karol Horodecki. *Quantum entanglement*. Reviews of Modern Physics, **81** 865–942, Jun 2009.
- [52] Géza Tóth and Dénes Petz. *Extremal properties of the variance and the quantum fisher information*. Physical Review A, **87** 032324, Mar 2013.
- [53] N. Behbood, F. Martin Ciurana, G. Colangelo, M. Napolitano, Géza Tóth, R. J. Sewell, and M. W. Mitchell. *Generation of macroscopic singlet states in a cold atomic ensemble*. Physical Review Letters, **113** 093601, Aug 2014.

- [54] CD Hamley, CS Gerving, TM Hoang, EM Bookjans, and MS Chapman. *Spin-nematic squeezed vacuum in a quantum gas*. Nature Physics, **8** 305–308, 2012.
- [55] H Häffner, W Hänsel, CF Roos, J Benhelm, M Chwalla, T Körber, UD Rapol, M Riebe, PO Schmidt, C Becher, O Gühne, W Dür, and R Blatt. *Scalable multiparticle entanglement of trapped ions*. Nature, **438** 643–646, 2005.
- [56] Xing-Can Yao, Tian-Xiong Wang, Ping Xu, He Lu, Ge-Sheng Pan, Xiao-Hui Bao, Cheng-Zhi Peng, Chao-Yang Lu, Yu-Ao Chen, and Jian-Wei Pan. *Observation of eight-photon entanglement*. Nature Photonics, **6** 225–228, feb 2012.